ABSTRACT

SCHAAF, CECILIA RENEE. Mechanisms Driving Intestinal Stem Cell Mediated Epithelial Repair Following Severe Ischemic Injury. (Under the direction of Dr. Liara Gonzalez).

The following project was conducted in order to identify mechanisms controlling intestinal epithelial stem cell (ISC) activity, particularly in the context of intestinal epithelial repair following severe ischemic injury. Intestinal ischemia affects a variety of both veterinary and human patients, resulting in mortality rates up to 80%. Such high mortality is due, in part, to epithelial barrier loss. To mitigate further damage from luminal bacterial translocation and sepsis, rapid barrier repair is critical. In both homeostasis and other intestinal disease states, ISCs are responsible for this barrier renewal and repair. Previous work in the Gonzalez lab using a surgical porcine model of intestinal ischemia demonstrated that an ISC subpopulation is preserved through acute injury and these cells may contribute to epithelial repair post-injury. However, the potential mechanisms that control the ability of these cells to proliferate after severe ischemia warranted further investigation as they could serve as potential therapeutic targets.

This project, which utilized translational, porcine models of intestinal injury, necessitated the use of gene-editing to identify specific cellular mechanisms. Chapter 1 is a literature review that focuses on the importance of the porcine model as well as recent developments in gene-edited porcine intestinal disease models. While various diseases are covered in Chapter 1, a large portion focuses specifically on intestinal ischemic injury, the ISC subpopulations, and a potential cellular mechanism that may control post-injury ISC proliferation. Chapter 1 also highlights the development of a prospective ISC reporter porcine model, which, upon further validation, could positively impact numerous intestinal research fields including colorectal cancer and post-injury barrier repair.

Chapter 2 focuses specifically on post-ischemic injury ISC-mediated epithelial repair in the porcine intestinal model. Through histologic analysis, we showed that in days 0-3 following ischemic injury (DPI), the first signs of crypt-base epithelial regeneration were present at 2 DPI. By more detailed immunofluorescent analysis to identify ISC subsets and proliferation markers, we showed that while HOPX+ ISCs are initially enriched at 1 DPI, by 2 DPI, HOPX+ ISCs decrease while proliferative marker Ki67 increases within the crypt-base epithelium. This increased 2 DPI proliferative activity was confirmed by *in vitro* enteroid cell culture. Given both these results and our previous findings correlating decreased HOPX expression with increased cellular proliferation, we questioned if silencing HOPX could act as a switch to increase crypt-base cell proliferation post-ischemic injury. This hypothesis was confirmed using viral transduction of short hairpin RNA in acute ischemic injured crypts and subsequent enteroid culture.

While the findings from Chapter 2 highlighted HOPX as a driver of epithelial recovery after severe intestinal ischemia, more detailed, single ISC analyses was still precluded by the lack of a porcine transgenic ISC reporter model. Chapter 3 describes a collaborative project with the Dr. Jorge Piedrahita lab to validate the first ISC reporter pig – LGR5-H2B-GFP. Through histology, cell culture, gene expression, and fluorescent *in situ* hybridization, we confirmed that LGR5-H2B-GFP^{hi} cells are active ISCs. Furthermore, we showed the utility of this new model for colorectal cancer studies by replicating a key tumor driver gene mutation in LGR5-H2B-GFP colonoids.

Future work using this transgenic pig in studies of ISC-mediated repair post-ischemic injury are needed. These studies would further investigate additional signaling mechanisms driving the ISC response. Such work is outlined in Appendix A, an NIH grant proposal. This proposal

hypothesizes that cytokine signals from neighboring intestinal T-cell populations are modulating the ISC proliferative response. Determination of these signals will help to identify future therapeutic targets to accelerate barrier repair and ultimately reduce patient suffering.

Mechanisms Driving Intestinal Stem Cell Mediated Epithelial Repair Following Severe Ischemic Injury

by
Cecilia Renee Schaaf

A dissertation submitted to the Graduate Faculty of
North Carolina State University
in partial fulfillment of the
requirements for the degree of
Doctor of Philosophy

Comparative Biomedical Sciences

Raleigh, North Carolina
2022

APPROVED BY:

_____	_____
Dr. Liara Gonzalez Committee Chair	Dr. Christopher Dekaney
_____	_____
Dr. Tobias Kaeser	Dr. Samuel Jones

DEDICATION

I dedicate this dissertation to my family. You encouraged my love of animals and science from the beginning and have provided so much support for this continuing journey. And especially to my husband, George, for always keeping me grounded along the way. Thank you.

BIOGRAPHY

Cecilia Schaaf was born in Winston-Salem, North Carolina on November 10, 1991. She grew up with her older brother, rabbits, birds, dogs, hermit crabs, and even a few long-lived goldfish won at the fair. She graduated from R.J. Reynolds High School and went on to receive her Bachelor of Science in Biology from Wake Forest University (WFU) in 2014. Along the way, she picked up the first love of her life, a horse named Dill Pickle. Cecilia and Dill Pickle set off for veterinary school at North Carolina State University (NCSU) and by the time she graduated in 2018, they had also acquired a hedgehog (Olive), a corgi (Ada), and the second love of Cecilia's life, a fellow veterinary student named George. After veterinary school, the crew moved to Greensboro so Cecilia and George could continue their post-doctoral trainings at NCSU and WFU, respectively. While Cecilia worked on her PhD in Comparative Biomedical Sciences under the direction of Dr. Liara Gonzalez, she and George got married, and their little Greensboro farmstead welcomed another dog (Mae) and a few more horses (Bertrand Russell, Devotion, and Raisin). Besides her passion for animals, translational research, and veterinary medicine, Cecilia has a love of playing the violin and gardening. She looks forward to long career as a horseback-riding, music-playing, clinician scientist.

ACKNOWLEDGMENTS

First, I would like to acknowledge and appreciate the animals used in these studies. Their contributions will ultimately help alleviate suffering in veterinary and human patients alike. For that, we are all grateful.

There are also many people to thank for their help and guidance through this PhD process. Dr. Liara Gonzalez, your encouragement to start down the research path while doing the summer veterinary scholar's program has helped me discover a genuine, fulfilling career. Your guidance, mentorship, and friendship over the past 7 years has been a true gift. Thank you to the other members of my committee -- Drs. Chris Dekaney, Toby Kaeser, and Sam Jones -- for your insights and support through these various projects. Particularly, thank you Dr. Kaeser, the Kaeser Lab, and Javid Mohammed, for the endless flow cytometry assistance. To the Gonzalez lab members past and present – particularly John, Amy, Caroline, Elsa, and Brittany – your contributions made all of this work attainable. I am so grateful for our camaraderie. To Amber Carter, undergraduate student extraordinaire, I cannot thank you enough for your help the past year. Your work, alongside Breanna Sheahan's assistance and Kathryn Polkoff's guidance, was instrumental. Thanks to all of you. I am also very appreciative of the assistance from staff in the Central Procedures Laboratory and Laboratory Animal Resources in taking care of the animals. And finally, thank you to my husband and family for supporting me through this process and in the next steps to come.

TABLE OF CONTENTS

LIST OF TABLES

Chapter 1

Chapter 2

Appendix

LIST OF FIGURES

Chapter 1

Chapter 2

Chapter 3

Appendix

CHAPTER 1

USE OF TRANSLATIONAL, GENETICALLY MODIFIED PORCINE MODELS TO ULTIMATELY IMPROVE INTESTINAL DISEASE TREATMENT

ABSTRACT

For both human and veterinary patients, non-infectious intestinal disease is a major cause of morbidity and mortality. To improve treatment of intestinal disease, large animal models are increasingly recognized as critical tools to translate the basic science discoveries made in rodent models into clinical application. Large animal intestinal models, particularly porcine, more closely resemble human anatomy, physiology, and disease pathogenesis; these features make them critical to the pre-clinical study of intestinal disease treatments. Previously, large animal model use has been somewhat precluded by the lack of genetically altered large animals to mechanistically investigate non-infectious intestinal diseases such as colorectal cancer, cystic fibrosis, and ischemia-reperfusion injury. However, recent advances and increased availability of gene editing technologies has led to both novel use of large animal models in clinically relevant intestinal disease research and improved testing of potential therapeutics for these diseases.

INTRODUCTION

Gastrointestinal disease accounts for over 3.0 million hospitalizations and over $135.9 billion in health care expenditures per year. [1] To lessen this incredible burden to patients and our healthcare system, animal models play a critical role in discovery of intestinal disease pathogenesis and therapeutic innovation. For successful clinical translation, it is critical that animal models are properly validated. The criteria used to validate an animal model include certifying similarity in biology and clinical presentation between model and human disease (face validity), confirming that clinical interventions produce similar effects (predictive ability), and demonstrating that the target under investigation has a similar role in the model compared to human clinical disease (target validity). [2] Of intestinal disease animal models, rodents are historically preferred for use due to their low cost and maintenance, rapid reproduction, and readily available rodent-specific

reagents. However, it is now widely recognized that rodents do not fully mimic human disease, physiology, immunology, or drug metabolism, thus limiting their use as pre-clinical models for disease treatment. [3-7] For example, despite promising pre-clinical murine anti-cancer therapeutic studies, success rate of these therapeutics in human clinical trial is only around 5%. [4, 8] Furthermore, the small size of rodents makes it difficult to model and advance surgical and endoscopic techniques. The differences between rodents and humans have left gaps in both basic science research and pre-clinical model development for intestinal diseases.

To better represent both human physiology and disease, and aid in the discovery of new treatments, porcine models are gaining popularity. With similar genome, size and architecture of the intestine, omnivorous diet, microbiome, immunology, and physiology to humans, pigs are increasingly the preferred model of enteric diseases (Table 1). [3, 6, 9-16] The large size of the pig allows for multiple, longitudinal sampling from the same individual. Their large litter size of around 12 piglets allows for ease of gender and sibling matching. These attributes reduce both experimental variation as well as overall animal use. Additionally, for toxicology and drug discovery testing, pigs have oral and parenteral dosing rates similar to humans as well as similar responses to a variety of drug classes. [17]

Table 1. Summary of comparisons between human and porcine intestinal physiology and anatomy as well as advantages and disadvantages of porcine models.

Porcine Intestine Similarities to Human	**Porcine Intestine Differences from Human**
• Intestinal length • Omnivorous diet • Microbiome • Immune response resembles human in 80% of analyzed parameters (compared to less than 10% in mice) • High genome homology	• Presence of spiral colon • Inverted lymph node structure • Distribution and frequency of intestinal lymphocyte populations • Continuous ileal Peyer's patch
Porcine Model Advantages	**Porcine Model Disadvantages**
• Husbandry well understood • Outbred breeds better mimic variation between human individuals • Large litters for gender/sibling matching • Large animal size allows for improving surgical/endoscopy techniques using human equipment for diseases like Cystic Fibrosis and colorectal cancer • Longer lifespan permits longitudinal studies • Oral/parenteral dosing and responses to many drug classes similar to humans • More accepted on ethical basis compared to non-human primates or other large animals • Numerous *in vitro* applications such as advanced 3D organoid cultures	• Necessitate large, specialized housing facilities • More expensive than mice • Not as many species-specific reagents as mice

Grossly, both human and porcine adult intestine are at a ratio of 0.1 length per kilogram of body weight. [18] The anatomy of the small intestine is similar between pig and human, though the large intestine varies slightly in the pig due to a larger cecum, lack of appendix, and the presence of the spiral colon (Figure 1). [3] Microscopically, for both species, the small and large intestine are comprised of a single layer of epithelial cells, interspersed with intra-epithelial lymphocytes, to serve as a barrier between luminal contents and systemic circulation. The single layer epithelium covers villus projections (present only in small intestine) and extends down into

the crypts of Lieberkuhn. Located at the crypt-base are the intestinal epithelial stem cells (ISCs), which are responsible for renewing the epithelial cell populations on a continuous 3-5 day cycle. [9, 19-21] In the human, the ISCs are interspersed with Paneth cells, a specialized secretory cell type that both supports ISC function and releases antimicrobial factors into the intestinal lumen. [22, 23] While a similar cell population expressing the same biomarkers and intracellular structures has been identified in the pig, the porcine Paneth cell has yet to be fully defined. [24, 25]

Beneath the epithelial barrier is the lamina propria compartment. While the lamina propria is made up of a mix of structural elements including blood and lymph vessels, connective tissue, and mesenchymal cells, immune cells constitute a major population, including dendritic cells and lymphocytes. These immune cells are responsible for discriminating between harmless luminal antigens and potential enteropathogens. [26-28] Some differences exist between the immunologic organization between human and pig intestine such as the distribution and frequency of lamina propria and intraepithelial lymphocyte populations, the inverted structure of porcine peripheral and gut-associated lymph nodes, and the aggregated lymphoid follicles (Peyer's patches) which form one long continuous band in the porcine ileum. [15, 28, 29] However, despite these differences, pigs are still recognized as useful models in several enteric immunologic studies including infectious disease, oral vaccination, small bowel transplantation, food hypersensitivity, and immune development. [14, 15, 30-33]

With these similarities in both physiology and architecture between human and porcine intestine (Table 1), porcine models of various intestinal injuries such as ischemia-reperfusion injury, intestinal transplantation, short gut syndrome, and necrotizing enterocolitis have progressed the field of gastroenterology. [31, 34-38] Furthermore, *in vitro* advancements continue to broaden the utility of porcine enteric disease models. These advancements include an increase in porcine

specific reagents and the use of primary intestinal epithelial cell culture in 2-D monolayers, 3-D organoid culture, and co-culture with microbes and lamina-propria derived cells to better understand intestinal barrier function. [11, 12, 25, 34, 35, 39, 40]. However, for more mechanistic studies and to better understand human genetic diseases in the wide array of intestinal maladies, advancements in porcine gene-edited models are needed. Fortunately, enhanced strategies to edit the porcine genome and develop transgenic models, as well as approaches to genetically modify porcine-derived intestinal organoids, have increased the availability of pre-clinical modeling for Cystic Fibrosis (CF), colorectal cancer (CRC), and ischemia-reperfusion injury (Table 2). This review summarizes the current use of pre-clinical, gene edited porcine intestinal disease and injury models and evaluates future additional needs to ultimately improve treatment of intestinal disease.

Table 2. Summary of findings from gene-edited porcine models of non-infectious intestinal disease.

Gene-Edited Porcine Model	Key Findings for Intestinal Disease	Sources
Cystic Fibrosis		
CFTR$^{-/-}$	Intestinal gene editing to correct cystic fibrosis transmembrane conductance regulator (CFTR) expression alleviates Cystic Fibrosis induced obstructions	[41]
Colorectal Cancer		
APC^{1311}	Adenomatous polyposis coli (*APC*) mutation model reproduces colonic and rectal polyps as seen in familial adenomatous polyposis (FAP)	[42]
	Identification of gene expression, micro-RNAs associated with FAP	[43-46]
	Development of nanoparticles to improve endoscopic identification of dysplastic lesions and adenomas	[47, 48]
TP53^{R167H}	Porcine TP53 isoforms expressed similarly to humans; TP53 variants and circular RNA overexpressed in colon	[49, 50]
KRAS^{G12D} *TP53*^{R167H}	Cre-recombinase inducible *TP53* and Kirsten rat sarcoma viral oncogene homolog (*KRAS*) mutation model leads to intestinal carcinoma development	[51]
Ischemia-Reperfusion Injury		
Enteroid Culture	*In vitro* gene-editing of ischemic injured intestinal epithelium identifies cellular mechanisms of repair	[35]
Future Directions: Stem Cell Reporter		
LGR5-H2B-GFP	*In vivo* and *in vitro* tracking of LGR5^{+} intestinal stem cells, further model validation necessary	[52]

Gene Therapy in Porcine Cystic Fibrosis Models to Alleviate Intestinal Obstruction

Cystic Fibrosis (CF) is a life-threatening disease due to various mutations in the CF transmembrane conductance regulator (*CFTR*) gene. [53] This critical gene encodes for an anion channel widely expressed in epithelium including lung, pancreas, kidney, and intestine; its loss of function inhibits chloride and bicarbonate transport across cell membranes. This leads to thick mucoid secretions with low pH, subsequent pathogen colonization, and dysregulated inflammation. [53, 54] While cause of death in patients afflicted with CF is primarily due to respiratory failure, intestinal disease also contributes significantly to patient morbidity. [55] Up to 20% of infants with CF suffer from meconium ileus at birth, followed by distal intestinal obstructive syndrome due to intestinal atresia, diverticulosis, and microcolon. [41, 53] While genetically modified murine models of CF assisted in basic understanding of *CFTR* functions, these mice fail to fully recreate human clinical disease. [55] These limitations in the mouse models impeded further discovery of disease pathogenesis and potential therapeutics.

In 2008, in an effort to develop an animal model that better represents CF clinical disease, Rogers et al. utilized recombinant adeno-associated virus (rAAV) vectors to create the first *CFTR*-null piglets ($CFTR^{-/-}$). These piglets also demonstrated immediate clinical signs of intestinal obstruction similar to that in human infants with CF. [56] These clinical signs include intestinal atresia, microcolon, and diverticulosis. [53] Other gene editing strategies have since been used to generate $CFTR^{-/-}$ pigs including bacterial artificial chromosome vectors [57] as well as rAAVs to introduce a point mutation within the *CFTR* gene, *CFTR*-ΔF508 mutation. [55, 58] This specific *CFTR* mutation is the most common CF-causing mutation in human patients – it accounts for about 70% of CF alleles. [58] Murine models with this same induced point mutation fail to develop airway disease, pushing the need for a porcine model of this common mutation. While *CFTR*-

ΔF508 porcine models display the same features of human disease in the lung and intestine, the rate of meconium ileus is 100% in the newborn pigs, in contrast to a rate of 20% in human infants. [41] As in humans, meconium ileus requires immediate medical and/or surgical correction, which inhibited the use of the porcine model due to cost and complexity. These factors pushed researchers to utilize additional gene editing techniques to alleviate meconium ileus in the porcine model. Stoltz et al. was able to correct this phenotype by inducing *CFTR* expression under the control of intestinal fatty acid-binding protein (*iFABP*) in *CFTR*$^{-/-}$ pig fibroblasts. [41] These findings indicated that correcting the expression of *CFTR* by gene editing in the intestine is sufficient to prevent intestinal obstruction. Further work in the porcine CF models is necessary to identify exactly how much *CFTR* function is required for proper intestinal function. With these findings, novel gene therapy approaches can be developed such as somatic tissue gene editing to restore endogenous *CFTR* function. It is critical that this research is done in a porcine model, similarly sized to humans, so that delivery of therapeutics can be modeled using human equipment such as endoscopy. The information gained from a translational porcine model of CF will lead to the development of innovative gene therapy treatment approaches to alleviate CF-induced intestinal obstruction.

Improved Modeling and Detection of Colorectal Cancer in Gene Edited Pigs

As of 2020 in the US, colorectal cancer (CRC) is the second leading cause of cancer related deaths for men and women combined. [59] For many patients, including those with precursor familial adenomatous polyposis condition (FAP), CRC begins with germline or somatic mutations in the tumor-suppressor, adenomatous polyposis coli (*APC*) gene. This key driver mutation initiates polyp formation in the colonic epithelium. Subsequent compounding epigenetic changes and genetic mutations progresses tumorigenesis through the adenoma-carcinoma sequence, often

culminating in metastatic cancer. [60] For reasons unknown, CRC incidence has recently risen for young and middle-aged adults. Furthermore, many CRC tumor subtypes exist which remain without treatments. [59] Without a doubt, there is a critical need for animal models to better understand CRC pathogenesis and develop targeted therapies. Attempts to recreate the polyp-adenoma-carcinoma pathogenesis sequence by mutating *Apc* (*Apc*$^{+/min}$) in the mouse usually only leads to non-invasive, non-metastatic neoplasia. Furthermore, this neoplasia only typically occurs in the murine small intestine instead of the colon (Figure 1). [42, 61-63] Moreover, the small size of mice and critical differences in drug metabolism make these mice impractical for development of human CRC drug therapies, progress in endoscopic imaging techniques, or improving surgical interventions.

To overcome these barriers and create an improved, human-scale CRC model, the first gene-targeted APC mutated pig line was developed by inserting a translational stop signal at codon 1311 (*APC*^{1311}). This mutation is orthologous to the germline mutations in patients with familial adenomatous polyposis condition (FAP). [42] In these genetically modified pigs, colonic, and rectal polyps and adenomas develop such as those found in human FAP and CRC patients (Figure 1). [64] Since their development, these pigs have contributed greatly to the discovery of epigenetic modifications, dysplastic polyp premalignant progression, and the function of genes other than *APC* that contribute to the varying severity and progression of disease in patients with FAP. [43-45, 65] One pivotal study by Stachowiak et al., using *APC*^{1311} pigs, was the first to reveal that microRNAs are associated with premalignant transformation of colon polyps and can serve as potential useful biomarkers of disease development. [46] Tan et al. attempted to replicate the *APC* mutation porcine model by transcription activator-like effector nucleases (TALENs) introduction of a stop signal at codon 902; however, these pigs have yet to develop CRC phenotype. [66]

In addition to the *APC*^{1311} line, other mutated tumor suppressor gene porcine models are now available to study tumorigenesis. One such group carries a latent Cre-activated tumor protein *p53* gene (*TP53*) mutated allele (*TP53*^{R167H}). [49] This mutation is orthologous to the oncogenic human mutant *TP53* allele that plays a role in numerous human cancers including CRC. Previously, studies using the *APC*^{1311} pigs reported that in severe cases of polyposis, there is an increase in expression of polymorphic *TP53*. [44] A more recent study using the *TP53*^{R167H} pig demonstrated that these pigs express *TP53* isoforms in a more similar manner to humans, further underscoring the benefits of porcine cancer models compared to murine. The *TP53*^{R167H} porcine model showed that *TP53* variants and circular RNA are overexpressed in the colon, indicating likely oncogenic function. [50] These findings highlight the important role of porcine oncogenic models to improve our understanding of the genetic and epigenetic changes that contribute to CRC pathogenesis. Further developments on the *TP53*^{R167H} model include the addition of inducible Kirsten rat sarcoma viral oncogene homolog (*KRAS*) mutation. [51, 67] Mutated *KRAS* is present in over 25% of human tumors, including CRC, and is one of the more commonly activated oncogenes. [68] Schook et al. showed that these Cre recombinase inducible *KRAS*^{G12D} *TP53*^{R167H} transgenic pigs developed rapid and reproducible mesenchymal tumors. For more specific study of intestinal cancer, Callesen et al. refined the combined *KRAS* and *TP53* mutation model by directing the control of the inducible recombination events under an intestinal epithelial specific gene promoter, which led to development of duodenal carcinoma. Further model establishment studies using the *KRAS*^{G12D} *TP53*^{R167H} pigs are warranted to establish carcinoma development in the lower intestine in order to better understand CRC carcinogenesis in a translational large animal model.

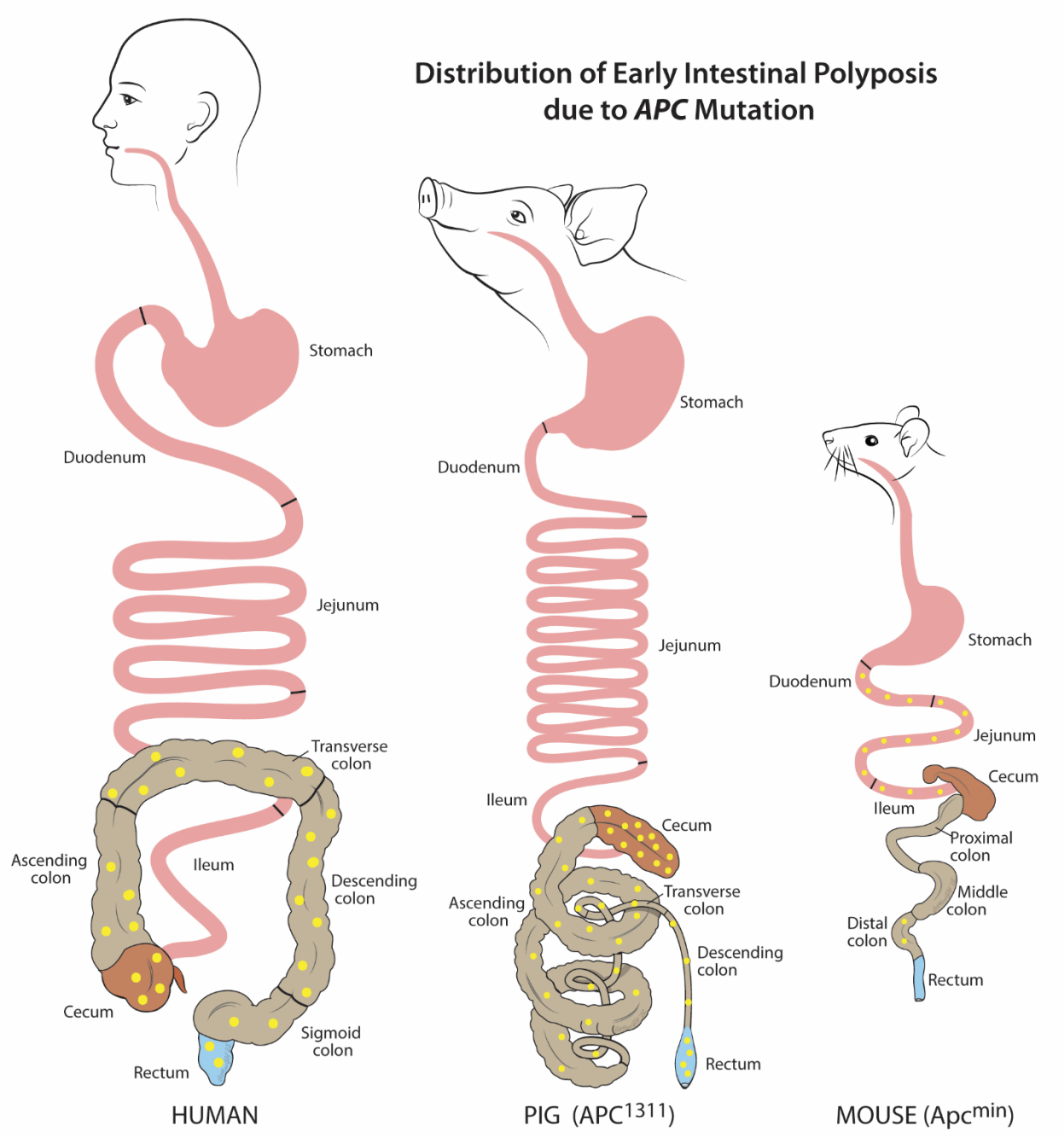

Figure 1. Distribution of Early Intestinal Polyposis due to APC Mutation. Human and porcine (APC^{1311}) early adenoma/polyp distribution is similar within the colon and rectum, while murine (Apc^{min}) is mostly localized to the small intestine. Adenoma/polyps shown in yellow.

While these gene-targeted porcine CRC models have served an important role for cellular mechanistic studies, they can also afford clinicians and researchers opportunities to improve endoscopy skills for minimally invasive surgery, conduct longitudinal sampling and monitoring

during treatment and enhance detection systems for pre-malignancies in a human-sized animal model. In general, porcine models have been popular for testing and advancing endoscopic techniques, particularly for colonoscopy. [69-71] Early diagnostic detection of colon dysplasia and adenomas typically relies on white-light endoscopy. [72] However, due to the subtle appearance of adenomas *in situ*, early-stage CRC lesions are often missed, especially in patients with abnormal colonic mucosa due to inflammatory bowel disease. [47, 48] To improve real-time detection of colorectal adenomas, one group developed biodegradable near-infrared fluorescent silica nanoparticles (FSNs). [48] These FSNs, administered intravascularly, permeate into cancerous tissue and 'mark' a lesion because tumor and dysplasia-associated blood and lymph vessels are typically leaky. [48, 73] Additionally, development of these biodegradable FSNs ensured no long-term sequestration within the body, as is typical of traditional nanoparticles. [48] In that study, nanoparticle application was tested by administering FSNs to APC^{1311} pigs intravenously. Twenty-four hours later, colons were surveyed using near-infrared fluorescence-assisted white light endoscopy and adenomas were successfully highlighted by the FSNs. [48] Since this study, additional work has successfully tested other probes in the APC^{1311} pigs to serve as CRC polyp markers. [47] This pre-clinical application testing made possible by the APC^{1311} pigs was critical to develop new techniques to accurately identify clinically significant colorectal dysplasia in human patients.

Gene Editing in Porcine *In Vitro* Model of Ischemia-Reperfusion Injury

Ischemic injury occurs when there is reduction or complete loss of blood flow to an organ. In the intestine, ischemic events can occur due to numerous pathologic events including thrombi, emboli, shock, cardiac insult, mechanical obstruction such as a hernia or intussusception, or necrotizing enterocolitis. [13] In all of these disease states, decreased blood flow to the intestine

diminishes the oxygen supply necessary for normal aerobic cellular metabolism and ATP production. Cells result to anaerobic metabolism which leads to decreased intracellular pH and accumulation of hypoxanthine. Within the ischemic injury period, cell damage and death via apoptosis, autophagy, necrosis, or necroptosis quickly follows. [74]

If blood flow is re-established, such as during surgical attempts to rescue the intestine, cell damage is compounded by reperfusion injury. Oxygen supplied by reperfusion leads to hypoxanthine-derived superoxide formation. Sequential superoxide-induced lipid membrane peroxidation and leukotriene B4 production quickly attracts activated neutrophils and ultimately leads to marked inflammation and production of additional harmful reactive oxygen species. This cascade of events leads to additional cell death, particularly within intestinal epithelial cells. [74] The epithelium is responsible for maintaining a critical barrier between harmful luminal microbes and systemic vasculature. Microbial and/or enterotoxin translocation across a compromised epithelial barrier can develop into systemic inflammatory response syndrome, intestinal necrosis, and remote organ failure. [75] Ultimately, severe ischemia-reperfusion injury progression results in over 50% patient mortality. [74, 76, 77] To lessen the high mortality rate, intestinal ischemia animal models are critical to better understand the pathophysiology of ischemic injury, identify factors driving epithelial repair, and develop potential therapeutics. [34-36, 78]

The process of ischemia-induced epithelial cell loss, as described in numerous animal models, begins at the villus tip and progressively extends down to the crypt-base intestinal epithelial stem cell (ISC) compartment with increasing durations of ischemia. [34, 79-82] In the ISC compartment, two populations of ISCs exist: active, proliferating ISCs that are sensitive to injury (aISCs) and quiescent, reserve ISCs that are injury resistant (rISCs). These two populations were first described using murine models. [83, 84] Accepted markers for the aISC population

include leucine-rich repeat-containing G protein-coupled receptor 5 (LGR5), olfactomedin-4 (OLFM4), and achaete scute-like 2 (ASCL2). [85-87] The rISC is often identified by B cell specific Moloney murine leukemia virus integration site 1 (BMI1), homeodomain only protein X (HOPX), tolemerase reverse transcriptase (TERT), or leucine rich repeats and immunoglobulin like domains (LRIG). [27, 84, 88]

New evidence has shown overlap of gene expression between these active and reserve markers. These findings suggest a degree of cellular plasticity and begs the question of if there are truly discrete active and reserve stem cell populations. [89, 90] However, even in light of these findings, slowly-cycling ISCs with high expression of the reserve markers have been shown to be more injury resistant. This injury resistant ISC population both replenishes the aISC pool and contributes to epithelial repair after other non-ischemia injury insults such as irradiation or chemical damage. [90-94]

In the context of severe intestinal ischemia, the impact of injury on the ISC populations was only recently described. Previously, small rodent models were unable to accurately represent severe human ischemic injury, likely due to differences in intestinal microvascular anatomy and overall small intestinal size. [9] The recent introduction of a porcine surgical model of mesenteric vascular occlusion finally made translational severe ischemic injury experiments possible. [9, 40] With similar sized intestine and more similar microvascular anatomy as humans, pigs make for a better model of intestinal ischemia. [9, 95] Using the surgical porcine model of mesenteric vascular occlusion, researchers identified that severe ischemic injury differentially impacts the two known ISC populations: aISCs undergo apoptosis while rISCs are preserved and are likely responsible for epithelial recovery after injury. [34] In this model, rISCs were identified *in vivo* by HOPX. [84] When ischemic-injured tissue, initially enriched in $HOPX^+$ rISCs, was recovered *in vivo* for up to

3 days post injury, increased signs of crypt-base epithelial regeneration corresponded to a decrease in HOPX. [35]

In organ development, HOPX is an important transcription factor for anterior-posterior patterning. [96] Once organogenesis is complete, HOPX remains present in a variety of cell types including alveolar epithelial cells, hair follicle stem cells, ISCs, and immune cells. [97] In cancer literature, HOPX promoter methylation, which leads to decreased *HOPX* mRNA and protein expression, was frequently found in lung, gastric, esophageal and colorectal cancer tumors. Using colorectal cancer cell lines, forced expression of HOPX suppressed cellular proliferation and invasion. Furthermore, in a xenograft model where colon cancer cell lines were stably transfected with HOPX and injected into nude mouse flanks, HOPX inhibited tumorigenesis. [98, 99]

In the lung, HOPX is expressed by a subset of alveolar epithelial type (AT) cells. In terms of barrier function and regeneration, alveolar epithelial type cells serve many of the same functions as the intestinal epithelium and ISC populations. A recent study in mice found that silencing HOPX in the subset of HOPX+ AT cells resulted in activation of cellular proliferation in culture. [96] For small intestinal rISCs until now, HOPX had served as merely a biomarker. To clarify the potential role of HOPX as a switch to control ISC proliferation after severe ischemia, genetic modification of the porcine ischemic injury model was necessary.

Whole animal, genetically-modified porcine models have yet to be used in intestinal ischemia-reperfusion studies. However, recent advances in genetic modification of porcine intestinal crypt culture are a promising first step for more mechanistic studies. Culture techniques for porcine enteroids, 3D organoids derived from intestinal stem cells that recapitulate the intestinal epithelium, have been well described. [20, 25, 40] Using lentivirus, Khalil et al. group was the first to genetically modify uninjured porcine intestinal crypts to create GFP expressing

enteroids. [100] To better understand epithelial recovery after ischemic injury and the specific role of HOPX function in epithelial crypt cells, Stewart et al. utilized adenovirus mediated transduction of short hairpin RNA to silence *HOPX* within ischemic injured crypt epithelium and showed that inhibiting HOPX increases cellular proliferation in resultant enteroids. [35]

Future work in the translational porcine model of severe intestinal ischemia is warranted to decipher the potential mechanisms controlling the changes in HOPX expression such as chromatin remodeling or microRNAs, as well as the cellular proliferation mechanisms downstream of HOPX. [93, 101] Additionally, $HOPX^+$ injury resistant ISCs may not be the sole players in regeneration from severe ischemic injury. Other intestinal damage models have shown that differentiated epithelial cells have remarkable flexibility and can de-differentiate to acquire stem cell characteristics. These cell types include Paneth cells, tuft cells, enteroendocrine cells, and progenitor cells. [93, 102] Various signaling pathways such as WMT/ASCL2, Hippo/YAP, Notch, and stem cell factor/c-Kit promote this cellular plasticity, dedifferentiation, and repair. [93] Even cytokine signals from intestinal immune cell populations have been shown to promote the epithelial regeneration process in both homeostasis and non-ischemic injury repair. [103-105] Use of the translational porcine model has identified a piece of the mechanistic puzzle controlling epithelial repair after ischemic injury, in part through novel advancement in porcine enteroid gene editing. Further work in gene edited porcine models is needed to understand the full extent of these cellular repair mechanisms in clinically relevant intestinal ischemic injury.

Future Directions: Development of Transgenic Porcine ISC Reporter Models

To improve studies of the cellular mechanisms involved in cancer and various types of intestinal injury such as ischemia reperfusion, transgenic reporter porcine models are warranted for *in vivo* and *in vitro* cell tracking of intestinal cell populations. Intestinal epithelial stem cell

reporter pigs are of particular interest as ISCs play critical roles in both the generation of colorectal cancer and in epithelial barrier regeneration during homeostasis and disease. [106-108] With the development of high efficiency genome editing tools, one group generated a novel porcine cell reporter model via CRISPR-Cas9 insertion of fused histone 2B (H2B) to green fluorescent protein (GFP) under the *ACTB* locus. [109] With successful ubiquitous nuclear expression of GFP demonstrated within these pigs, the same group went on to insert the H2B-GFP sequence under control of leucine-rich repeat-containing G protein-coupled receptor 5 (*LGR5)*, a known biomarker expressed by ISCs (LGR5-H2B-GFP). [52, 83] Histologic sections of colon demonstrated nuclear GFP in the crypt base cell populations in this novel model.

To truly utilize this translational model and isolate ISCs for mechanistic studies in intestinal disease, further work is necessary to conclude that these GFP expressing cells are in fact $LGR5^+$ ISCs. With this information, researchers would then have access to the first ever large animal ISC reporter model. Such a translational model would be ground-breaking for intestinal disease models such as intestinal barrier function/repair and colorectal cancer (CRC). Numerous studies have implicated the role of $LGR5^+$ cancer stem cells (CSCs) in CRC development by deleting *Apc* in murine LGR5+ ISCs. [107, 110, 111] These mutations led to adenoma development that maintained a stem cell/progenitor cell hierarchy, supporting the idea of CSCs. [107] More recently, the presence of LGR5+ CSCs was found to be closely related to drug resistance, and tumor recurrence and metastasis specifically in human samples. [108, 111] The availability of a LGR5+ stem cell reporter large animal model, which could be further gene edited to induce the specific gene mutations associated with CRC tumorogenesis, would aid in the improved understanding of tumorigenesis and production of effective CSC-targeted treatments.

Future Directions: Transgenic Porcine Models of Inflammatory Bowel Disease

Inflammatory Bowel Disease (IBD) is a multifactorial disease that is typically categorized as Crohn's Disease (CD) or Ulcerative Colitis (UC). These syndromes are characterized by inflammation of the intestinal mucosa, influx of immune cells, and dysregulated cytokine production. Subsequently, patients suffer from episodes of abdominal pain, diarrhea, bloody stools, and weight loss. [112] Historically, gene edited rodent models have been used to determine underlying etiologies and test therapeutic targets. [113] Murine models of IBD include knock-outs of cytokines such as IL-10, TGF-β, IL-2, and IL-23. Loss of these cytokines disrupts regulation of inflammation in the intestine, leading to intestinal lesions similar to those seen in IBD. [114-117] Mice have also been engineered to over express signals such as IL-7 or STAT4 to upregulate immune cell activity and induce IBD. [118, 119] However, given the immunological differences known between man and mouse, [5, 7] alternative models that better emulate human immune physiology are needed to test surgical interventions and pharmaceutical therapeutics. A host of factors have been identified to contribute to IBD including gut microbiota, environmental factors, and abnormal innate and adaptive immune responses. [112] Pigs, with similar intestinal microbiota, immunology, and anatomy to humans, are the clear choice for IBD models. [3, 6, 10-16] Chemical-induction of IBD by dextran sulfate sodium (DSS) or trinitrobenzenesulfonic acid (TNBS) has been shown to reproduce intestinal lesions in the pig similar to those found in UC and CD, respectively. [120-124] These models have been used to test advanced endoscopic techniques to correct strictures and supplemental amino acid therapy. To study IBD on a more mechanistic level within a translationally relevant large animal model, transgenic induced IBD porcine models, parallel to the IBD murine models, are needed to mimic the specific immune cell dysregulations seen with IBD.

CONCLUSIONS

The need for large animal models, particularly porcine, to improve pre-clinical intestinal disease translational research is well known. As described in this review, innovative applications of gene-edited porcine models of Cystic Fibrosis, colorectal cancer, and ischemia-reperfusion injury have progressed both the mechanistic understanding of disease pathophysiology as well as led to novel therapeutic treatment development. With continued improvement of gene-editing systems such as CRISPR/Cas, additional porcine models to track intestinal stem cells or simulate disorders such as Inflammatory Bowel Disease can be made available to further progress translational intestinal disease research.

REFERENCES

[1] Peery AF, Crockett SD, Murphy CC, Lund JL, Dellon ES, Williams JL, Jensen ET, Shaheen NJ, Barritt AS, Lieber SR, Kochar B, Barnes EL, Fan YC, Pate V, Galanko J, Baron TH, Sandler RS. Burden and Cost of Gastrointestinal, Liver, and Pancreatic Diseases in the United States: Update 2018. Gastroenterology 2019;156(1):254-72.e11.

[2] Denayer T, Stöhr T, Van Roy M. Animal models in translational medicine: Validation and prediction. New Horizons in Translational Medicine 2014;2(1):5-11.

[3] Kararli TT. Comparison of the gastrointestinal anatomy, physiology, and biochemistry of humans and commonly used laboratory animals. Biopharmaceutics & Drug Disposition 1995;16(5):351-80.

[4] Mak IW, Evaniew N, Ghert M. Lost in translation: animal models and clinical trials in cancer treatment. American journal of translational research 2014;6(2):114-8.

[5] Mestas J, Hughes CCW. Of Mice and Not Men: Differences between Mouse and Human Immunology. The Journal of Immunology 2004;172(5):2731.

[6] Lunney Joan K, Van Goor A, Walker Kristen E, Hailstock T, Franklin J, Dai C. Importance of the pig as a human biomedical model. Science Translational Medicine;13(621):eabd5758.

[7] Seok J, Warren HS, Cuenca AG, Mindrinos MN, Baker HV, Xu W, Richards DR, McDonald-Smith GP, Gao H, Hennessy L, Finnerty CC, López CM, Honari S, Moore EE, Minei JP, Cuschieri J, Bankey PE, Johnson JL, Sperry J, Nathens AB, Billiar TR, West MA, Jeschke MG, Klein MB, Gamelli RL, Gibran NS, Brownstein BH, Miller-Graziano C, Calvano SE, Mason PH, Cobb JP, Rahme LG, Lowry SF, Maier RV, Moldawer LL, Herndon DN, Davis RW, Xiao W, Tompkins RG. Genomic responses in mouse models poorly mimic human inflammatory diseases. Proc Natl Acad Sci U S A 2013;110(9):3507-12.

[8] Hutchinson L, Kirk R. High drug attrition rates—where are we going wrong? Nature Reviews Clinical Oncology 2011;8(4):189-90.

[9] P. Nejdfors MEBJBRW. Mucosal in Vitro Permeability in the Intestinal Tract of the Pig, the Rat, and Man: Species- and Region-Related Differences. Scandinavian Journal of Gastroenterology 2000;35(5):501-7.

[10] Käser T. Swine as biomedical animal model for T-cell research—Success and potential for transmittable and non-transmittable human diseases. Molecular Immunology 2021;135:95-115.

[11] Dawson HD, Lunney JK. Porcine cluster of differentiation (CD) markers 2018 update. Research in Veterinary Science 2018;118:199-246.

[12] Dawson HD, Sang Y, Lunney JK. Porcine cytokines, chemokines and growth factors: 2019 update. Research in Veterinary Science 2020.

[13] Gonzalez LM, Moeser AJ, Blikslager AT. Porcine models of digestive disease: the future of large animal translational research. Translational Research 2015;166(1):12-27.

[14] Meurens F, Summerfield A, Nauwynck H, Saif L, Gerdts V. The pig: a model for human infectious diseases. Trends in microbiology 2012;20(1):50-7.

[15] Mair KH, Sedlak C, Käser T, Pasternak A, Levast B, Gerner W, Saalmüller A, Summerfield A, Gerdts V, Wilson HL, Meurens F. The porcine innate immune system: An update. 45. 2014:321-43.

[16] Nguyen TLA, Vieira-Silva S, Liston A, Raes J. How informative is the mouse for human gut microbiota research? Disease Models & Mechanisms 2015;8(1):1-16.

[17] Walters EM, Prather RS. Advancing swine models for human health and diseases. Missouri medicine 2013;110(3):212-5.

[18] Patterson JK, Lei XG, Miller DD. The pig as an experimental model for elucidating the mechanisms governing dietary influence on mineral absorption. Exp Biol Med (Maywood) 2008;233(6):651-64.

[19] Marshman E, Booth C, Potten CS. The intestinal epithelial stem cell. Bioessays 2002;24(1):91-8.

[20] Gonzalez LM, Williamson I, Piedrahita JA, Blikslager AT, Magness ST. Cell Lineage Identification and Stem Cell Culture in a Porcine Model for the Study of Intestinal Epithelial Regeneration. Public Library of Science One 2013;8(6).

[21] Vega-López MA, Arenas-Contreras G, Bailey M, González-Pozos S, Stokes CR, Ortega MG, Mondragón-Flores R. Development of intraepithelial cells in the porcine small intestine. Developmental immunology 2001;8(2):147-58.

[22] Sato T, van Es JH, Snippert HJ, Stange DE, Vries RG, van den Born M, Barker N, Shroyer NF, van de Wetering M, Clevers H. Paneth cells constitute the niche for Lgr5 stem cells in intestinal crypts. Nature 2011;469(7330):415-8.

[23] Wehkamp J, Chu H, Shen B, Feathers RW, Kays RJ, Lee SK, Bevins CL. Paneth cell antimicrobial peptides: Topographical distribution and quantification in human gastrointestinal tissues. FEBS Letters 2006;580(22):5344-50.

[24] Dekaney CM, Bazer FW, Jaeger LA. Mucosal morphogenesis and cytodifferentiation in fetal porcine small intestine. The Anatomical Record 1997;249(4):517-23.

[25] van der Hee B, Loonen LMP, Taverne N, Taverne-Thiele JJ, Smidt H, Wells JM. Optimized procedures for generating an enhanced, near physiological 2D culture system from porcine intestinal organoids. Stem Cell Research 2018;28:165-71.

[26] Hunyady B, Mezey E, Palkovits M. Gastrointestinal immunology: cell types in the lamina propria--a morphological review. Acta physiologica Hungarica 2000;87(4):305-28.

[27] Powell Anne E, Wang Y, Li Y, Poulin Emily J, Means Anna L, Washington Mary K, Higginbotham James N, Juchheim A, Prasad N, Levy Shawn E, Guo Y, Shyr Y, Aronow Bruce J, Haigis Kevin M, Franklin Jeffrey L, Coffey Robert J. The Pan-ErbB Negative Regulator Lrig1 Is an Intestinal Stem Cell Marker that Functions as a Tumor Suppressor. Cell 2012;149(1):146-58.

[28] Burkey TE, Skjolaas KA, Minton JE. BOARD-INVITED REVIEW: Porcine mucosal immunity of the gastrointestinal tract1. Journal of Animal Science 2009;87(4):1493-501.

[29] Vega-López MA, Arenas-Contreras G, Bailey M, González-Pozos S, Stokes CR, Ortega MG, Mondragón-Flores R. Development of lntraepithelial Cells in the Porcine Small Intestine. Developmental Immunology 2001;8:025301.

[30] Helm RM, Furuta GT, Stanley JS, Ye J, Cockrell G, Connaughton C, Simpson P, Bannon GA, Burks AW. A neonatal swine model for peanut allergy. J Allergy Clin Immunol 2002;109(1):136-42.

[31] Gruessner RWG, Nakhleh RE, Benedetti E, Pirenne J, Belani KG, Beebe D, Carr R, Troppmann C, Gruessner AC. Combined Liver—Total Bowel Transplantation Has No Immunologic Advantage Over Total Bowel Transplantation Alone: A Prospective Study in a Porcine Model. Archives of Surgery 1997;132(10):1077-85.

[32] Azevedo MP, Vlasova AN, Saif LJ. Human rotavirus virus-like particle vaccines evaluated in a neonatal gnotobiotic pig model of human rotavirus disease. Expert Review of Vaccines 2013;12(2):169-81.

[33] Stokes CR, Bailey M, Wilson AD. Immunology of the porcine gastrointestinal tract. Veterinary Immunology and Immunopathology 1994;43(1):143-50.

[34] Gonzalez LM, Amy SS, Freund J, Cecilia RK, Dekaney CM, Magness ST, Blikslager AT. Preservation of reserve intestinal epithelial stem cells following severe ischemic injury. American Journal of Physiology-Gastrointestinal and Liver Physiology 2019;316(4):G482-G94.

[35] Stewart AS, Schaaf CR, Luff JA, Freund JM, Becker TC, Tufts SR, Robertson JB, Gonzalez LM. HOPX+ injury-resistant intestinal stem cells drive epithelial recovery after severe intestinal ischemia. American Journal of Physiology-Gastrointestinal and Liver Physiology 2021;321(5):G588-G602.

[36] Yandza T, Tauc M, Saint-Paul MC, Ouaissi M, Gugenheim J, Hebuterne X. The pig as a preclinical model for intestinal ischemia-reperfusion and transplantation studies. Journal of Surgical Research 2012;178(2):807-19.

[37] Llanos JC, Bakonyi Neto A, Lerco MM, Clark RMO, Polachini do Valle A, Sousa MMF. Induction of Short Gut Syndrome and Transplantation in a Porcine Model. Transplantation Proceedings 2006;38(6):1855-6.

[38] Sangild PT, Siggers RH, Schmidt M, Elnif J, Bjornvad CR, Thymann T, Grondahl ML, Hansen AK, Jensen SK, Boye M, Moelbak L, Buddington RK, Weström BR, Holst JJ, Burrin DG. Diet- and Colonization-Dependent Intestinal Dysfunction Predisposes to Necrotizing Enterocolitis in Preterm Pigs. Gastroenterology 2006;130(6):1776-92.

[39] Cui T, Theuns S, Desmarets LMB, Xie J, De Gryse GMA, Yang B, Van den Broeck W, Nauwynck HJ. Establishment of porcine enterocyte/myofibroblast co-cultures for the growth of porcine rota- and coronaviruses. Scientific Reports 2018;8(1):15195.

[40] Stewart AS, Freund JM, Blikslager AT, Gonzalez LM. Intestinal Stem Cell Isolation and Culture in a Porcine Model of Segmental Small Intestinal Ischemia. Journal of Visualized Experiments 2018;135:57647.

[41] Stoltz DA, Rokhlina T, Ernst SE, Pezzulo AA, Ostedgaard LS, Karp PH, Samuel MS, Reznikov LR, Rector MV, Gansemer ND, Bouzek DC, Alaiwa MHA, Hoegger MJ,

Ludwig PS, Taft PJ, Wallen TJ, Wohlford-Lenane C, McMenimen JD, Chen J-H, Bogan KL, Adam RJ, Hornick EE, Nelson GAIV, Hoffman EA, Chang EH, Zabner J, McCray PB, Jr., Prather RS, Meyerholz DK, Welsh MJ. Intestinal CFTR expression alleviates meconium ileus in cystic fibrosis pigs. The Journal of Clinical Investigation 2013;123(6):2685-93.

[42] Flisikowska T, Merkl C, Landmann M, Eser S, Rezaei N, Cui X, Kurome M, Zakhartchenko V, Kessler B, Wieland H, Rottmann O, Schmid RM, Schneider G, Kind A, Wolf E, Saur D, Schnieke A. A Porcine Model of Familial Adenomatous Polyposis. Gastroenterology 2012;143(5):1173-5.e7.

[43] Sikorska A, Stachowiak M, Flisikowska T, Stachecka J, Flisikowski K, Switonski M. Polymorphisms of CSF1R and WISP1 genes are associated with severity of familial adenomatous polyposis in APC(1311) pigs. Gene 2020;759:144988.

[44] Sikorska A, Flisikowska T, Stachowiak M, Kind A, Schnieke A, Flisikowski K, Switonski M. Elevated expression of p53 in early colon polyps in a pig model of human familial adenomatous polyposis. J Appl Genet 2018;59(4):485-91.

[45] Perkowska A, Flisikowska T, Perleberg C, Flisikowski K, Stachowiak M, Nowacka-Woszuk J, Saur D, Kind A, Schnieke A, Switonski M. The expression of TAP1 candidate gene, but not its polymorphism and methylation, is associated with colonic polyp formation in a porcine model of human familial adenomatous polyposis. Animal Biotechnology 2020;31(4):306-13.

[46] Stachowiak M, Flisikowska T, Bauersachs S, Perleberg C, Pausch H, Switonski M, Kind A, Saur D, Schnieke A, Flisikowski K. Altered microRNA profiles during early colon adenoma progression in a porcine model of familial adenomatous polyposis. Oncotarget 2017;8(56):96154-60.

[47] Yim JJ, Harmsen S, Flisikowski K, Flisikowska T, Namkoong H, Garland M, van den Berg NS, Vilches-Moure JG, Schnieke A, Saur D, Glasl S, Gorpas D, Habtezion A, Ntziachristos V, Contag CH, Gambhir SS, Bogyo M, Rogalla S. A protease-activated, near-infrared fluorescent probe for early endoscopic detection of premalignant gastrointestinal lesions. Proceedings of the National Academy of Sciences 2021;118(1):e2008072118.

[48] Rogalla S, Flisikowski K, Gorpas D, Mayer AT, Flisikowska T, Mandella MJ, Ma X, Casey KM, Felt SA, Saur D, Ntziachristos V, Schnieke A, Contag CH, Gambhir SS, Harmsen S. Biodegradable Fluorescent Nanoparticles for Endoscopic Detection of Colorectal Carcinogenesis. Advanced Functional Materials 2019;29(51):1904992.

[49] Leuchs S, Saalfrank A, Merkl C, Flisikowska T, Edlinger M, Durkovic M, Rezaei N, Kurome M, Zakhartchenko V, Kessler B, Flisikowski K, Kind A, Wolf E, Schnieke A. Inactivation and Inducible Oncogenic Mutation of p53 in Gene Targeted Pigs. PLOS ONE 2012;7(10):e43323.

[50] Niu G, Hellmuth I, Flisikowska T, Pausch H, Rieblinger B, Carrapeiro A, Schade B, Böhm B, Kappe E, Fischer K, Klinger B, Steiger K, Burgkart R, Bourdon J-C, Saur D, Kind A, Schnieke A, Flisikowski K. Porcine model elucidates function of p53 isoform in carcinogenesis and reveals novel circTP53 RNA. Oncogene 2021;40(10):1896-908.

[51] Callesen MM, Árnadóttir SS, Lyskjær I, Ørntoft M-BW, Høyer S, Dagnæs-Hansen F, Liu Y, Li R, Callesen H, Rasmussen MH, Berthelsen MF, Thomsen MK, Schweiger PJ, Jensen KB, Laurberg S, Ørntoft TF, Elverløv-Jakobsen JE, Andersen CL. A genetically inducible porcine model of intestinal cancer. Molecular Oncology 2017;11(11):1616-29.

[52] Polkoff KM, Chung J, Simpson SG, Gleason K, Piedrahita JA. In Vitro Validation of Transgene Expression in Gene-Edited Pigs Using CRISPR Transcriptional Activators. The CRISPR Journal 2020;3(5):409-18.

[53] Yan Z, Stewart ZA, Sinn PL, Olsen JC, Hu J, McCray PB, Engelhardt JF. Ferret and Pig Models of Cystic Fibrosis: Prospects and Promise for Gene Therapy. Human Gene Therapy Clinical Development 2014;26(1):38-49.

[54] Zhou ZP, Yang LL, Cao H, Chen ZR, Zhang Y, Wen X-Y, Hu J. In Vitro Validation of a CRISPR-Mediated CFTR Correction Strategy for Preclinical Translation in Pigs. Human Gene Therapy 2019;30(9):1101-16.

[55] Rogers CS, Hao Y, Rokhlina T, Samuel M, Stoltz DA, Li Y, Petroff E, Vermeer DW, Kabel AC, Yan Z, Spate L, Wax D, Murphy CN, Rieke A, Whitworth K, Linville ML, Korte SW, Engelhardt JF, Welsh MJ, Prather RS. Production of CFTR-null and CFTR-ΔF508 heterozygous pigs by adeno-associated virus–mediated gene targeting and somatic cell nuclear transfer. The Journal of Clinical Investigation 2008;118(4):1571-7.

[56] Meyerholz DK, Stoltz DA, Pezzulo AA, Welsh MJ. Pathology of Gastrointestinal Organs in a Porcine Model of Cystic Fibrosis. The American Journal of Pathology 2010;176(3):1377-89.

[57] Klymiuk N, Mundhenk L, Kraehe K, Wuensch A, Plog S, Emrich D, Langenmayer MC, Stehr M, Holzinger A, Kröner C, Richter A, Kessler B, Kurome M, Eddicks M, Nagashima H, Heinritzi K, Gruber AD, Wolf E. Sequential targeting of CFTR by BAC vectors generates a novel pig model of cystic fibrosis. Journal of Molecular Medicine 2012;90(5):597-608.

[58] Ostedgaard Lynda S, Meyerholz David K, Chen J-H, Pezzulo Alejandro A, Karp Philip H, Rokhlina T, Ernst Sarah E, Hanfland Robert A, Reznikov Leah R, Ludwig Paula S, Rogan Mark P, Davis Greg J, Dohrn Cassie L, Wohlford-Lenane C, Taft Peter J, Rector Michael V, Hornick E, Nassar Boulos S, Samuel M, Zhang Y, Richter Sandra S, Uc A, Shilyansky J, Prather Randall S, McCray Paul B, Zabner J, Welsh Michael J, Stoltz David A. The ΔF508 Mutation Causes CFTR Misprocessing and Cystic Fibrosis–Like Disease in Pigs. Science Translational Medicine 2011;3(74):74ra24-74ra24.

[59] Siegel RL, Miller KD, Goding Sauer A, Fedewa SA, Butterly LF, Anderson JC, Cercek A, Smith RA, Jemal A. Colorectal cancer statistics, 2020. CA: A Cancer Journal for Clinicians 2020;70(3):145-64.

[60] Huang D, Sun W, Zhou Y, Li P, Chen F, Chen H, Xia D, Xu E, Lai M, Wu Y, Zhang H. Mutations of key driver genes in colorectal cancer progression and metastasis. Cancer and Metastasis Reviews 2018;37(1):173-87.

[61] Boivin GP, Washington K, Yang K, Ward JM, Pretlow TP, Russell R, Besselsen DG, Godfrey VL, Doetschman T, Dove WF, Pitot HC, Halberg RB, Itzkowitz SH, Groden J,

Coffey RJ. Pathology of mouse models of intestinal cancer: Consensus report and recommendations. Gastroenterology 2003;124(3):762-77.

[62] Stastna M, Janeckova L, Hrckulak D, Kriz V, Korinek V. Human Colorectal Cancer from the Perspective of Mouse Models. Genes 2019;10(10).

[63] Su L-K, Kinzler KW, Vogelstein B, Preisinger AC, Moser AR, Luongo C, Gould KA, Dove WF. Multiple Intestinal Neoplasia Caused by a Mutation in the Murine Homolog of the APC Gene. Science 1992;256(5057):668-70.

[64] Cancer Genome Atlas N. Comprehensive molecular characterization of human colon and rectal cancer. Nature 2012;487(7407):330-7.

[65] Flisikowska T, Stachowiak M, Xu H, Wagner A, Hernandez-Caceres A, Wurmser C, Perleberg C, Pausch H, Perkowska A, Fischer K, Frishman D, Fries R, Switonski M, Kind A, Saur D, Schnieke A, Flisikowski K. Porcine familial adenomatous polyposis model enables systematic analysis of early events in adenoma progression. Scientific Reports 2017;7(1):6613.

[66] Tan W, Carlson Daniel F, Lancto Cheryl A, Garbe John R, Webster Dennis A, Hackett Perry B, Fahrenkrug Scott C. Efficient nonmeiotic allele introgression in livestock using custom endonucleases. Proceedings of the National Academy of Sciences 2013;110(41):16526-31.

[67] Schook LB, Collares TV, Hu W, Liang Y, Rodrigues FM, Rund LA, Schachtschneider KM, Seixas FK, Singh K, Wells KD, Walters EM, Prather RS, Counter CM. A Genetic Porcine Model of Cancer. PLOS ONE 2015;10(7):e0128864.

[68] Beganoyic S. CLINICAL SIGNIFICANCE OF THE KRAS MUTATION. Bosnian Journal of Basic Medical Sciences 2009;9(Suppl 1):S17-S20.

[69] Obstein KL, Valdastri P. Advanced endoscopic technologies for colorectal cancer screening. World journal of gastroenterology 2013;19(4):431-9.

[70] Choi WJ, Moon J-H, Min JS, Song YK, Lee SA, Ahn JW, Lee SH, Jung HC. Real-time detection system for tumor localization during minimally invasive surgery for gastric and colon cancer removal: In vivo feasibility study in a swine model. Journal of Surgical Oncology 2018;117(4):699-706.

[71] Ciuti G, Skonieczna-Żydecka K, Marlicz W, Iacovacci V, Liu H, Stoyanov D, Arezzo A, Chiurazzi M, Toth E, Thorlacius H, Dario P, Koulaouzidis A. Frontiers of Robotic Colonoscopy: A Comprehensive Review of Robotic Colonoscopes and Technologies. Journal of Clinical Medicine 2020;9(6).

[72] Winawer S, Fletcher R, Rex D, Bond J, Burt R, Ferrucci J, Ganiats T, Levin T, Woolf S, Johnson D, Kirk L, Litin S, Simmang C. Colorectal cancer screening and surveillance: clinical guidelines and rationale-Update based on new evidence. Gastroenterology 2003;124(2):544-60.

[73] Jiang T, Jin K, Liu X, Pang Z. 8 - Nanoparticles for tumor targeting. In: Jana S, Maiti S, Jana S, editors. Biopolymer-Based Composites. Woodhead Publishing; 2017, p. 221-67.

[74] Kalogeris T, Baines CP, Krenz M, Korthuis RJ. Chapter Six - Cell Biology of Ischemia/Reperfusion Injury. In: Jeon KW, editor International Review of Cell and Molecular Biology. Academic Press; 2012, p. 229-317.

[75] Kinross J, Warren O, Basson S, Holmes E, Silk D, Darzi A, Nicholson JK. Intestinal ischemia/reperfusion injury: defining the role of the gut microbiome. Biomarkers in Medicine 2009;3(2):175-92.

[76] Reginelli A, Genovese EA, Cappabianca S, Iacobellis F, Berritto D, Fonio P, Coppolino F, Grassi R. Intestinal Ischemia: US-CT findings correlations. Critical Ultrasound Journal 2013;5(1):S7.

[77] Kassahun WT, Schulz T, Richter O, Hauss J. Unchanged high mortality rates from acute occlusive intestinal ischemia: six year review. Langenbeck's Archives of Surgery 2008;393(2):163-71.

[78] Nolan LS, Wynn JL, Good M. Exploring Clinically-Relevant Experimental Models of Neonatal Shock and Necrotizing Enterocolitis. Shock (Augusta, Ga) 2020;53(5):596-604.

[79] Chiu C-J, McArdle AH, Brown R, Scott HJ, Gurd FN. Intestinal Mucosal Lesion in Low-Flow States: I. A Morphological, Hemodynamic, and Metabolic Reappraisal. Archives of Surgery 1970;101(4):478-83.

[80] Park PO, Haglund U, Bulkley GB, Fält K. The sequence of development of intestinal tissue injury after strangulation ischemia and reperfusion. Surgery 1990;107(5):574-80.

[81] Parks DA, Granger DN. Ischemia-induced vascular changes: role of xanthine oxidase and hydroxyl radicals. American Journal of Physiology-Gastrointestinal and Liver Physiology 1983;245(2):G285-G9.

[82] Robinson JW, Mirkovitch V, Winistörfer B, Saegesser F. Response of the intestinal mucosa to ischaemia. Gut 1981;22(6):512-27.

[83] Barker N, van Es JH, Kuipers J, Kujala P, van den Born M, Cozijnsen M, Haegebarth A, Korving J, Begthel H, Peters PJ, Clevers H. Identification of stem cells in small intestine and colon by marker gene Lgr5. Nature 2007;449(7165):1003-7.

[84] Takeda N, Jain R, LeBoeuf MR, Wang Q, Lu MM, Epstein JA. Interconversion Between Intestinal Stem Cell Populations in Distinct Niches. Science 2011;334(6061):1420.

[85] Barker N, Clevers H. Leucine-rich repeat-containing G-protein-coupled receptors as markers of adult stem cells. Gastroenterology 2010;138(5):1681-96.

[86] van der Flier LG, van Gijn ME, Hatzis P, Kujala P, Haegebarth A, Stange DE, Begthel H, van den Born M, Guryev V, Oving I, van Es JH, Barker N, Peters PJ, van de Wetering M, Clevers H. Transcription factor achaete scute-like 2 controls intestinal stem cell fate. Cell 2009;136(5):903-12.

[87] van der Flier LG, Haegebarth A, Stange DE, van de Wetering M, Clevers H. OLFM4 Is a Robust Marker for Stem Cells in Human Intestine and Marks a Subset of Colorectal Cancer Cells. Gastroenterology 2009;137(1):15-7.

[88] Montgomery RK, Carlone DL, Richmond CA, Farilla L, Kranendonk MEG, Henderson DE, Baffour-Awuah NY, Ambruzs DM, Fogli LK, Algra S, Breault DT. Mouse telomerase

reverse transcriptase (mTert) expression marks slowly cycling intestinal stem cells. Proceedings of the National Academy of Sciences of the United States of America 2011;108(1):179-84.

[89] Muñoz J, Stange DE, Schepers AG, van de Wetering M, Koo B-K, Itzkovitz S, Volckmann R, Kung KS, Koster J, Radulescu S, Myant K, Versteeg R, Sansom OJ, van Es JH, Barker N, van Oudenaarden A, Mohammed S, Heck AJR, Clevers H. The Lgr5 intestinal stem cell signature: robust expression of proposed quiescent '+4' cell markers. The EMBO journal 2012;31(14):3079-91.

[90] Bankaitis ED, Ha A, Kuo CJ, Magness ST. Reserve Stem Cells in Intestinal Homeostasis and Injury. Gastroenterology 2018;155(5):1348-61.

[91] Buczacki SJA, Zecchini HI, Nicholson AM, Russell R, Vermeulen L, Kemp R, Winton DJ. Intestinal label-retaining cells are secretory precursors expressing Lgr5. Nature 2013;495(7439):65-9.

[92] Tian H, Warming S, Leong KG, Rangell L, Klein OD, de Sauvage FJ. A reserve stem cell population in small intestine renders Lgr5-positive cells dispensable. Nature 2011;478:255-9.

[93] Meyer AR, Brown ME, McGrath PS, Dempsey PJ. Injury-Induced Cellular Plasticity Drives Intestinal Regeneration. Cellular and Molecular Gastroenterology and Hepatology 2022;13(3):843-56.

[94] Higa T, Okita Y, Matsumoto A, Nakayama S, Oka T, Sugahara O, Koga D, Takeishi S, Nakatsumi H, Hosen N, Robine S, Taketo MM, Sato T, Nakayama KI. Spatiotemporal reprogramming of differentiated cells underlies regeneration and neoplasia in the intestinal epithelium. Nature Communications 2022;13(1):1500.

[95] Bellamy JE, Latshaw WK, Nielsen NO. The vascular architecture of the porcine small intestine. Canadian journal of comparative medicine : Revue canadienne de medecine comparee 1973;37(1):56-62.

[96] Ota C, Ng-Blichfeldt J-P, Korfei M, Alsafadi HN, Lehmann M, Skronska-Wasek W, M. De Santis M, Guenther A, Wagner DE, Königshoff M. Dynamic expression of HOPX in alveolar epithelial cells reflects injury and repair during the progression of pulmonary fibrosis. Scientific Reports 2018;8(1):12983.

[97] Liu Y, Zhang W. The role of HOPX in normal tissues and tumor progression. Bioscience reports 2020;40(1):BSR20191953.

[98] Katoh H, Yamashita K, Waraya M, Margalit O, Ooki A, Tamaki H, Sakagami H, Kokubo K, Sidransky D, Watanabe M. Epigenetic Silencing of HOPX Promotes Cancer Progression in Colorectal Cancer. 14. 2012:559-IN6.

[99] Yamashita K, Katoh H, Watanabe M. The homeobox only protein homeobox (HOPX) and colorectal cancer. International journal of molecular sciences 2013;14(12):23231-43.

[100] Khalil HA, Lei NY, Brinkley G, Scott A, Wang J, Kar UK, Jabaji ZB, Lewis M, Martín MG, Dunn JCY, Stelzner MG. A novel culture system for adult porcine intestinal crypts. Cell and Tissue Research 2016;365(1):123-34.

[101] Liang H, Wang C, Gao K, Li J, Jia R. MicroRNA-421 promotes the progression of non-small cell lung cancer by targeting HOPX and regulating the Wnt/β-catenin signaling pathway. Molecular medicine reports 2019;20(1):151-61.

[102] Tetteh PW, Farin HF, Clevers H. Plasticity within stem cell hierarchies in mammalian epithelia. Trends in Cell Biology 2015;25(2):100-8.

[103] Biton M, Haber AL, Rogel N, Burgin G, Beyaz S, Schnell A, Ashenberg O, Su C-W, Smillie C, Shekhar K, Chen Z, Wu C, Ordovas-Montanes J, Alvarez D, Herbst RH, Zhang M, Tirosh I, Dionne D, Nguyen LT, Xifaras ME, Shalek AK, von Andrian UH, Graham DB, Rozenblatt-Rosen O, Shi HN, Kuchroo V, Yilmaz OH, Regev A, Xavier RJ. T Helper Cell Cytokines Modulate Intestinal Stem Cell Renewal and Differentiation. Cell 2018;175(5):1307-20.e22.

[104] Hanash AM, Dudakov JA, Hua G, O'Connor MH, Young LF, Singer NV, West ML, Jeng RR, Holland AM, Kappel LW, Ghosh A, Tsai JJ, Rao UK, Yim NL, Smith OM, Velardi E, Hawryluk EB, Murphy GF, Liu C, Fouser LA, Kolesnick R, Blazar BR, van den Brink MR. Interleukin-22 protects intestinal stem cells from immune-mediated tissue damage and regulates sensitivity to graft versus host disease. Immunity 2012;37(2):339-50.

[105] Lindemans CA, Calafiore M, Mertelsmann AM, O'Connor MH, Dudakov JA, Jenq RR, Velardi E, Young LF, Smith OM, Lawernce G, Ivanov JA, Fu Y, Takashima S, Hua G, Martin ML, O'Rourke KP, Lo YMM, Romera-Hernandez M, Cupedo T, Dow LE, Nieuwenhuis EE, Shroyer NF, Liu C, Kolesnick R, van der Brink MRM, Hanash AM. Interleukin-22 promotes intestinal-stem-cell-mediated epithelial regeneration. Nature 2015;528(24/31):560-4.

[106] Potten CS, Hume WJ, Reid P, Cairns J. The segregation of DNA in epithelial stem cells. Cell 1978;15(3):899-906.

[107] Barker N, Ridgway RA, van Es JH, van de Wetering M, Begthel H, van den Born M, Danenberg E, Clarke AR, Sansom OJ, Clevers H. Crypt stem cells as the cells-of-origin of intestinal cancer. Nature 2009;457(7229):608-11.

[108] Baker A-M, Graham TA, Elia G, Wright NA, Rodriguez-Justo M. Characterization of LGR5 stem cells in colorectal adenomas and carcinomas. Scientific Reports 2015;5(1):8654.

[109] Sper RB, Koh S, Zhang X, Simpson S, Collins B, Sommer J, Petters RM, Caballero I, Platt JL, Piedrahita JA. Generation of a Stable Transgenic Swine Model Expressing a Porcine Histone 2B-eGFP Fusion Protein for Cell Tracking and Chromosome Dynamics Studies. PloS one 2017;12(1):e0169242-e.

[110] Morgan RG, Mortensson E, Williams AC. Targeting LGR5 in Colorectal Cancer: therapeutic gold or too plastic? British Journal of Cancer 2018;118(11):1410-8.

[111] Zhou Y, Xia L, Wang H, Oyang L, Su M, Liu Q, Lin J, Tan S, Tian Y, Liao Q, Cao D. Cancer stem cells in progression of colorectal cancer. Oncotarget 2017;9(70):33403-15.

[112] Fiocchi C. Inflammatory bowel disease: Etiology and pathogenesis. Gastroenterology 1998;115(1):182-205.

[113] Prattis S, Jurjus A. Spontaneous and transgenic rodent models of inflammatory bowel disease. Laboratory animal research 2015;31(2):47-68.

[114] Lees CW, Barrett JC, Parkes M, Satsangi J. New IBD genetics: common pathways with other diseases. Gut 2011;60(12):1739.

[115] Baumgart DC, Olivier W-A, Reya T, Peritt D, Rombeau JL, Carding SR. Mechanisms of Intestinal Epithelial Cell Injury and Colitis in Interleukin 2 (IL2)-Deficient Mice. Cellular Immunology 1998;187(1):52-66.

[116] Shull MM, Ormsby I, Kier AB, Pawlowski S, Diebold RJ, Yin M, Allen R, Sidman C, Proetzel G, Calvin D, Annunziata N, Doetschman T. Targeted disruption of the mouse transforming growth factor-β1 gene results in multifocal inflammatory disease. Nature 1992;359(6397):693-9.

[117] Berg DJ, Davidson N, Kühn R, Müller W, Menon S, Holland G, Thompson-Snipes L, Leach MW, Rennick D. Enterocolitis and colon cancer in interleukin-10-deficient mice are associated with aberrant cytokine production and CD4(+) TH1-like responses. The Journal of Clinical Investigation 1996;98(4):1010-20.

[118] Simpson SJ, Shah S, Comiskey M, de Jong YP, Wang B, Mizoguchi E, Bhan AK, Terhorst C. T Cell–mediated Pathology in Two Models of Experimental Colitis Depends Predominantly on the Interleukin 12/Signal Transducer and Activator of Transcription (Stat)-4 Pathway, but Is Not Conditional on Interferon γ Expression by T Cells. Journal of Experimental Medicine 1998;187(8):1225-34.

[119] Watanabe M, Ueno Y, Yajima T, Okamoto S, Hayashi T, Yamazaki M, Iwao Y, Ishii H, Habu S, Uehira M, Nishimoto H, Ishikawa H, Hata J-i, Hibi T. Interleukin 7 Transgenic Mice Develop Chronic Colitis with Decreased Interleukin 7 Protein Accumulation in the Colonic Mucosa. Journal of Experimental Medicine 1998;187(3):389-402.

[120] Lukas M, Kolar M, Ryska O, Juhas S, Juhasova J, Kalvach J, Pazin J, Kocisova T, Foltan O, Kristianova H, Ptacnik J, Vitkova I, Bortlik M, Lukas M. Novel porcine model of Crohn's disease anastomotic stricture suitable for evaluation and training of advanced endoscopic techniques. Gastrointestinal Endoscopy 2021;93(1):250-6.

[121] Ziv Y, Nevler A, Willenz E, Doron O, Zbar A, Shperber A, Sandbank J. A novel porcine model for chemically inducible Crohn's-like reaction. The Israel Medical Association journal : IMAJ 2015;17(1):19-23.

[122] Kim CJ, Kovacs-Nolan J, Yang C, Archbold T, Fan MZ, Mine Y. L-cysteine supplementation attenuates local inflammation and restores gut homeostasis in a porcine model of colitis. Biochimica et Biophysica Acta (BBA) - General Subjects 2009;1790(10):1161-9.

[123] Kim CJ, Kovacs-Nolan JA, Yang C, Archbold T, Fan MZ, Mine Y. l-Tryptophan exhibits therapeutic function in a porcine model of dextran sodium sulfate (DSS)-induced colitis. The Journal of Nutritional Biochemistry 2010;21(6):468-75.

[124] Negaard A, Loberg EM, Naess PA, Eriksen M, Klow N-E. Feasibility of MRI in Experimentally Induced Inflammatory Small Bowel Disease: A Pilot Study in a Porcine Model. Digestive Diseases and Sciences 2010;55(1):14-20.

CHAPTER 2

HOPX+ INJURY-RESISTANT INTESTINAL STEM CELLS DRIVE EPITHELIAL RECOVERY AFTER SEVERE INTESTINAL ISCHEMIA

This article was published in the American Journal of Physiology: Gastrointestinal and Liver Physiology on November 1st, 2021.

Original citation: 10.1152/ajpgi.00165.2021

PMCID: PMC8616590

Preface: Co-authorship Contribution

As the second co-author to this manuscript, my contributions included conceptualizing the experimental design for Figures 3, 4, and 5. This involved developing the technique to isolate epithelial cells from recovering tissue for fluorescence activated cell sorting as well as the protocol to transfect crypt epithelial cells with adenovirus to express the short hairpin RNA and GFP reporter in order to silence *HOPX* expression. I managed the data collection for each of these experiments including imaging and measuring growth of enteroids in culture (Figures 3 and 4), counting enteroid bud units (Figure 3), and counting total and proliferating cells (Figure 5). I analyzed the bud count and cell number data for statistical analysis and collaborated with the statistician to analyze the enteroid area measurements. I drafted the figure legends, methods, and results sections pertaining to each of these figures, as well as revised the introduction and discussion sections and provided final approval for the published version. These contributions directly relate to the overall dissertation as they reveal the mechanistic role of HOPX in post-ischemic injured crypt epithelial cells.

Am J Physiol Gastrointest Liver Physiol 321: G588–G602, 2021.
First published September 22, 2021; doi:10.1152/ajpgi.00165.2021

american physiological society

AMERICAN JOURNAL OF PHYSIOLOGY
GASTROINTESTINAL AND LIVER PHYSIOLOGY

RESEARCH ARTICLE

HOPX$^+$ injury-resistant intestinal stem cells drive epithelial recovery after severe intestinal ischemia

Amy Stieler Stewart,[1] Cecilia Renee Schaaf,[1] Jennifer A. Luff,[1] John M. Freund,[1] Thomas C. Becker,[2] Sara R. Tufts,[1] James B. Robertson,[1] and Liara M. Gonzalez[1]

[1]*College of Veterinary Medicine, North Carolina State University, Raleigh, North Carolina and* [2]*Duke Molecular Physiology Institute and Sarah W. Stedman Nutrition and Metabolism Center, Duke University Medical Center, Durham, North Carolina*

Abstract

Intestinal ischemia is a life-threatening emergency with mortality rates of 50%–80% due to epithelial cell death and resultant barrier loss. Loss of the epithelial barrier occurs in conditions including intestinal volvulus and neonatal necrotizing enterocolitis. Survival depends on effective epithelial repair; crypt-based intestinal epithelial stem cells (ISCs) are the source of epithelial renewal in homeostasis and after injury. Two ISC populations have been described: *1*) active ISC [aISC; highly proliferative; leucine-rich-repeat-containing G protein-coupled receptor 5 (LGR5$^+$)-positive or sex-determining region Y-box 9 -antigen Ki67-positive (SOX9$^+$Ki67$^+$)] and *2*) reserve ISC [rISC; less proliferative; homeodomain-only protein X positive (HOPX$^+$)]. The contributions of these ISCs have been evaluated both in vivo and in vitro using a porcine model of mesenteric vascular occlusion to understand mechanisms that modulate ISC recovery responses following ischemic injury. In our previously published work, we observed that rISC conversion to an activated state was associated with decreased *HOPX* expression during in vitro recovery. In the present study, we wanted to evaluate the direct role of *HOPX* on cellular proliferation during recovery after injury. Our data demonstrated that during early in vivo recovery, injury-resistant HOPX$^+$ cells maintain quiescence. Subsequent early regeneration within the intestinal crypt occurs around 2 days after injury, a period in which HOPX expression decreased. When *HOPX* was silenced in vitro, cellular proliferation of injured cells was promoted during recovery. This suggests that HOPX may serve a functional role in ISC-mediated regeneration after injury and could be a target to control ISC proliferation.

NEW & NOTEWORTHY This paper supports that rISCs are resistant to ischemic injury and likely an important source of cellular renewal following near-complete epithelial loss. Furthermore, we have evidence that *HOPX* controls ISC activity state and may be a critical signaling pathway during ISC-mediated repair. Finally, we use multiple novel methods to evaluate ISCs in a translationally relevant large animal model of severe intestinal injury and provide evidence for the potential role of rISCs as therapeutic targets.

epithelial repair; HOPX; ischemia; large animal models; stem cell

INTRODUCTION

Intestinal ischemia is a life-threatening condition with mortality rates of >50% due to difficulties in early diagnosis, leading to delays in treatment and ultimate intestinal epithelial loss that results in sepsis and remote organ failure (1–4). The intestinal epithelium, made up of a single layer of cells, serves as a barrier to selectively allow for absorption of nutrients while playing a key role in the defense against intraluminal toxins and pathogens (5). Disruption of this barrier occurs during both intestinal ischemia and subsequent tissue reperfusion injury (6). As acute intestinal ischemia is rarely preventable, research efforts must be focused on the development of new therapeutics targeting the postischemic period (7) and more importantly, repair of the damaged mucosa and epithelial barrier. Intestinal epithelial stem cells (ISCs) are responsible for epithelial cell renewal during both homeostasis and after injury. Therefore, ISCs serve as a promising target to improve healing after intestinal injury (8–11).

Published literature supports two pools of intestinal crypt-based ISCs during homeostasis: *1*) an actively cycling population (aISC), identified by leucine-rich repeat-containing G protein-coupled receptor 5 (LGR5) gene expression (12) or sex-determining region Y-box 9 and antigen Ki67 (SOX9$^+$Ki67$^+$) protein coexpression (13) that are responsible for self-renewal and daily cellular turnover (13, 14) and *2*) a quiescent, slow cycling population (rISCs) that express HOPX (homeodomain-only protein homeobox), BMI1 (B-cell-specific moloney murine leukemia virus integration site-1), or TERT (telomerase reverse transcriptase) that can become activated after intestinal injury (15–18). The ISC compartment has been shown, in mouse models, to respond and to regenerate the intestinal epithelium following a variety of injuries including ionizing radiation, chemotherapeutics, and intestinal resection (19–

Correspondence: L. M. Gonzalez (Lmgonza4@ncsu.edu).
Submitted 12 May 2021 / Revised 11 August 2021 / Accepted 13 September 2021

22). More recent studies have highlighted plasticity within the crypt compartment and the ability of absorptive and secretory progenitor cells to revert to a stem-like state and also contribute to repair (23–26). At this time, the porcine models required to investigate crypt plasticity remain unavailable; however, as both progenitor cells and aISCs are lost following prolonged ischemic injury, it is likely that crypt regeneration depends on remaining rISCs (19). Despite this near complete epithelial loss after severe ischemia, we have previously shown that the small intestinal crypt compartment can regenerate in vivo by 3 days postinjury (DPI). In addition, $HOPX^+$ ISCs are injury resistant and the likely source of new epithelium (13). Our in vitro recovery of crypt epithelium postischemic injury, which included the $HOPX^+$ ISCs, further showed that resultant spheroids initially had increased *HOPX* gene expression and diminished growth when compared with uninjured cells (13). Subsequent increases in spheroid area corresponded to decreases in *HOPX* expression, suggesting that *HOPX* may serve as a functional, molecular switch to control proliferation of recovering ISCs.

HOPX, the smallest homeodomain protein, has been identified as a critical transcription factor in a variety of tissues (27). Direct modulation of *HOPX* expression has been shown to influence cellular proliferation and differentiation in several cell types including trophoblasts, keratinocytes, T cells, lung alveolar cells, and myocytes (28–32). In addition, *HOPX* has been labeled a tumor suppressor gene in multiple forms of cancer including both gastric and esophageal (33–35). In colorectal cancer, decreased *HOPX* expression has also been associated with increased cellular proliferation (36). These works highlight the influence of *HOPX* expression on cellular proliferation within numerous cell types. To date, HOPX has been frequently used as a rISC biomarker; however, its mechanistic role within these cells, particularly after severe ischemic injury, has yet to be evaluated.

In the present study, we utilized an established model of porcine mesenteric vascular occlusion (13, 37, 38) to evaluate epithelial recovery both in vivo and in vitro immediately following prolonged ischemic injury to both define how ISCs contribute to barrier repair and to understand ISC mechanisms that modulate the recovery response. Based on our previous work, we hypothesized that $HOPX^+$ ISCs contribute actively to the repair process and that peak activation of these cells occurs within 2 days after injury. In addition, we wanted to evaluate whether *HOPX* expression levels played a direct role on cellular proliferation during recovery after injury; we hypothesized that *HOPX* silencing would result in increased enteroid growth and cellular proliferation. Our results supported our hypothesis that peak ISC activation occurs by 2 days after injury and further demonstrated that *HOPX* silencing led to increased cellular proliferation during recovery after ischemic injury. This suggests that HOPX may serve a more functional role in regeneration after injury and may be a potential target to control proliferation.

MATERIALS AND METHODS

Experimental Animals

All animal studies were approved by the Institutional Animal Care and Use Committee (IACUC) of North Carolina State University. Yorkshire crossbred pigs (8- to 10-wk old) of either sex weighing between 15 and 25 kg were used.

Recombinant Adenovirus Construction and Generation

Adenoviral vectors engineered to coexpress a short hairpin RNA (shRNA) and enhanced green fluorescent protein (eGFP) reporter were created using gBlock Gene Fragments (IDT, Inc.) and the recently described Gateway-based (Invitrogen, Inc) pMVP system (39). In brief, gBlocks (IDT, Inc.) containing the human H1 RNA promoter, and one of two shRNA sequences (porcine *HOPX*-specific GGTCATTCCGATTCATAAA; NM_213792.2) or a scrambled control (Sc) sequence GCCTTACGACCAGTCGTATT), flanked by 5′ and 3′ *att*L1 and *att*R5 sequences, and plasmids containing the cytomegalovirus (CMV) promoter (*att*L5-CMV-*att*L4 plasmid IH401), the eGFP open reading frame (*att*R4-eGFP-*att*R3 plasmid IO001), and the human growth hormone polyadenylation signal (*att*L3-hGH-*att*L2 plasmid HB901) were recombined into the Gateway adenoviral acceptor plasmid pAd-PL-DEST, according to the manufacturer's instructions (Invitrogen, Inc.). The Gateway recombination reactions were transformed into *Escherichia coli* stbl3 cells (Gibco) and grown overnight at 37°C on LBcarb plates. Colonies were screened in a QuantStudio6 real-time PCR machine (ABI, Inc) using SYBR green primers specific for the H1 RNA promoter (oligos TB1025/TB1026), CMV promoter (TB1507/TB1508), eGFP (TB916/TB917), and Ad5 hexon (TB10145/TB1046). Positive clones were grown in 5 mL of LBcarb for 15 h at 37°C, 225 rpm. Clones were then sequenced with CMV forward oligo TB1013 (GeneWiz). To produce recombinant, replication-deficient adenoviruses, the recombinant adenovirus genomes containing either *HOPX*- or Sc-shRNA sequences were transfected into HEK293 cells (Invitrogen) for adenovirus generation and propagation (Ad-siHOPX and Ad-Sc). Cells were collected just before lysis in a small volume of media, pelleted, and lysed for an approximate viral titer of 10^{10} pfu/mL for both Ad-siHOPX and Ad-Sc.

Operative Technique and Tissue Collection

Before surgery, pigs were fasted for 16–18 h. General anesthesia was induced using xylazine (1.5 mg/kg im) and ketamine (11–20 mg/kg im). Orotracheal intubation was performed, and pigs were maintained under general anesthesia with isoflurane (2%–5%) vaporized in 100% O_2 until recovery. Before induction of intestinal ischemia, pigs were placed on heating pads and their temperature monitored. Lactated Ringer solution was administered intravenously through the auricular vein at a maintenance rate of 15 mL/kg/h. Anesthetic monitoring included pulse oximetry, electrocardiography, and indirect blood pressure measurements. Pigs were placed in dorsal recumbency and the abdomen was accessed through a 12-cm ventral midline incision centered at the umbilicus. The jejunum was identified 40 cm oral to the ileocecal junction. In terminal surgeries of ischemia without recovery, 10-cm-long loops of jejunum were delineated by circumferentially ligating the bowel with suture. Mesenteric vasculature to the loop was occluded by suture ligation for 3 and 4 h, and animals were subsequently euthanized. In animals recovered after ischemia, intestinal loops were atraumatically delineated using longitudinal

doyen intestinal forceps. The local mesenteric vasculature was clamped using Hopkin's bulldog clamps for 3 and 4 h after which time the clamps were removed. An additional segment was identified at the start of surgery to serve as an internal normal control. To decrease adhesion formation in recovery animals, carboxymethylcellulose (CMC) was instilled into the abdomen after clamp placement and again before closure (40, 41). After clamp removal was completed, an abdominal lavage was performed using sterile saline. The abdomen was then closed in three layers and animals were recovered for 1 (18–20 h), 2 (40–44 h), or 3 (66–70 h) days after injury (DPI). Postoperatively, pigs were maintained on a soft, canned food diet (Hills Pet Nutrition, Topeka, KS) and were administered intramuscular buprenorphine (0.02–0.05 mg/kg) every 8–12 h as needed for pain. Before being euthanized, animals were reanesthetized using xylazine and ketamine. After animals were euthanized with pentobarbital (85–100 mg/kg iv), intestinal tissue was immediately collected. Tissues were rinsed with 1X phosphate-buffered saline (PBS) and either opened longitudinally along the antimesenteric boarder for histomorphology or sectioned into smaller pieces for epithelial crypt dissociation and enteroid culture.

Tissue Histomorphometric Evaluation

For histomorphological analysis, tissue was fixed in 10% neutral buffered formalin, embedded in paraffin, and sectioned (~5–8 μm thickness). Slides were stained with hematoxylin and eosin to visualize tissue architecture. A small subset of slides at each time point after injury were examined unblinded by a boarded pathologist (JL) to define each time point of recovery and create an objective scoring system. The different categories and criteria for assessment are shown in Table 1. Slides were then blinded and evaluated by the pathologist. Peracute injury was defined by loss of surface epithelium and contracted villi, but relatively normal crypts characterized by well-differentiated epithelium with tall columnar cells, presence of brush border, basal polarity, rare mitotic figures, and presence of goblet cell differentiation (Fig. 1*A*). Acute injury was defined by loss of surface epithelium in >75% of the section, absent villi, and abnormal crypts characterized by crypt dilation, loss of crypt epithelium in >75% of the section with remaining cells vacuolated or attenuated, and <10% of crypt epithelium showing signs of early regeneration (Fig. 1*A*). Early regeneration was defined by loss of surface epithelium in >60% of the section, loss of villi, and early regenerative crypt epithelium characterized by cytoplasmic basophilia, cuboidal to low columnar epithelium, lack of basal polarity, ill-defined brush border, and prominent mitoses. In early regeneration, less than 10% of the crypt epithelium had characteristics of differentiation (Fig. 1*A*). Late regeneration was defined by an intact surface epithelium over 75% of the section, blunted to absent villi, and >75% of crypts lined by epithelium with characteristics of early to late differentiation. Differentiation within the crypt epithelium was characterized by crypt elongation, low to tall columnar epithelial cells, presence of brush border, restoration of basal polarity, and goblet cell differentiation (Fig. 1*A*).

Table 1. *Criteria for histological scoring of intestinal biopsies after ischemic injury*

					Evidence Regeneration Crypt Epithelium				Evidence Differentiation Crypt Epithelium		
Classification	Surface Epithelium (% covered)	Villi (Contracted/ Absent/Normal)	Percentage of Crypts Lined by Epithelium	Normal Crypts Epithelial Cells	Basophilic Cells	Loss Polarity	Cuboidal	Mitoses	Loss of Basophilia	Basal Polarity	Tall Columnar
Normal	90%–100%	Normal	95%–100%	Yes							
Peracute	<25%	Contracted	>75%	Yes							
Acute	<25%	Absent	<25%	No	No	No	No	No	No	No	No
Early regeneration	<40%	Absent	25%–80%	No	Yes	Yes	Yes	Prominent	No/rare	No/rare	No/rare
Late regeneration	>25%	Absent/blunted	>75%	No	No/rare	No/rare	No/rare	Rare	Yes	Yes	Yes

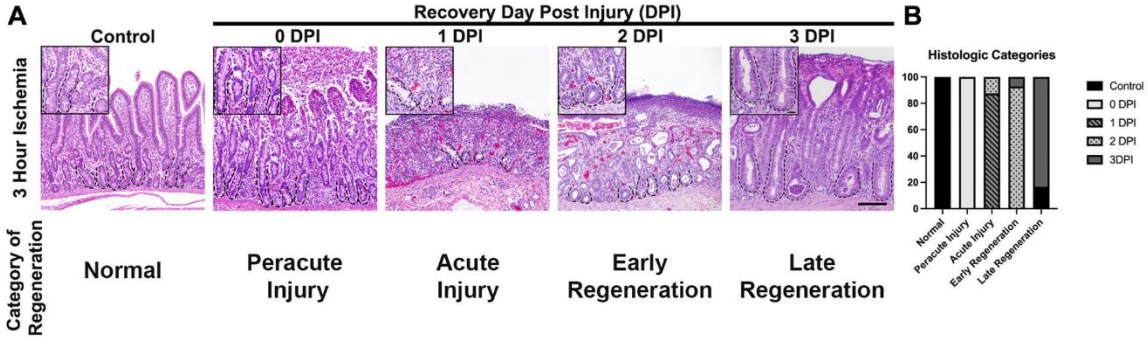

Figure 1. Histomorphometric analysis of recovering small intestine after 3 h of ischemic injury demonstrates that early epithelial regeneration begins 2 DPI. *A*: immediately after injury, there is significant surface epithelial loss and contraction of villi to their base (0 DPI). By 1 DPI, the villi are absent and there is loss of crypt epithelial cells. By 2 DPI, the crypts are lined by plump, cuboidal epithelial cells with prominent mitoses. Epithelial differentiation is seen by 3 DPI with tall columnar cells lining crypts, basal polarity, and evidence of crypt elongation. Scale bar *inset* 20 μm. Scale bar panel 100 μm. *B*: stack graph defining the histological categories of epithelial recovery and demonstrating that early regeneration occurs at 2 DPI; $n = 3–6$ pigs. DPI, days postinjury.

Fluorescent Multiplex Immunohistochemistry with Tyramide Signal Amplification

For immunofluorescence analysis, rinsed tissue was fixed in 4% paraformaldehyde (PFA) solution for 16–18 h at 4°C. The tissue was transferred to 30% sucrose solution for at least 24 h at 4°C, embedded in optimal cutting temperature (OCT) media, then frozen and subsequently sectioned at 5–8 μm thickness using a cryotome. Before being stained, sections were washed with PBS to remove OCT. When necessary, heat-induced epitope retrieval (HIER) was performed by placing slides into reveal decloaker solution (Biocare Medical, Concord, CA) for 30 s at 120°C and then 90°C for 10 s, in a pressure cooker. Tissue permeabilization was performed with PBS-0.3% Triton X-100. Antibodies were diluted in antibody diluent (SignalStain, Cell Signaling Technology, Danvers, MA), applied to tissue and incubated for 1 h at room temperature in a humidified chamber. Dilutions for functional antibodies were as follows: αß-catenin (mouse, 1:200, Cell Signaling Technology), αSOX9 (rabbit, 1:2,000, Chemicon/Millipore, Temecula, CA), αKi67 (mouse, 1:1,600, Dako, Santa Clara, CA), and αHOPX (rabbit, 1:500, Santa Cruz Biotechnology, Santa Cruz, CA). After incubation with the first antibody, slides were washed in TBS-T and boosted with a HRP Signal Stain Boost (host specific, rabbit or mouse) for 30 min. A specific fluorophore-conjugated tyramide signal amplification color reagent (Cyanine 3 for HOPX/SOX9, Fluorescein green (GFP) for Ki67, Cyanine 5 for β-catenin; PerkinElmer) was then applied for 10 min. To utilize multiple antibodies raised in the same host, slides were boiled in 10 mM sodium citrate buffer (SignalStain Citrate Unmasking Solution, Cell Signaling Technology), held at a subboiling temperature (95°) for 10 min and then cooled. After this stripping procedure, a different primary antibody and subsequent color reaction was applied. After all reactions, slides were counterstained with bisBenzimide H 33258 nuclear stain (1:1,000, Sigma-Aldrich, St. Louis, MO) and coverslipped (Hydromount; National Diagnostics). Background staining was negligible as determined by nonspecific IgG staining.

For each slide evaluated, well-oriented crypts were used to obtain cell counts. A well-oriented crypt was identified as one with a crypt base in close apposition to the muscularis mucosa and that extended and opened fully into the gut lumen. At least 10 well-oriented crypts for each protein biomarker were imaged, positive cells per crypt counted, and the results averaged for each time point (13, 20, 42).

Image Acquisition

Images were captured on an inverted fluorescence microscope (Olympus IX83, Tokyo, Japan) fitted with a monochrome digital camera (ORCA-flash 4.0, Hamamatsu, Japan) and color camera (DP26, Olympus). The objective lenses used were ×10, ×20, and ×40 with numerical apertures of 0.3, 0.45 and 0.6, respectively (LUC Plan FLN, Olympus).

Intestinal Epithelial Crypt Isolation, Adenovirus Transduction, and Culture

The excised jejunum was washed in cold phosphate-buffered saline solution (PBS) and opened longitudinally. Tissue was cut into small 0.5-cm pieces and incubated for 30 min in a 50-mL conical tube with PBS containing 30 mM ethylenediaminetetraacetic acid (EDTA), 10 mM Y-27632 (Selleck Chemicals, Houston, TX), 1 mM DTT (Sigma-Aldrich), 1X antibiotic-antimycotic (Life Technologies Corporation, Carlsbad, CA), and Primocin (InvivoGen, San Diego, CA). The conical tube was shaken every 5–10 min and kept on ice. Tissue pieces were transferred into a 37°C prewarmed PBS solution containing 30 mM EDTA and 10 mM Y-27632. The tissue was incubated in this solution at 37°C for 10 min and shaken to help mobilize the crypt/villi units. After this step, tissues were placed in ice-cold PBS wash and shaken for 1–2 min. Tissue was transferred into additional washes and shaken until crypt units were seen with minimal background debris. After the final washes, the remnant intestine was removed from the solution. Crypts were aliquoted into RNAse-free microtubes for viral transduction and culture.

Appropriate volumes of isolated crypts suspended in PBS from control (uninjured) and 3-h ischemic-injured pigs were separately pelleted by centrifugation (300 *g* for 5 min at 4°C) to achieve 50 crypts per 50-μL Matrigel (BD Bioscience, San Jose, CA). Similar to the previously described "mix and seed"

approach (43), crypt pellets were resuspended in the appropriate volume of ice-chilled Matrigel. Then either Ad-Sc or Ad-siHOPX virus, diluted 1:10 in 1% bovine serum albumin (BSA, Sigma-Aldrich) in PBS, was added to the suspended crypts at 500 multiplicities of infection (MOI) with gentle mixing. Matrigel containing crypts and virus was immediately plated on 24-well plates in 50-μL patties, allowed to set for 30 min at 37°C, then overlayed with 250 μL of Advanced DMEM/F12 containing the supplements 1X N-2 supplement (Life Technologies Corporation, Carlsbad, CA), 1X B-27 supplement minus vitamin A (Life Technologies Corporation), 1X Glutamax (Life Technologies Corporation), 100 mg/mL penicillin-streptomycin, and 1 mM HEPES buffer (Life Technologies Corporation). An additional 250 μL of WRN conditioned media [Wnt-3a (conditioned media, 50% final volume), R-spondin 3 (conditioned medium, 50% final volume), Noggin (conditioned media, 50% final volume)] was also added to each well. Conditioned media were produced from L-WRN cells derived by transfecting L-Wnt3A (ATCC CRL-2647) with an R-spondin 3 and noggin coexpressing vector. Stable clones were selected in medium containing G418 and Hygromycin B. Media were also supplemented with growth factors [50 ng/mL recombinant human EGF (Life Technologies Corporation), 10 mM nicotinamide (Sigma-Aldrich), 10 nM gastrin (Sigma-Aldrich), 10 mM Y-27632, 10 mM SB202190 (Sigma-Aldrich), 500 nM LY2157299 (Selleck Chemicals), and 2.5 μM glycogen synthase kinase 3 inhibitor (GSK3i, CHIR99021)]. Control and 3-h ischemic-injured crypts were also grown without virus and with 1% BSA to serve as negative and vehicle controls, respectively. Growth factors and fresh conditioned media were added 48 h after plating and subsequent 48-h intervals. Successfully transduced resultant spheroid/enteroids, conferred by GFP expression at 24 h in culture, were imaged daily out to 72 h for area measurements. A MOI of 500 resulted in 100% of plated crypts having at least one transduced cell (GFP^+, data not shown).

Epithelial Single-Cell Isolation

To isolate epithelial cells ($EpCAM^+$) and ensure collection of ISCs from tissue recovering 1–2 DPI, the entire mucosa was fully dissociated into a single-cell suspension for fluorescence-activated cell sorting (FACS) (44). Full-thickness sections from control and 3-h ischemic-injured jejunum with in vivo recovery were excised and cut into 2-cm square pieces. Each piece was washed in cold 1X Hank's balanced salt solution wash (HBSS without Ca and Mg, Gibco; 10 mM HEPES; and 0.47% sodium bicarbonate, Corning). For each piece, the serosa was dissected and the remaining mucosa minced, placed in predigest buffer (HBSS wash, 5 mM EDTA, 1.25% BSA, 1 mM DTT, and 10 mM Y-27632), and incubated for 10 min at 37°C, 250 rpm. Tissue pieces were filtered using a 110-μm mesh filter and the cellular filtrate collected. Tissue pieces were then rinsed in HBSS wash with 1.25% BSA, transferred to a gentleMACS C Tube (Miltenyi Biotec) with 0.78 WU Liberase TM (Millipore Sigma), 250 μg DNase (Roche), 3.6 U Dispase (Gibco), and R1.25 (RPMI 1640 + L-glutamine media (Gibco) with 1.25% BSA), and then incubated for 30 min, 37°C, 225 rpm for enzymatic digestion. Then, the C Tube containing tissue was mounted on a gentleMACs dissociator (Miltenyi Biotec) and preset program m_intestine_01 run for further mechanical dissociation. Resultant dissociated single cells were combined with collected cells from predigest A step, filtered, and red blood cells lysed by 1X RBC Lysis Buffer (Invitrogen). Single cells were suspended in flow buffer (PBS with 2% fetal bovine serum and 2 mM EDTA) and counted by trypan blue (Gibco) exclusion in a hemocytometer. Single cells were then incubated with α-CD 326 (EpCAM) (Biolegend, Cat. No. 118211, Alexa Fluor-647 conjugated; 1:200 per 10^6 cells in 100 μL flow buffer) for 15 min on ice. After being washed, cells were incubated with 7AAD live/dead stain (Novus) and FACS sorted on a Beckman Coulter MoFlo XDP for $EpCAM^+$ live single cells (45–47). $EpCAM^+$ single cells were collected in culture media for three-dimensional (3–D) culture. Approximately 15,000 cells per 50 μL Matrigel were plated on 24-well plates and overlaid with WRN conditioned media, as earlier described. Resultant spheroid/enteroids were imaged and counted daily out to 168 h for area measurements, plating efficiency, and ISC expansion potential (bud count) (48).

Spheroid/Enteroid Area Measurement

Spheroid/enteroid area measurement was obtained after image acquisition using the Freehand Polygon Selection Tool and Measurement Function (NIH ImageJ). Ten to twenty spheroids/enteroids per time point per animal were measured and averaged.

Spheroid/Enteroid Isolation, RNA Extraction, and cDNA Conversion

Adenovirus-transduced spheroids/enteroids were isolated from Matrigel using Corning Cell Recovery Solution (REF 354253), as per manufacturer's instructions at 24, 48, and 72 h postplating. Spheroids/enteroids were pelleted and snap frozen in liquid nitrogen and stored at −80°C. RNA was extracted using the Ambion PureLink RNA Mini Kit (Thermo Fisher Scientific). Yield and quality control of the extracts were determined by an Agilent 2100 BioAnalyzer performed by the North Carolina State University Genomic Sciences Laboratory Core using Agilent Eukaryote Total Pico Series II chips (Agilent Technologies, Santa Clara, CA). RNA was used if integrity score was >6 and RNA concentration >100 pg/μL. RNA (1 μg) was converted to cDNA using the iScript cDNA synthesis kit (Bio-Rad). Expression of *HOPX* was determined by quantitative real-time PCR (QuantStudio 6 Flex; Applied Biosystems) on cDNA samples using iTaq Universal SYBR green Supermix (Bio-Rad). The $\Delta\Delta C_t$ method was used to measure relative changes in gene expression. Samples were tested in triplicate.

Primer Sequences

Primer sequences are presented in Table 2. Additional primers, including HOPX, (GGAGGAGACCCAGAAATGGTT and TCTTGGTGGAAGGAAGCAGC) have been previously published (13).

Spheroid/Enteroid Whole Mount Immunofluorescence

Before fixation, spheroids were incubated with 5-ethynyl-2′-deoxyuridine (EdU Click-iT, Thermo Fisher Scientific) for 1 h before being fixated with 4% PFA. Briefly, spheroids were fixed in 4% PFA at room temperature for 30 min, washed in PBS, and incubated with 0.1% Triton X-100 at room temperature for 30 min to permeabilize. Cells were then incubated in

Table 2. *Primer sequences*

Pligo	Forward/Reverse	Target	Sequence
TB916	For	EGFP	TGACCCTGAAGTTCATCTGCACCA
TB917	Rev		TCTTGTAGTTGCCGTCGTCCTTGA
TB1025	For	H1 RNA promoter	TCATCAACCCGCTCCAAGGAAT
TB1026	Rev		CCCAGAACACATAGCGACATGCAA
TB1045	For	Ad5 Hexon	TTGGCGCATCCCATTCTCCAGTAA
TB1046	Rev		ATAAAGAAGGGTGGGCTCGTCCAT
TB1507	For	CMV promoter (proximal)	CCCACTTGGCAGTACATCAA
TB1508	Rev		CCAAGTAGGAAAGTCCCGTAAG
TB1013	For	CMV promoter	TTGGCTCATGTCCAATATGACCGC
TB1014	Rev		GGCGGGCCATTTACCGTAAGTTAT

5% BSA blocking medium at room temperature for 60 min. After a wash, the Click-iT EdU Imaging Kit (Thermo Fisher Scientific) was used to label proliferating cells. Briefly, the cells were incubated in the Click-iT reaction cocktail for 30 min at room temperature. After a 3% BSA wash, cells were stained with 1X Hoescht 33342 for 30 min. At least 15–20 spheroids were counted per pig and evaluated.

Statistics

In general, statistical analyses were performed using Prism 9.0.0 (GraphPad Software, La Jolla, CA) software, unless noted. Outliers were identified using the ROUT method. A Shapiro–Wilk normality test was performed on raw data. For simple comparisons, a Mann–Whitney test was performed. One-way ANOVA was used to evaluate normally distributed data. The Kruskal–Wallis test was performed when any data were either not normally distributed or when sample size was too small to determine normality. A two-way ANOVA was used to evaluate the impact of both animal and recovery time point on number of ISCs during immunofluorescent imaging and the number of buds resultant from single-cell culture. For analyses with significance detected, Tukey's test, Sidak's test, or Dunn's test were utilized for post hoc pairwise multiple comparisons. The α-level for statistical significance was defined as $P \leq 0.05$.

To examine the change over time for spheroid/enteroid area from both FACS-sorted EpCAM$^+$ single cells and the virus-transduced crypts, linear mixed models were fit. Model selection used Satterthwaite's method for degrees of freedom. The full model consisted of the $\log_{10}$-transformed area predicted by the fixed effects of time, treatment, and time squared. Two-way interactions were allowed. Pig was included as a blocking factor and a potential interaction with time. The random effect included was a random intercept for image within pig. After fit, residuals were examined for constant variance, and quantile-quantile plots were generated to check the normality of errors (R version 4.0.2 with lme4, lmerTest, and ggplot2 packages).

RESULTS

After Prolonged Ischemic Injury, Crypt-Based Epithelial Cells Recover, with the Earliest Signs of Histologic Regeneration Occurring 2 DPI

Previous studies from our laboratory have shown histological evidence of crypt disruption occurring at durations of acute ischemia beyond 3 h. This disruption is characterized by dramatic loss of both aISCs and transit-amplifying cells but preservation of the rISCs (13). However, the dynamics of crypt epithelial regeneration and the specific contributions of each ISC population to recovery remain unknown. To better define when epithelial regeneration is initiated after prolonged ischemic injury, we first established a histologic time course of recovery using a new scoring system. This system was developed based upon the expected observable histologic response of the intestinal mucosa following ischemic injury (49). Among these expectations, early regenerating crypt epithelium is characterized by epithelial cells with deeply basophilic cytoplasm, loss of regular basal nuclear polarity, low columnar to cuboidal shape with an ill-defined brush border, and high mitotic activity. After early regeneration, crypt epithelial cell differentiation begins, marked by the presence of goblet cells and tall columnar epithelial cells with basal orientation of nuclei and well-defined brush border. Based on our previous work, cell differentiation, crypt expansion, and evidence of epithelial restitution by 3 DPI (13, 37), we postulated that early epithelial regeneration and subsequent stem cell activation occurred on 1 or 2 DPI.

Histological analysis of ischemic (0 DPI) and recovering jejunum revealed that within the first day following the onset of ischemia (1 DPI), injury appeared to be ongoing, evidenced by severe crypt disruption, loss of crypt epithelial cells, and villous contraction followed by complete loss of villi (Fig. 1*A*). Surviving epithelial cells within the crypts appear flattened and attenuated with loss of the normal brush border. Signs of early epithelial regeneration including presence of plump, cuboidal, deeply basophilic epithelial cells with prominent cellular mitoses were first noted at 2 DPI. The consistency of these early regeneration histological markers at 2 DPI were confirmed by masked evaluation of recovering tissue sections (Fig. 1*B*). Similar to previous work, crypt expansion, epithelial differentiation, and epithelial restitution, signifying late regeneration, were present by 3 DPI. Once a time course of recovery was established and signs of early epithelial regeneration were identified before 3 DPI, we next wanted to investigate the contribution of ISCs to this early regeneration. Based on our previous work, we postulated that rISCs (HOPX$^+$) were likely responsible for this repair.

Intestinal Stem Cell Quiescence Dominates after Prolonged Ischemic Injury with a Shift to Cellular Proliferation Occurring between 1 and 3 DPI as HOPX$^+$ Cells Steadily Decrease

To investigate ISC population numbers in repair after severe ischemic injury, immunofluorescent protein biomarkers were

used to first identify recovering epithelial cells (B-catenin$^+$) and subsequently characterize them as aISCs (SOX9$^+$Ki67$^+$), rISCs (HOPX$^+$), and general proliferative cells (Ki67$^+$) (Fig. 2*A*). To first identify proliferating cells throughout recovery, total Ki67$^+$ cells per crypt were counted at 0–3 DPI (Fig. 2*B*). The overall number of proliferating cells significantly increased between 1 and 3 DPI (P = <0.0001), which correlated to the increased crypt expansion seen histologically (Fig. 1).

We have previously reported an initial loss of SOX9$^+$Ki67$^+$ aISCs due to apoptosis immediately after severe ischemic injury (13). Further investigation into the specific dynamics of aISC and rISC population numbers in recovery confirmed a decrease in aISC numbers at 0 DPI (P = 0.0046) (Fig. 2*C*). Numbers of aISCs began to recover at 1 DPI but remained significantly decreased compared with control (P = 0.014). In contrast, the relative number of HOPX$^+$ rISCs per intestinal crypt remained unchanged at 0 DPI and then significantly increased to reach a peak 1 DPI ($P \leq 0.0001$). A significant number of these cells were also colocalized with Ki67 at 1 and 2 DPI (Fig. 2*D*). Subsequently, as HOPX$^+$ cell number decreased at 2 DPI, the number of SOX9$^+$Ki67$^+$ cells within the recovering crypt increased, marking a shift in the ISCs contributing to repair.

To further examine epithelial regenerative capacity after injury, we next sought to isolate the epithelial cells that remained from 1 or 2 DPI mucosal tissue, likely enriched in rISCs or aISCs, respectively, to monitor their growth and proliferation potential in vitro. Traditional crypt isolation techniques were not successful in isolating epithelial cells from the actively recovering mucosa; therefore, tissues were chemically and mechanically digested into single cells, stained with a pan-epithelial marker (EpCAM) (44) and fluorescence-activated cell sorted (FACS) for culture.

Epithelial Cells Isolated from 2 DPI Demonstrate Superior Growth When Compared with Cells Isolated from Control and 1 DPI Tissue

Epithelial (EpCAM$^+$) cells were successfully isolated from both control and recovering tissue and grown in culture out to 168 h (Fig. 3, *A* and *B*). With a demonstrated loss of villus epithelium and aISCs following severe ischemic injury [Fig. 1*A*, (13)], the EpCAM$^+$ epithelial cells isolated from 1 DPI tissue were likely enriched in injury-resistant cells including

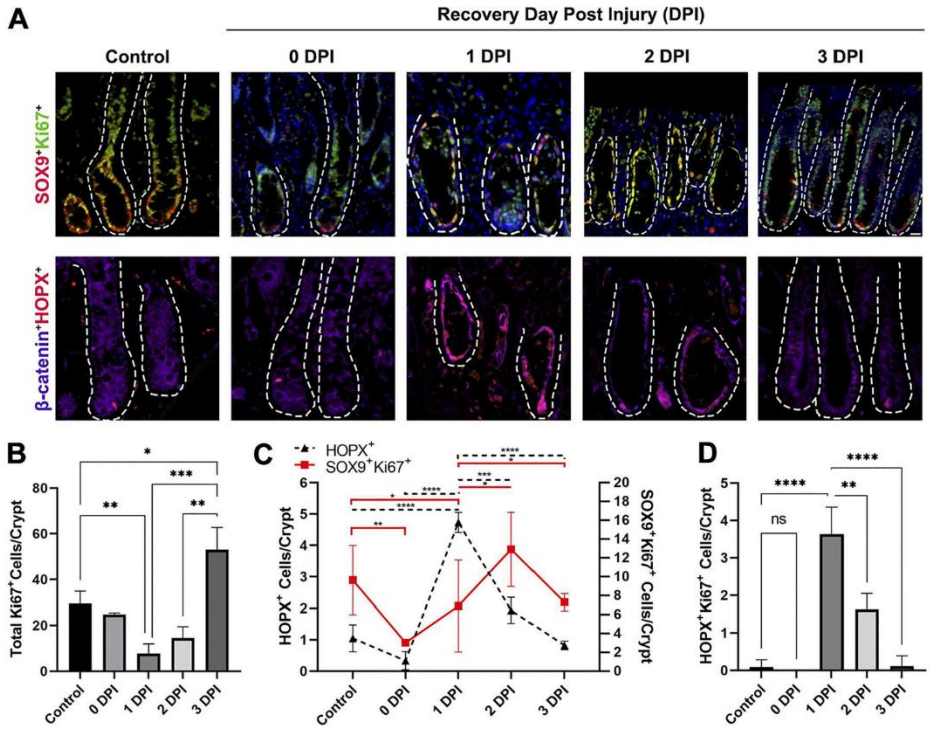

Figure 2. After severe ischemic injury, HOPX$^+$ cell numbers are initially enriched and begin to decrease as active intestinal epithelial stem cells (ISCs) recover and proliferate. *A*: immunofluorescent images of aISC (SOX9$^+$Ki67$^+$, yellow) and rISC (HOPX$^+$, red) cells after severe ischemic injury and during recovery. Epithelium marked by B-catenin (purple). Nuclei were stained with bisbenzimide H 33258 (blue). Dotted line outlines crypts extending down to the muscularis mucosa. Scale bar 20 μm. *B*: total number of proliferating cells (Ki67$^+$) decrease after ischemic injury and subsequent tissue reperfusion and begin to recover between 1 and 3 DPI. C: total number of active and reserve ISCs postinjury demonstrate that HOPX$^+$ rISCs are injury resistant and numbers are enriched after injury, whereas SOX9$^+$Ki67$^+$ aISCs are lost and recover between 1 and 2 DPI. *D*: HOPX$^+$ rISCs also colocalize with Ki67 at 1 and 2 DPI. Values are means ± SD. Analysis by two-way ANOVA with post hoc Tukey's test, *P < 0.05 **P < 0.01 ***P < 0.001 ****P < 0.0001, n = 3–5 pigs per recovery time point, 10 crypts were counted per animal per time point.

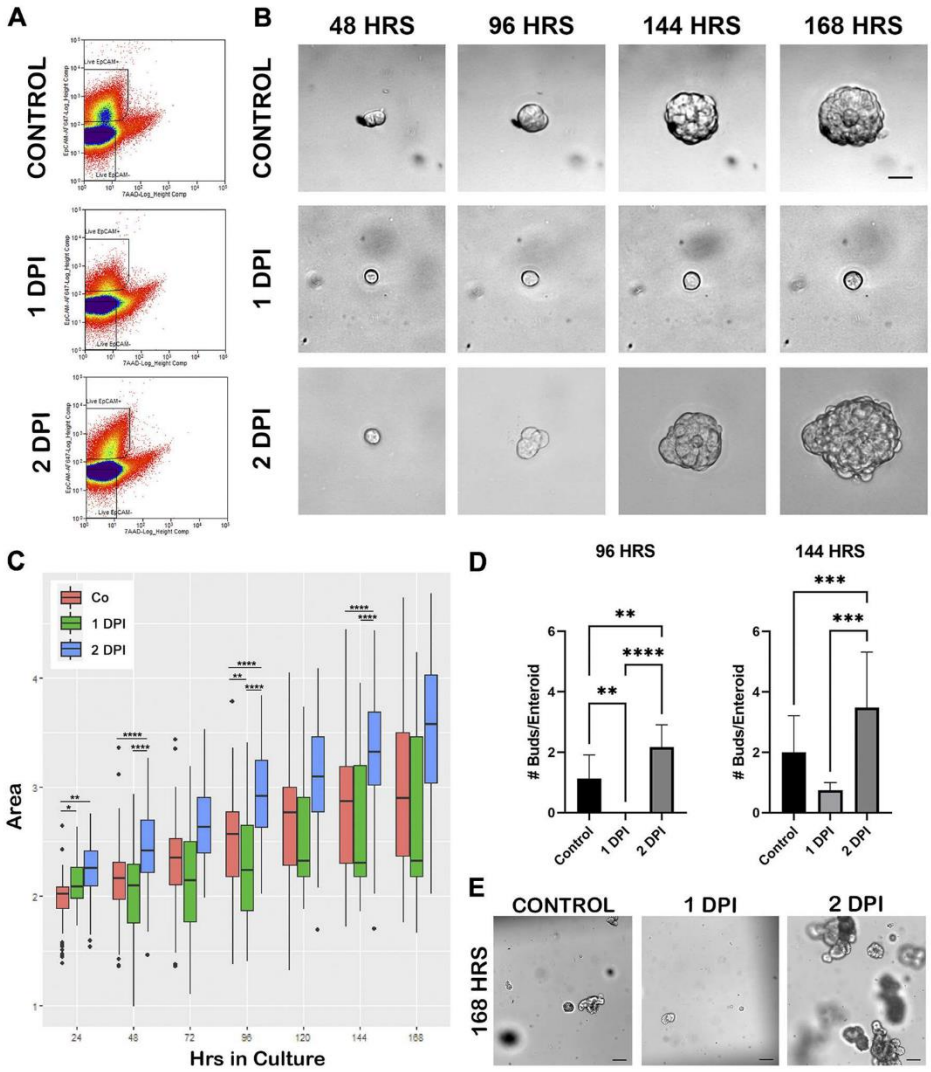

Figure 3. Two days postinjury (DPI) in vivo recovered epithelial cells grown in culture demonstrate increased size and proliferation compared with control and 1 DPI cells. *A*: representative gating strategy for FACS-sorted cells isolated from control, 1 DPI, and 2 DPI jejunum based on live/dead (7 AAD) and EpCAM-Alexa647. *B*: representative time course images of enteroid growth in culture from FACS-sorted EpCAM$^+$ cells from control, 1 DPI, and 2 DPI out to 168 h in culture. Scale bar 20 μm. *C*: box plots of log transformed daily enteroid area measurements from enteroids in *B*, showing increased growth of 2 DPI enteroids compared with control and 1 DPI, $n = 4$ pigs for each recovery day, 15,000 cells plated per 50 μL Matrigel, 15–20 enteroids measured per pig. *D*: means ± SD of bud counts per enteroid, showing significantly increased proliferative capacity for 2 DPI enteroids at 96 and 144 h in culture compared with control and 1 DPI. Analysis by two-way ANOVA with post hoc Tukey's test, $^{**}P < 0.01$, $^{***}P < 0.001$, $^{****}P < 0.0001$. Data collected from same enteroids in C. *E*: culture overview images at 168 h, demonstrating increased size and bud count for 2 DPI enteroids. Scale bar 100 μm. FACS, fluorescence-activated cell sorting.

rISCs (Fig. 2). Cells successfully plated from this group (1 DPI) grew 22.0% slower compared with control ($P = 0.00639$) supporting a quiescent phenotype, whereas overtime, cells isolated from 2 DPI grew 8.6% faster each day than control ($P = 0.000122$) suggesting increased proliferation at this time. To determine differences between groups at specific time points, the resultant spheroid and/or enteroid log-transformed areas were compared between recovery groups at 24, 48, 96, and 144 h in culture (Fig. 3*C*). Spheroids are the developmental structures that first form during culture before morphological evidence of more complex enteroid growth such as budding. Compared with uninjured control, spheroids from 1 DPI cells, while initially larger at 24 h ($P = 0.0102$, 51.9% larger), were no different at 48 h ($P = 0.1526$). At 96 h in culture, 1 DPI

spheroids/enteroids were significantly smaller than control (P = 0.005629, 41.9% smaller). In contrast, spheroids from 2 DPI cells demonstrated significantly increased size; they started larger than control at 24 h and continued to be significantly larger at 48, 96, and 144 h (P = 0.0026, 46.3% larger; $P < 0.0001$, 106.3% larger; $P = 6.411 \times 10^{-11}$, 159.8% larger; $P = 2.198 \times 10^{-8}$, 204.2% larger, respectively). Furthermore, spheroids/enteroids from 2 DPI cells were also significantly larger than those from 1 DPI at all time points including 48, 96, and 144 h ($P = 4.606 \times 10^{-9}$, $P = 8.058 \times 1\,0^{-11}$, and $P = 1.485 \times 10^{-6}$, respectively).

To further quantify enteroid proliferation, the number of bud units per enteroid were counted at 96 and 144 h in culture. Resultant enteroids grown from 2 DPI cells had significantly more buds per enteroid than both control (P = 0.004) and 1 DPI ($P < 0.0001$) at 96 h (Fig. 3, *D* and *E*). By 144 h, 2 DPI enteroids remained more proliferative with increased bud counts when compared with control (P = 0.0005) and 1 DPI (P = 0.0002). One DPI spheroid/enteroids remained small with few buds, suggesting both that signals for cellular activation and proliferation occur between 1 and 2 DPI and that these early cultures are enriched in quiescent rISCs. Despite the marked changes in bud count and area, there were no significant differences in growth efficiency throughout the 7 days (Supplemental Fig. S1, see https://figshare.com/articles/figure/Supplemental_Figure_1/15145038).

Our previous work demonstrated that resultant spheroid/enteroid cultures derived from 0 DPI ischemic-injured crypts had significantly higher levels of *HOPX* gene expression; this expression remained increased until 120 h. At that point, a decrease in *HOPX* gene expression correlated with a significant increase in spheroid size (13). In the current study, we both confirmed preservation of $HOPX^+$ cells at 0 DPI and demonstrated a relative increase in the numbers of $HOPX^+$ cells at 1 DPI (Fig. 2). The same 1 DPI cells plated in culture had decreased growth and proliferative potential (Fig. 3), similar to our previous in vitro recovery findings. However, by 2 DPI, $HOPX^+$ cell numbers decreased (Fig. 2), and growth in culture of 2 DPI cells was significantly increased (Fig. 3). Therefore, given the evidence that decreased HOPX gene and protein expression was associated with increased enteroid growth, we hypothesized that HOPX plays a functional role in the modulation of cellular proliferation. To investigate this hypothesis, an adenovirus coexpressing a HOPX-specific short hairpin RNA (shRNA) and an EGFP reporter (Ad-siHOPX) was developed and used to transduce isolated crypt epithelium.

Decreased HOPX Leads to Increased Spheroid Growth and Cellular Proliferation of Ischemic-Injured Epithelial Crypts

To validate that the adenoviral transduction resulted in silencing of *HOPX* gene expression, isolated control crypts were first transduced with either Ad-siHOPX or a control adenovirus coexpressing a scrambled shRNA and the EGFP reporter (Ad-Sc), as described. After transduction, resultant cultures were collected at 48 h for RNA isolation and qRT-PCR. *HOPX* gene expression was significantly decreased in cultures transduced with Ad-siHOPX when compared with Ad-Sc (P = 0.05, Fig. 4*A*). To determine the functional role of HOPX and assess whether silencing *HOPX* impacted the growth of ischemic-injured ISCs, crypts isolated immediately after 3 h of ischemic injury (3hrI) were transduced with either Ad-siHOPX or Ad-Sc. Successful transduction was confirmed by the presence of GFP-positive cells within plated crypts at 24 h (Fig. 4*B*). Area measurements of resultant spheroids in culture were performed every 24 h and the log-transformed values compared between groups (Fig. 4*C*). At 24 h, spheroids grown from 3hrI crypts transduced with the Ad-siHOPX were significantly larger than both Ad-Sc transduced (36% larger, P = 0.000461) and no virus spheroids (41.6% larger, P = 0.0000533); no virus spheroids were no different from Ad-Sc spheroids (P = 0.498305). At 48 h, Ad-siHOPX spheroids from 3hrI crypts remained larger than both Ad-Sc (29% larger, P = 0.00834) and no virus spheroids (43.9% larger, P = 0.000315); no virus spheroids remained no different from Ad-Sc at 48 h (P = 0.27073). At 72 h, Ad-siHOPX spheroids remained larger than the Ad-Sc group (P = 0.0206) but not the no virus control group (P = 0.2670).

To determine whether silencing *HOPX* impacted growth in homeostasis, uninjured control crypts were transduced with Ad-siHOPX and Ad-Sc and evaluated. No significant differences in resultant spheroid area were found between the groups at any time point (Fig. 4*D*). Although Ad-siHOPX transduction resulted in significant reduction of *HOPX* expression in uninjured control crypts (Fig. 4*A*), it is likely that aISC and progenitor cell activity present in all control crypt conditions mitigated any potential spheroid growth effects due to silencing *HOPX*. Conversely, ischemic injury leads to a loss of crypt-based aISC and progenitor cells. The remaining rISCs transduced with Ad-siHOPX lead to increased spheroid growth rate (Fig. 4*C*). These data suggest that HOPX is paramount during recovery after injury but not homeostasis.

Based on these results, we postulated that the increased spheroid area of previously injured and *HOPX*-silenced ISCs was due to increased cellular proliferation. To test this hypothesis, we performed whole mount staining of spheroids grown from 3hrI crypts for DAPI and EdU at 48 h in culture (Fig. 5). Ad-siHOPX spheroids had significantly more $DAPI^+$ cells compared with both Ad-Sc (P = 0.0013) and no virus controls (P = 0.0042), which confirmed that the increased spheroid area (Fig. 4*C*) was due to an increase in overall cellular number (Fig. 5*B*). Resultant Ad-siHOPX spheroids were more proliferative when compared with Ad-Sc with significantly more EdU^+ cells/spheroid (P = 0.0052, Fig. 5*C*). There was no difference in the number of EdU^+ cells/spheroid between Ad-siHOPX and no virus control (P = 0.2975). Despite an increased total number of EdU^+ cells in the Ad-siHOPX group when compared with Ad-Sc, there was no increase in the number of virus-infected, proliferative cells (GFP^+EdU^+) between groups (P = 0.333, Fig. 5*D*). It is likely that some of the EdU^+ cells seen within the Ad-siHOPX spheroids were replicating daughter cells resulting from the original transduction that would not express GFP. To assess the influence of overall size and total cell count on the number of EdU^+ cells/spheroid, the percentage of EdU^+ cells relative to the number of total $DAPI^+$ cells/spheroid was calculated and compared between groups (Fig. 5*E*). Ad-siHOPX spheroids had a higher percentage of EdU^+ cells/spheroid when compared with Ad-Sc (P = 0.0369). No virus spheroids

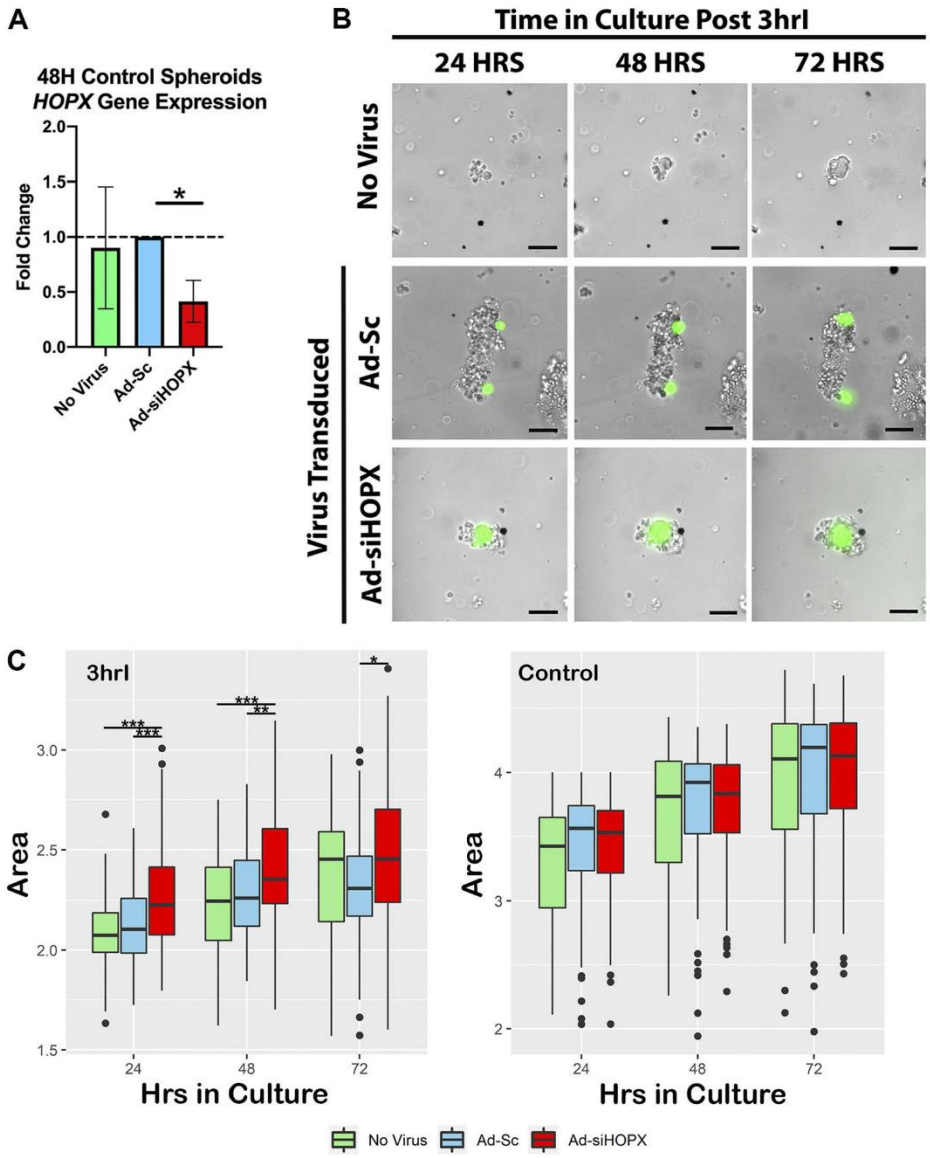

Figure 4. Ad-siHOPX silences *HOPX* in culture and leads to increased size of spheroids grown from 3-h ischemic-injured (3hrI) crypts. *A*: *HOPX* expression is significantly decreased in control crypts transduced with Ad-siHOPX compared with Ad-Sc at 48 h in culture. Fold changes were calculated relative to Ad-Sc samples and *GAPDH* as housekeeping gene. Statistics analyzed by two-way ANOVA with $*P = 0.05$, $n = 8$. *B*: representative images of spheroids at 24, 48, and 72 h in culture, grown from no virus, Ad-Sc, and Ad-siHOPX transduced 3hrI crypts. Transduction confirmed by GFP expression (green). Scale bar 20 μm. *C*: box plots of log transformed daily spheroid area measurements from no virus (green), Ad-Sc (blue), and Ad-siHOPX (red) transduced 3hrI and control crypts, $*P < 0.05$ $**P < 0.01$ $***P < 0.001$, $n = 5$ pigs, 15–20 spheroid/enteroids per condition measured.

had a significantly higher percentage of EdU^+ cells relative to DAPI when compared with Ad-Sc ($P = 0.0022$) but not the Ad-siHOPX group ($P = 0.2179$, Fig. 5*E*). Taken together, the data presented in Fig. 5 support that shRNA-mediated suppression of HOPX results in increased cellular proliferation as evidenced by an increased number of total $DAPI^+$ cells/spheroid and EdU^+ cells/spheroid when compared with the scrambled shRNA control.

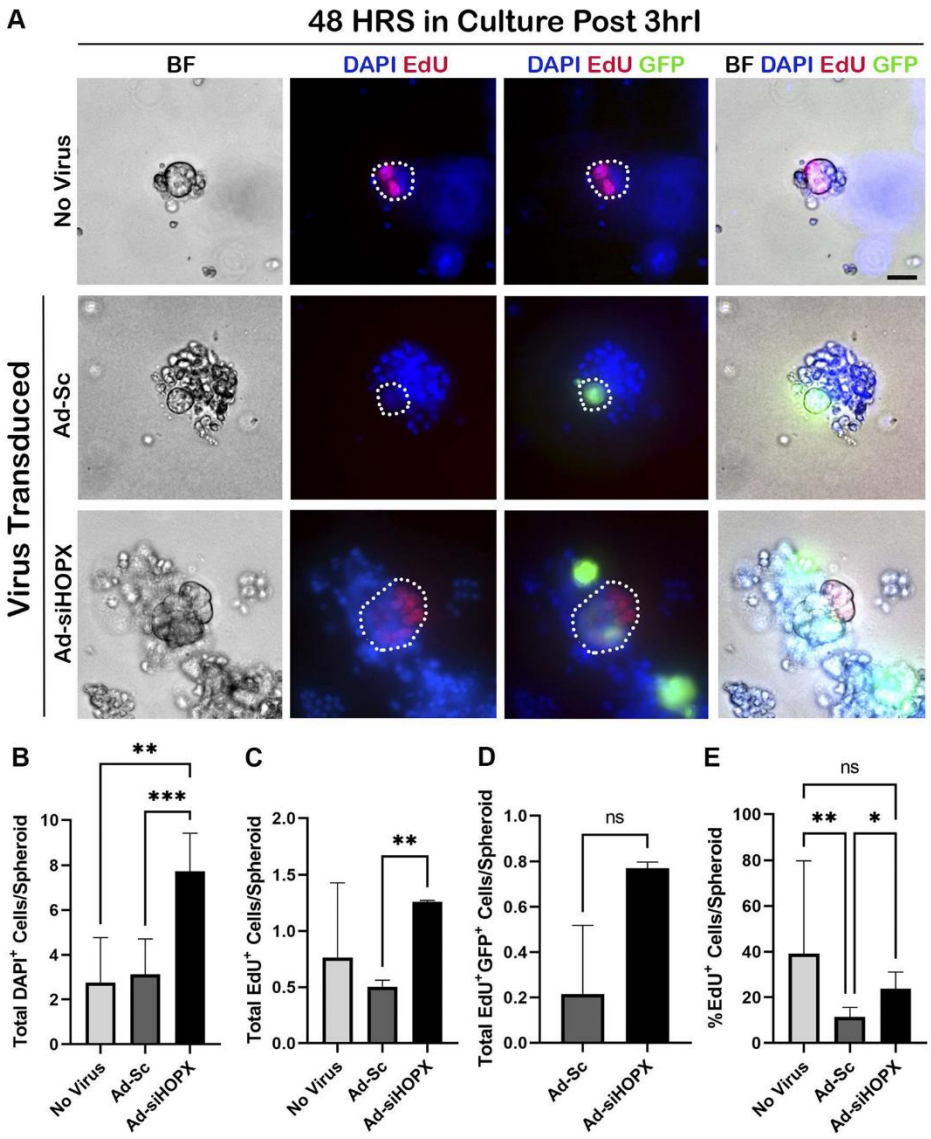

Figure 5. Silencing *HOPX* in 3-h ischemic injured (3hrl) crypt epithelium leads to increased overall cell and proliferating cell counts at 48 h in culture. *A*: representative bright field (BF) and immunofluorescent images of 48 h spheroids from no virus, Ad-Sc, and Ad-siHOPX-transduced 3hrl crypts. Proliferating cells were identified by EdU (red) and Ad-Sc and Ad-siHOPX cells identified by their GFP reporter (green). Nuclei were stained with Hoescht 33342 (blue). Scale bar 20 μm. *B*: means and standard deviations of total cell count per spheroid, showing significantly increased total cell counts for Ad-siHOPX compared with both Ad-Sc and no virus. *C*: means and standard deviations of total EdU^+ cell counts per spheroid, showing significantly increased EdU^+ cells in Ad-siHOPX compared with Ad-Sc. *D*: means and standard deviations of total EdU^+ GFP^+ colocalized cells per spheroid, showing no difference between Ad-siHOPX and Ad-Sc. No virus spheroids are not included as they did not contain a GFP reporter. *E*: means and standard deviations of the percentage of EdU^+ cells per total cells per spheroid, showing that with Ad-siHOPX leads to significantly increased percentage of proliferating cells. Analysis by two-way ANOVA with post hoc Tukey's test, $^*P < 0.05$ $^{**}P < 0.01$ $^{***}P < 0.001$, $n = 1$ or 2 pigs, 15–28 enteroids counted per pig.

DISCUSSION

After prolonged ischemic injury, the epithelium has a remarkable healing capacity with evidence of epithelial restitution and crypt expansion by 3 DPI (Fig. 1). The driving force behind this restitution and repair is the ISC compartment, composed of primarily injury-resistant $HOPX^+$ rISCs. Based on our data shown, $HOPX^+$ rISCs survive after severe

ischemia and are enriched within the surviving crypt as the remainder of the epithelium including $Ki67^+$ proliferating cells, $SOX9^+Ki67^+$ aISCs and early progenitors are lost (Fig. 2). As the intestine recovers, the population numbers of each ISC pool change, marked by a decrease in $HOPX^+$ rISCs and a subsequent rebound and increase in $SOX9^+Ki67^+$ cells. These cells are likely aISCs or early progenitor cells derived from the injury-resistant rISCs. More importantly, with this decline in crypt $HOPX^+$ cells, there is an increase in the number of $Ki67^+$ cells. These findings suggest a role of HOPX to serve as a switch to trigger cellular proliferation.

At this time, the inability to lineage trace porcine epithelial cells in vivo precludes investigations into the specific contributions of each ISC population during recovery. However, by utilizing FACS sorting, we were able to isolate and culture recovering $EpCAM^+$ epithelial cells from 1 and 2 DPI tissue. To the authors' knowledge, this is the first report of this technique in a porcine model of intestinal injury. When placed in culture, recovering $EpCAM^+$ cells were monitored for 7 days and provided further insight into the dynamics of ISC recovery. Surviving $EpCAM^+$ cells isolated from 1 DPI likely represent injury-resistant rISCs. As shown, cultured cells from this time point survive but grow significantly less than those from control or 2 DPI (Fig. 3). Furthermore, resultant 1 DPI spheroids remain small in culture with minimal growth and budding throughout the 7 days. These data suggest that at 1 DPI, signals within the intestinal crypt support quiescence and dormancy. Immunofluorescent data presented here also showed that in vivo at this time point, there appeared to be a relative increase in the number of HOPX protein-expressing cells (Fig. 2). Interestingly, many of those cells were also positive for the proliferation marker $Ki67^+$ yet remained less proliferative when isolated in culture, supporting that these cells may be noncycling or cycle arrested despite expressing Ki67 protein in immunofluorescence (50). Our previous work (13) also demonstrated that spheroids derived from crypts immediately after ischemic injury that were recovered in vitro had an overall decreased growth and increased levels of *HOPX* gene expression when compared with uninjured crypts. As *HOPX* expression decreased over time, the cultures began to grow and proliferate. These experiments support the hypothesis that HOPX serves a more functional role in ISC dynamics during recovery after injury than has been previously reported in the ISC literature.

It has been demonstrated that *HOPX* expression modulates cellular proliferation and differentiation in a variety of cell types (28–32, 51); direct upregulation of *HOPX* has also been shown to decrease cellular proliferation in several cancer cell lines including both esophageal squamous cell carcinoma and colorectal cancer (34, 36, 52, 53). Therefore, we utilized adenoviral transduction to directly influence the recovery of ischemic-injured intestinal crypts in culture by silencing *HOPX*. Successful transduction of injured crypts led to a significant increase in the growth and proliferation of resultant spheroids in culture (Figs. 4 and 5). This increase in size when compared with the scrambled virus and no virus control was significant up through 72 h further supporting a functional role of HOPX in the modulation of cellular proliferation during severe injury. Effects of the virus, while significant, were short lived, with no differences between groups after 72 h (data not shown). This is likely due to the high MOI used in our model to ensure efficient transduction of whole crypt epithelium. It has been shown that high adenoviral loads can influence cellular behavior in culture leading to growth retardation and apoptosis (54). This may have also contributed to the lack of significant difference between no virus and Ad-siHOPX observed in in vitro proliferation assays after 72 h in culture. In addition, it is possible that other cell types within close proximity to the intestinal stem cells, such as intraepithelial lymphocytes, could be isolated and inadvertently cultured during crypt dissociation thus influencing cellular behavior after a viral infection (55, 56). To minimize the potential impact of neighboring niche cells, future studies should focus on manipulating *HOPX* expression in isolated epithelial stem cells.

Currently, the mechanisms that control *HOPX* expression are not completely understood. It has been demonstrated that *HOPX* gene expression is likely controlled via methylation within the promoter region (36). Hypermethylation of the *HOPX* promoter results in loss of gene expression and increased cellular proliferation in a variety of body systems (53, 57–59). DNA methylation, a form of epigenetic change, can be influenced by a variety of factors including age, environment, lifestyle, and disease state (60). Interestingly, in hypoxic disease states including colorectal cancer, reactive oxygen species (ROS), and subsequent oxidative stress have been shown to influence epigenetic regulation and gene expression (61, 62). In diseases of ischemia-reperfusion injury where hypoxia-induced ROS production is known to impact tissue damage and recovery following intestinal ischemia-reperfusion injury (7, 63), ROS could also influence gene expression, including *HOPX*, within injury-resistant rISCs. Additional potential mechanisms to repress *HOPX* gene expression after ischemia-reperfusion injury include transcription factors. Cellular exposure to hypoxia, as occurs during ischemic injury, results in altered induction of transcription factors to regulate gene expression. Hypoxia-inducible factor (HIF) is a well-described adaptive mechanism by which hypoxia-induced stabilization of HIF then controls expression of cell survival and proliferation genes (64). Another recently described transcription factor in hypoxic injury is Repressor Element 1-Silencing Transcription (REST) factor, which regulates ~20% of hypoxia-repressed genes. By targeting downstream cell cycle and proliferation genes, REST could play a role in the regulation of *HOPX* (65). Finally, at the posttranscriptional level, endogenous intracellular mechanisms such as microRNAs play an important role in cellular resistance to injury. Hypoxia-regulated microRNAs have been shown to influence cellular differentiation, proliferation, death, and metabolism via translational repression and mRNA degradation in response to ischemic injury (66, 67). The mechanisms by which $HOPX^+$ injury-resistant rISCs become activated to proliferate would offer further insight into early epithelial repair after ischemic injury.

We have demonstrated the functional impact of HOPX expression on intestinal stem cells following a severe ischemic insult. High levels of *HOPX* expression correlated to a quiescent state with minimal growth during in vitro recovery (13), whereas silencing of *HOPX* led to improved growth and increased cellular proliferation (Figs. 4 and 5). Along with the in vivo data demonstrating an increased number of cells

positive for HOPX protein expression at 1 DPI (Fig. 2) and a subsequent quiescence of EpCAM$^+$ cells cultured from this time point (Fig. 3), it is likely that a switch occurs around 2 DPI that drives recovering ISCs to become active once again. This switch to proliferation is first demonstrated histologically at 2 DPI, as the earliest signs of epithelial regeneration occur consistently at this time point (Fig. 1). Decreased HOPX protein expression (Fig. 2) and increased growth of EpCAM$^+$ cells cultured at 2 DPI (Fig. 3) further support that additional signals are likely present within the recovering intestine at this time point that drive cellular proliferation and recovery after injury.

Intestinal epithelial stem cells are supported by a variety of other cells and both soluble and cell-associated growth factors crucial in homeostasis and during repair (68). The ISC niche contains subepithelial mesenchymal elements such as myofibroblasts and telocytes as well as hematopoietic cells including lymphocytes and macrophages (69). Niche cells are a known critical source of growth factors for ISCs including Wnt, which promotes epithelial proliferation (70, 71). Additional factors produced by neighboring cells such as T helper cell cytokines may also play a role in the modulation of ISC behavior (72). Future research will investigate the role of supporting factors that signal ISCs during repair with a specific focus on the modulation of cellular proliferation within HOPX$^+$ injury-resistant ISCs. Additional identification of intracellular pathways downstream of HOPX to signal ISC proliferation following intestinal ischemic injury may offer a unique approach to treat ischemic injury by promoting cellular proliferation and improving epithelial repair.

SUPPLEMENTAL DATA

Supplemental Fig. S1: https://figshare.com/articles/figure/Supplemental_Figure_1/15145038.

ACKNOWLEDGMENTS

The authors thank Dr. Elsa Ludwig for assistance in performing the porcine surgeries; Dr. Brittany Veerasammy, Dr. Caroline McKinney, Seth Kodikara, Mallory Thomas, and Nichol Henderson for assistance in data acquisition; NCSU-CVM Histology Lab for processing histologic samples and Javid Mohammed (NCSU-CVM Flow Cytometry Core) for patience and assistance with FACS in this project. In addition, we thank all of the technicians and laboratory animal veterinarians of North Carolina State Laboratory Animal Resources for assistance with animal care before, during, and after procedures, as well as for their dedication to this project.

GRANTS

This study was supported by National Institutes of Health Grants T32 OD011130 (to A. S. Stewart), K01 OD019911-01A1 (to L. M. Gonzalez), R03 OD026598-01 (to L. M. Gonzalez), and National Institute of Diabetes and Digestive and Kidney Diseases Grant P30 DK034987 (to L. M. Gonzalez).

DISCLOSURES

No conflicts of interest, financial or otherwise, are declared by the authors.

AUTHOR CONTRIBUTIONS

A.S.S., C.R.S., and L.M.G. conceived and designed research; A.S.S., C.R.S., J.M.F., T.C.B., S.R.T., and L.M.G. performed experiments; A.S.S., C.R.S., J.B.R., and L.M.G. analyzed data; A.S.S., C.R.S., J.A.L., and L.M.G. interpreted results of experiments; A.S.S., C.R.S., and J.A.L. prepared figures; A.S.S., C.R.S., and L.M.G. drafted manuscript; A.S.S., C.R.S., and L.M.G. edited and revised manuscript; A.S.S., C.R.S., J.A.L., J.M.F., T.C.B., S.R.T., J.B.R., and L.M.G. approved final version of manuscript.

REFERENCES

1. **Aliosmanoglu I, Gul M, Kapan M, Arikanoglu Z, Taskesen F, Basol O, Aldemir M.** Risk factors effecting mortality in acute mesenteric ischemia and mortality rates: a single center experience. *Int Surg* 98: 76–81, 2013. doi:10.9738/CC112.1.
2. **Bobadilla JL.** Mesenteric ischemia. *Surg Clin North Am* 93: 925–940, ix, 2013. doi:10.1016/j.suc.2013.04.002.
3. **Heys SD, Brittenden J, Crofts TJ.** Acute mesenteric ischaemia: the continuing difficulty in early diagnosis. *Postgrad Med J* 69: 48–51, 1993. doi:10.1136/pgmj.69.807.48.
4. **Park WM, Gloviczki P, Cherry KJ Jr, Hallett JW Jr, Bower TC, Panneton JM, Schleck C, Ilstrup D, Harmsen WS, Aa N.** Contemporary management of acute mesenteric ischemia: factors associated with survival. *J Vasc Surg* 35: 445–452, 2002. doi:10.1067/mva.2002.120373.
5. **Groschwitz KR, Hogan SP.** Intestinal barrier function: molecular regulation and disease pathogenesis. *J Allergy Clin Immunol* 124: 3–20, 2009. doi:10.1016/j.jaci.2009.05.038.
6. **Grootjans J, Lenaerts K, Derikx JP, Matthijsen RA, de Bruïne AP, van Bijnen AA, van Dam RM, Dejong CH, Buurman WA.** Human intestinal ischemia-reperfusion-induced inflammation characterized: experiences from a new translational model. *Am J Pathol* 176: 2283–2291, 2010. doi:10.2353/ajpath.2010.091069.
7. **Gonzalez LM, Moeser AJ, Blikslager AT.** Animal models of ischemia-reperfusion-induced intestinal injury: progress and promise for translational research. *Am J Physiol Gastrointest Liver Physiol* 308: G63–G75, 2015. doi:10.1152/ajpgi.00112.2013.
8. **Markel TA, Crisostomo PR, Lahm T, Novotny NM, Rescorla FJ, Tector J, Meldrum DR.** Stem cells as a potential future treatment of pediatric intestinal disorders. *J Pediatr Surg* 43: 1953–1963, 2008. doi:10.1016/j.jpedsurg.2008.06.019.
9. **Potten CS, Booth C, Pritchard DM.** The intestinal epithelial stem cell: the mucosal governor. *Int J Exp Pathol* 78: 219–243, 1997. doi:10.1046/j.1365-2613.1997.280362.x.
10. **Yui S, Nakamura T, Sato T, Nemoto Y, Mizutani T, Zheng X, Ichinose S, Nagaishi T, Okamoto R, Tsuchiya K, Clevers H, Watanabe M.** Functional engraftment of colon epithelium expanded in vitro from a single adult Lgr5(+) stem cell. *Nat Med* 18: 618–623, 2012. doi:10.1038/nm.2695.
11. **Fordham RP, Yui S, Hannan NR, Soendergaard C, Madgwick A, Schweiger PJ, Nielsen OH, Vallier L, Pedersen RA, Nakamura T, Watanabe M, Jensen KB.** Transplantation of expanded fetal intestinal progenitors contributes to colon regeneration after injury. *Cell stem cell* 13: 734–744, 2013. doi:10.1016/j.stem.2013.09.015.
12. **Sato T, Vries RG, Snippert HJ, van de Wetering M, Barker N, Stange DE, van Es JH, Abo A, Kujala P, Peters PJ, Clevers H.** Single Lgr5 stem cells build crypt-villus structures in vitro without a mesenchymal niche. *Nature* 459: 262–265, 2009. doi:10.1038/nature07935.
13. **Gonzalez LM, Stewart AS, Freund J, Kucera CR, Dekaney CM, Magness ST, Blikslager AT.** Preservation of reserve intestinal epithelial stem cells following severe ischemic injury. *Am J Physiol Gastrointest Liver Physiol* 316: G482–G494, 2019. doi:10.1152/ajpgi.00262.2018.
14. **Barker N, van Es JH, Kuipers J, Kujala P, van den Born M, Cozijnsen M, Haegebarth A, Korving J, Begthel H, Peters PJ, Clevers H.** Identification of stem cells in small intestine and colon by marker gene Lgr5. *Nature* 449: 1003–1007, 2007. doi:10.1038/nature06196.

15. **Takeda N**, **Jain R**, **LeBoeuf MR**, **Wang Q**, **Lu MM**, **Epstein JA.** Interconversion between intestinal stem cell populations in distinct niches. *Science* 334: 1420–1424, 2011. doi:10.1126/science.1213214.
16. **Henning SJ**, **von Furstenberg RJ.** GI stem cells - new insights into roles in physiology and pathophysiology. *J Physiol* 594: 4769–4779, 2016. doi:10.1113/JP271663.
17. **Richmond CA**, **Shah MS**, **Carlone DL**, **Breault DT.** An enduring role for quiescent stem cells. *Dev Dyn* 245: 718–726, 2016. doi:10.1002/dvdy.24416.
18. **Bankaitis ED**, **Ha A**, **Kuo CJ**, **Magness ST.** Reserve stem cells in intestinal homeostasis and injury. *Gastroenterology* 155: 1348–1361, 2018. doi:10.1053/j.gastro.2018.08.016.
19. **Van Landeghem L**, **Santoro MA**, **Krebs AE**, **Mah AT**, **Dehmer JJ**, **Gracz AD**, **Scull BP**, **McNaughton K**, **Magness ST**, **Lund PK.** Activation of two distinct Sox9-EGFP-expressing intestinal stem cell populations during crypt regeneration after irradiation. *Am J Physiol Gastrointest Liver Physiol* 302: G1111–G1132, 2012. doi:10.1152/ajpgi.00519.2011.
20. **Dekaney CM**, **Gulati AS**, **Garrison AP**, **Helmrath MA**, **Henning SJ.** Regeneration of intestinal stem/progenitor cells following doxorubicin treatment of mice. *Am J Physiol Gastrointest Liver Physiol* 297: G461–G470, 2009. doi:10.1152/ajpgi.90446.2008.
21. **Helmrath MA**, **Fong JJ**, **Dekaney CM**, **Henning SJ.** Rapid expansion of intestinal secretory lineages following a massive small bowel resection in mice. *Am J Physiol Gastrointest Liver Physiol* 292: G215–G222, 2007. doi:10.1152/ajpgi.00188.2006.
22. **Kim CK**, **Yang VW**, **Bialkowska AB.** The role of intestinal stem cells in epithelial regeneration following radiation-induced gut injury. *Curr Stem Cell Rep* 3: 320–332, 2017 [Erratum in *Curr Stem Cell Rep* 4: 95, 2018]. doi:10.1007/s40778-017-0103-7.
23. **Tetteh PW**, **Basak O**, **Farin HF**, **Wiebrands K**, **Kretzschmar K**, **Begthel H**, **van den Born M**, **Korving J**, **de Sauvage F**, **van Es JH**, **van Oudenaarden A**, **Clevers H.** Replacement of lost Lgr5-positive stem cells through plasticity of their enterocyte-lineage daughters. *Cell Stem Cell* 18: 203–213, 2016. doi:10.1016/j.stem.2016.01.001.
24. **Ayyaz A**, **Kumar S**, **Sangiorgi B**, **Ghoshal B**, **Gosio J**, **Ouladan S**, **Fink M**, **Barutcu S**, **Trcka D**, **Shen J**, **Chan K**, **Wrana JL**, **Gregorieff A.** Single-cell transcriptomes of the regenerating intestine reveal a revival stem cell. *Nature* 569: 121–125, 2019. doi:10.1038/s41586-019-1154-y.
25. **Murata K**, **Jadhav U**, **Madha S**, **van Es J**, **Dean J**, **Cavazza A**, **Wucherpfennig K**, **Michor F**, **Clevers H**, **Shivdasani RA.** Ascl2-dependent cell dedifferentiation drives regeneration of ablated intestinal stem cells. *Cell Stem Cell* 26: 377–390, 2020. e376. doi:10.1016/j.stem.2019.12.011.
26. **Rees WD**, **Tandun R**, **Yau E**, **Zachos NC**, **Steiner TS.** Regenerative intestinal stem cells induced by acute and chronic injury: the saving grace of the epithelium? *Front Cell Dev Biol* 8: 583919, 2020. doi:10.3389/fcell.2020.583919.
27. **Liu Y**, **Zhang W.** The role of HOPX in normal tissues and tumor progression. *Biosci Rep* 40, 2020. doi:10.1042/BSR20191953.
28. **Cheung WK**, **Zhao M**, **Liu Z**, **Stevens LE**, **Cao PD**, **Fang JE**, **Westbrook TF**, **Nguyen DX.** Control of alveolar differentiation by the lineage transcription factors GATA6 and HOPX inhibits lung adenocarcinoma metastasis. *Cancer Cell* 23: 725–738, 2013. doi:10.1016/j.ccr.2013.04.009.
29. **Asanoma K**, **Kato H**, **Yamaguchi S**, **Shin CH**, **Liu ZP**, **Kato K**, **Inoue T**, **Miyanari Y**, **Yoshikawa K**, **Sonoda K**, **Fukushima K**, **Wake N.** HOP/NECC1, a novel regulator of mouse trophoblast differentiation. *J Biol Chem* 282: 24065–24074, 2007. doi:10.1074/jbc.M701380200.
30. **Kee HJ**, **Kim JR**, **Nam KI**, **Park HY**, **Shin S**, **Kim JC**, **Shimono Y**, **Takahashi M**, **Jeong MH**, **Kim N**, **Kim KK**, **Kook H.** Enhancer of polycomb1, a novel homeodomain only protein-binding partner, induces skeletal muscle differentiation. *J Biol Chem* 282: 7700–7709, 2007. doi:10.1074/jbc.M611198200.
31. **Obarzanek-Fojt M**, **Favre B**, **Kypriotou M**, **Ryser S**, **Huber M**, **Hohl D.** Homeodomain-only protein HOP is a novel modulator of late differentiation in keratinocytes. *Eur J Cell Biol* 90: 279–290, 2011. doi:10.1016/j.ejcb.2010.11.001.
32. **Hawiger D**, **Wan YY**, **Eynon EE**, **Flavell RA.** The transcription cofactor Hopx is required for regulatory T cell function in dendritic cell-mediated peripheral T cell unresponsiveness. *Nat Immunol* 11: 962–968, 2010. doi:10.1038/ni.1929.
33. **Ooki A**, **Yamashita K**, **Kikuchi S**, **Sakuramoto S**, **Katada N**, **Kokubo K**, **Kobayashi H**, **Kim MS**, **Sidransky D**, **Watanabe M.** Potential utility of HOP homeobox gene promoter methylation as a marker of tumor aggressiveness in gastric cancer. *Oncogene* 29: 3263–3275, 2010. doi:10.1038/onc.2010.76.
34. **Yamashita K**, **Kim MS**, **Park HL**, **Tokumaru Y**, **Osada M**, **Inoue H**, **Mori M**, **Sidransky D.** HOP/OB1/NECC1 promoter DNA is frequently hypermethylated and involved in tumorigenic ability in esophageal squamous cell carcinoma. *Mol Cancer Res* 6: 31–41, 2008. doi:10.1158/1541-7786.MCR-07-0213.
35. **Yap LF**, **Lai SL**, **Patmanathan SN**, **Gokulan R**, **Robinson CM**, **White JB**, **Chai SJ**, **Rajadurai P**, **Prepageran N**, **Liew YT**, **Lopes V**, **Wei W**, **Hollows RJ**, **Murray PG**, **Lambert DW**, **Hunter KD**, **Paterson IC.** HOPX functions as a tumour suppressor in head and neck cancer. *Sci Rep* 6: 38758, 2016. doi:10.1038/srep38758.
36. **Katoh H**, **Yamashita K**, **Waraya M**, **Margalit O**, **Ooki A**, **Tamaki H**, **Sakagami H**, **Kokubo K**, **Sidransky D**, **Watanabe M.** Epigenetic silencing of HOPX promotes cancer progression in colorectal cancer. *Neoplasia* 14: 559–571, 2012. doi:10.1593/neo.12330.
37. **Blikslager AT**, **Rhoads JM**, **Bristol DG**, **Roberts MC**, **Argenzio RA.** Glutamine and transforming growth factor-alpha stimulate extracellular regulated kinases and enhance recovery of villous surface area in porcine ischemic-injured intestine. *Surgery* 125: 186–194, 1999.
38. **Stieler Stewart A**, **Freund JM**, **Blikslager AT**, **Gonzalez LM.** Intestinal stem cell isolation and culture in a porcine model of segmental small intestinal ischemia. *J Vis Exp* 135: 57647, 2018. doi:10.3791/57647.
39. **Haldeman JM**, **Conway AE**, **Arlotto ME**, **Slentz DH**, **Muoio DM**, **Becker TC**, **Newgard CB.** Creation of versatile cloning platforms for transgene expression and dCas9-based epigenome editing. *Nucleic Acids Res* 47: e23, 2019. doi:10.1093/nar/gky1286.
40. **Hay WP**, **Mueller PO**, **Harmon B**, **Amoroso L.** One percent sodium carboxymethylcellulose prevents experimentally induced abdominal adhesions in horses. *Vet Surg* 30: 223–227, 2001. doi:10.1053/jvet.2001.17849.
41. **Reijnen MM**, **Skrabut EM**, **Postma VA**, **Burns JW**, **van Goor H.** Polyanionic polysaccharides reduce intra-abdominal adhesion and abscess formation in a rat peritonitis model. *J Surg Res* 101: 248–253, 2001. doi:10.1006/jsre.2001.6288.
42. **Pereira-Fantini PM**, **Thomas SL**, **Wilson G**, **Taylor RG**, **Sourial M**, **Bines JE.** Short- and long-term effects of small bowel resection: a unique histological study in a piglet model of short bowel syndrome. *Histochem Cell Biol* 135: 195–202, 2011. doi:10.1007/s00418-011-0778-2.
43. **Wang N**, **Zhang H**, **Zhang B-Q**, **Liu W**, **Zhang Z**, **Qiao M**, **Zhang H**, **Deng F**, **Wu N**, **Chen X**, **Wen S**, **Zhang J**, **Liao Z**, **Zhang Q**, **Yan Z**, **Yin L**, **Ye J**, **Deng Y**, **Luu HH**, **Haydon RC**, **Liang H**, **He T-C.** Adenovirus-mediated efficient gene transfer into cultured three-dimensional organoids. *PloS One* 9: e93608, 2014. doi:10.1371/journal.pone.0093608.
44. **Gonzalez LM**, **Williamson I**, **Piedrahita JA**, **Blikslager AT**, **Magness ST.** Cell lineage identification and stem cell culture in a porcine model for the study of intestinal epithelial regeneration. *PloS One* 8: e66465, 2013. doi:10.1371/journal.pone.0066465.
45. **Yoshida S**, **Miwa H**, **Kawachi T**, **Kume S**, **Takahashi K.** Generation of intestinal organoids derived from human pluripotent stem cells for drug testing. *Sci Rep* 10: 5989, 2020. doi:10.1038/s41598-020-63151-z.
46. **Luo H**, **Zheng J**, **Chen Y**, **Wang T**, **Zhang Z**, **Shan Y**, **Xu J**, **Yue M**, **Fang W**, **Li X.** Utility Evaluation of porcine enteroids as PDCoV infection model in vitro. *Front Microbiol* 11: 821, 2020. doi:10.3389/fmicb.2020.00821.
47. **Gracz AD**, **Puthoff BJ**, **Magness ST.** Identification, isolation, and culture of intestinal epithelial stem cells from murine intestine. *Methods Mol Biol* 879: 89–107, 2012. doi:10.1007/978-1-61779-815-3_6.
48. **Fuller MK**, **Faulk DM**, **Sundaram N**, **Shroyer NF**, **Henning SJ**, **Helmrath MA.** Intestinal crypts reproducibly expand in culture. *J Surg Res* 178: 48–54, 2012. doi:10.1016/j.jss.2012.03.037.
49. **Uzal FA**, **Brandon P**, **Hostetter J.** Alimentary system; intestinal ischemia and infarction. In: *Jubb, Kennedy & Palmer's Pathology of Domestic Animals*, edited by Maxie MG. St. Louis, MO: Elsevier, 2016, p. 81–82.

50. **van Oijen MG**, **Medema RH**, **Slootweg PJ**, **Rijksen G.** Positivity of the proliferation marker Ki-67 in noncycling cells. *Am J Clin Pathol* 110: 24–31, 1998. doi:10.1093/ajcp/110.1.24.
51. **Ota C**, **Ng-Blichfeldt JP**, **Korfei M**, **Alsafadi HN**, **Lehmann M**, **Skronska-Wasek W**, **Mds M**, **Guenther A**, **Wagner DE**, **Königshoff M.** Dynamic expression of HOPX in alveolar epithelial cells reflects injury and repair during the progression of pulmonary fibrosis. *Sci Rep* 8: 12983, 2018. doi:10.1038/s41598-018-31214-x.
52. **Yamaguchi S**, **Asanoma K**, **Takao T**, **Kato K**, **Wake N.** Homeobox gene HOPX is epigenetically silenced in human uterine endometrial cancer and suppresses estrogen-stimulated proliferation of cancer cells by inhibiting serum response factor. *Int J Cancer* 124: 2577–2588, 2009. doi:10.1002/ijc.24217.
53. **Waraya M**, **Yamashita K**, **Katoh H**, **Ooki A**, **Kawamata H**, **Nishimiya H**, **Nakamura K**, **Ema A**, **Watanabe M.** Cancer specific promoter CpG Islands hypermethylation of HOP homeobox (HOPX) gene and its potential tumor suppressive role in pancreatic carcinogenesis. *BMC Cancer* 12: 397, 2012. doi:10.1186/1471-2407-12-397.
54. **Brand K**, **Klocke R**, **Possling A**, **Paul D**, **Strauss M.** Induction of apoptosis and G2/M arrest by infection with replication-deficient adenovirus at high multiplicity of infection. *Gene Ther* 6: 1054–1063, 1999. doi:10.1038/sj.gt.3300914.
55. **Rogoz A**, **Reis BS**, **Karssemeijer RA**, **Mucida D.** A 3-D enteroid-based model to study T-cell and epithelial cell interaction. *J Immunol Methods* 421: 89–95, 2015. doi:10.1016/j.jim.2015.03.014.
56. **Kawabata S**, **Boyaka PN**, **Coste M**, **Fujihashi K**, **Yamamoto M**, **McGhee JR**, **Kiyono H.** Intraepithelial lymphocytes from villus tip and crypt portions of the murine small intestine show distinct characteristics. *Gastroenterology* 115: 866–873, 1998. doi:10.1016/s0016-5085(98)70258-6.
57. **Ren X**, **Yang X**, **Cheng B**, **Chen X**, **Zhang T**, **He Q**, **Li B**, **Li Y**, **Tang X**, **Wen X**, **Zhong Q**, **Kang T**, **Zeng M**, **Liu N**, **Ma J.** HOPX hypermethylation promotes metastasis via activating SNAIL transcription in nasopharyngeal carcinoma. *Nat Commun* 8: 14053, 2017. doi:10.1038/ncomms14053.
58. **Kikuchi M**, **Katoh H**, **Waraya M**, **Tanaka Y**, **Ishii S**, **Tanaka T**, **Nishizawa N**, **Yokoi K**, **Minatani N**, **Ema A**, **Kosaka Y**, **Tanino H**, **Yamashita K**, **Watanabe M.** Epigenetic silencing of HOPX contributes to cancer aggressiveness in breast cancer. *Cancer Lett* 384: 70–78, 2017. doi:10.1016/j.canlet.2016.10.017.
59. **Rodrigues MF**, **Esteves CM**, **Xavier FC**, **Nunes FD.** Methylation status of homeobox genes in common human cancers. *Genomics* 108: 185–193, 2016. doi:10.1016/j.ygeno.2016.11.001.
60. **Rodríguez-Paredes M**, **Esteller M.** Cancer epigenetics reaches mainstream oncology. *Nat Med* 17: 330–339, 2011. doi:10.1038/nm.2305.
61. **Zhang R**, **Kang KA**, **Kim KC**, **Na SY**, **Chang WY**, **Kim GY**, **Kim HS**, **Hyun JW.** Oxidative stress causes epigenetic alteration of CDX1 expression in colorectal cancer cells. *Gene* 524: 214–219, 2013. doi:10.1016/j.gene.2013.04.024.
62. **García-Guede Á**, **Vera O**, **Ibáñez-de-Caceres I.** When oxidative stress meets epigenetics: implications in cancer development. *Antioxidants (Basel)* 9, 2020. doi:10.3390/antiox9060468.
63. **Sasaki M**, **Joh T.** Oxidative stress and ischemia-reperfusion injury in gastrointestinal tract and antioxidant, protective agents. *J Clin Biochem Nutr* 40: 1–12, 2007. doi:10.3164/jcbn.40.1.
64. **Benita Y**, **Kikuchi H**, **Smith AD**, **Zhang MQ**, **Chung DC**, **Xavier RJ.** An integrative genomics approach identifies hypoxia inducible factor-1 (HIF-1)-target genes that form the core response to hypoxia. *Nucleic Acids Res* 37: 4587–4602, 2009. doi:10.1093/nar/gkp425.
65. **Cavadas MA**, **Mesnieres M**, **Crifo B**, **Manresa MC**, **Selfridge AC**, **Keogh CE**, **Fabian Z**, **Scholz CC**, **Nolan KA**, **Rocha LM**, **Tambuwala MM**, **Brown S**, **Wdowicz A**, **Corbett D**, **Murphy KJ**, **Godson C**, **Cummins EP**, **Taylor CT**, **Cheong A.** REST is a hypoxia-responsive transcriptional repressor. *Sci Rep* 6: 31355, 2016. doi:10.1038/srep31355.
66. **Kulshreshtha R**, **Davuluri RV**, **Calin GA**, **Ivan M.** A microRNA component of the hypoxic response. *Cell Death Differ* 15: 667–671, 2008. doi:10.1038/sj.cdd.4402310.
67. **Liang H**, **Wang C**, **Gao K**, **Li J**, **Jia R.** MicroRNA-421 promotes the progression of non-small cell lung cancer by targeting HOPX and regulating the Wnt/β-catenin signaling pathway. *Mol Med Rep* 20: 151–161, 2019. doi:10.3892/mmr.2019.10226.
68. **Sailaja BS**, **He XC**, **Li L.** The regulatory niche of intestinal stem cells. *J Physiol* 594: 4827–4836, 2016. doi:10.1113/JP271931.
69. **Santos AJ**, **Lo YH**, **Mah AT**, **Kuo CJ.** The intestinal stem cell niche: homeostasis and adaptations. *Trends Cell Biol* 28: 1062–1078, 2018. doi:10.1016/j.tcb.2018.08.001.
70. **Kaestner KH.** The intestinal stem cell niche: a central role for Foxl1-expressing subepithelial telocytes. *Cell Mol Gastroenterol Hepatol* 8: 111–117, 2019. doi:10.1016/j.jcmgh.2019.04.001.
71. **Shoshkes-Carmel M**, **Wang YJ**, **Wangensteen KJ**, **Tóth B**, **Kondo A**, **Massassa EE**, **Itzkovitz S**, **Kaestner KH.** Subepithelial telocytes are an important source of Wnts that supports intestinal crypts. *Nature* 557: 242–246, 2018. doi:10.1038/s41586-018-0084-4.
72. **Biton M**, **Haber AL**, **Rogel N**, **Burgin G**, **Beyaz S**, **Schnell A**, **Ashenberg O**, **Su C**, **Smillie C**, **Shekhar K**, **Chen Z**, **Wu C**, **Ordovas-Montanes J**, **Alvarez D**, **Herbst RH**, **Zhang M**, **Tirosh I**, **Dionne D**, **Nguyen LT**, **Xifaras ME**, **Shalek AK**, **von Andrian UH**, **Graham DB**, **Rozenblatt-Rosen O**, **Shi HN**, **Kuchroo V**, **Yilmaz OH**, **Regev A**, **Xavier RJ.** T helper cell cytokines modulate intestinal stem cell renewal and differentiation. *Cell* 175: 1307–1320, 2018. doi:10.1016/j.cell.2018.10.008.

CHAPTER 3

LGR5-H2B-GFP PORCINE MODEL FOR THE STUDY OF STEM CELLS IN INTESTINAL DISEASE

ABSTRACT

Introduction: Intestinal epithelial stem cells (ISCs) are responsible for intestinal epithelial barrier renewal; thereby, ISCs play a critical role in intestinal pathophysiology research involving both homeostasis and repair. While reporter transgenic mouse models are available to identify the ISCs in research settings, a translational large animal model has yet to be established. This study validates the identification of ISCs (LGR5+) by a newly developed porcine Leucine Rich Repeat Containing G Protein-Coupled Receptor 5 (LGR5) reporter line.

Methods: We applied histology, immunofluorescence, fluorescent *in situ* hybridization, fluorescence activated cell (FACS) sorting, flow cytometry, gene expression quantification, and 3D organoid culture techniques to whole tissue and single cells from duodenum, jejunum, ileum, and colon of LGR5-H2B-GFP and wild type pigs. LGR5-H2B-GFP, healthy human, and murine biopsies of ileum and colon were compared by mRNA fluorescent *in situ* hybridization (FISH). Colonoids from LGR5-H2B-GFP pigs were edited by CRISPR/Cas9 to introduce *APC* gene mutation.

Results: Green fluorescent protein (GFP) expressing cells were identified within the crypt-base of all intestine sections and co-localized with known ISC biomarkers. LGR5-H2B-GFP^{hi} cells FACS sorted by GFP expression had significantly higher *LGR5* expression ($p<0.01$) and enteroid forming efficiency in culture ($p<0.0001$) compared to LGR5-H2B-GFP$^{med/lo/neg}$ cells. Use of FISH identified similar *LGR5, OLFM4, HOPX, LYZ* and *SOX9* expression between both human and LGR5-H2B-GFP pig crypt-base cells. Loss of *APC* in LGR5-H2B-GFP colonoids led to cystic growth in WNT/R-spondin depleted media with up-regulation of Wnt/β-catenin signaling targets.

Conclusions: LGR5^{+} ISCs are reproducibly isolated in LGR5-H2B-GFP pigs. The development of this transgenic pig represents significant progress in the study of ISCs and their function by

utilizing a large animal model that shares similar anatomy and physiology to humans, thus serving as an improved translational model of intestinal pathophysiology research.

INTRODUCTION

The intestine is a complex organ that serves to absorb nutrients while simultaneously prevent translocation of potentially harmful luminal contents into systemic circulation. In part, these complex intestinal functions are maintained by a constant renewal of the inner-most epithelial cell layer separating the systemic circulation and gastrointestinal contents. This constant epithelial regeneration is the sole responsibility of intestinal epithelial stem cells (ISCs), which reside deep in the intestinal crypt structures. Intestinal stem cells constantly divide asymmetrically to give rise to all intestinal epithelial cell lineages; [1, 2] they are also critical to epithelial repair following acute and chronic injury. [3-5] However, in the disease state of colorectal cancer (CRC), the second leading cause of U.S. cancer related deaths, [6] mutated ISCs play a more deleterious role by contributing to tumor development. [7-9] The most common initiating gene mutation that drives adenoma formation is in the tumor-suppressor, adenomatous polyposis coli (*APC*) gene. This *APC* mutation is present in over 80% of colorectal cancers. [10-13] Several groups have shown that mutation of *Apc* specifically in murine ISCs resulted in large adenoma formation. [7, 8, 14] Given the multifaceted role of ISCs, it is critical to be able to isolate and understand ISC dynamics in intestinal research. [8, 15, 16]

To effectively study ISCs, tools to identify this cell population are necessary. Multiple biomarkers for ISCs have been identified; [5, 17-22] one of the more widely known and used ISC-specific biomarkers is the transmembrane protein Leucine Rich Repeat Containing G Protein-Coupled Receptor 5 (Lgr5). [2, 23] While antibody-based techniques have had limited success in identifying the discrete $Lgr5^+$ ISC population, [23, 24] the development of Lgr5 transgenic reporter

mice in 2007 allowed for reliable *in vivo* identification of the $Lgr5^+$ stem cells for studies including ISC biology, repair, and tumorigenesis. [2, 8, 16, 25]

Although transgenic reporter mice are both a beneficial scientific tool and the current standard for ISC research, mice do not fully replicate human physiology, disease, or drug metabolism. [26-29] Therefore, there is increasing interest in non-rodent translational models to better replicate and study human gastrointestinal disease. For this purpose, pigs serve as a particularly useful animal model of human gastrointestinal pathophysiology. [30, 31] Pigs, like humans, are monogastric animals with similar intestinal anatomic features including ratio of intestinal length per kilogram of body weight and vascular structure. With an omnivorous diet similar to humans, pigs share numerous parallel physiologic characteristics including comparable metabolic processes, nutrient requirements, analogous mucosal barrier physiology, enteric microbiota, immune cell populations, and susceptibility to enteric pathogens. [32-36] These similarities between humans and pigs make the study of intestinal diseases including ischemia-reperfusion, necrotizing enterocolitis, acute and chronic inflammation, and short bowel syndrome better represented by a porcine model in basic science translational research. [4, 30, 31, 37-39] Such porcine models better replicate human disease and overcome some of the limitations of small rodent models.

Thus far, one disadvantage of porcine models has been the lack of a transgenic model specifically developed to study ISCs in both homeostasis and disease. To remedy this gap in ISC research, our group validated a newly developed transgenic porcine model, LGR5-H2B-GFP, as a novel means to identify $LGR5^+$ ISCs for both *in vivo* and *ex vivo* studies. Here, we defined the LGR5-H2B-GFP^{hi} cells within the intestinal epithelium as the $LGR5^+$ ISC population, thus validating the LGR5-H2B-GFP porcine model as the first of its kind. This will provide improved

ways to specifically study ISCs in a non-murine species with gastrointestinal physiology that more closely resembles humans. Furthermore, we demonstrated that *APC* disruption via CRISPR-Cas9 editing in LGR5-H2B-GFP colonoids led to cystic, clonal organoid growth with constitutive WNT pathway activation. This colonoid platform demonstrates the novel and translational utility of this ISC reporter porcine model for CRC. Overall, this novel porcine model provides critical advancement to the field of translational gastrointestinal research.

RESULTS

LGR5-H2B-GFP porcine model generation

The LGR5-H2B-GFP pig model was developed using CRISPR/Cas9 mediated gene knock-in to insert a fused GFP and histone 2B (H2B) transgene into one allele of the LGR5 locus, under the control of the *LGR5* promoter (Figure 1). [40] Thus, any cells that express LGR5 also produce intranuclear GFP, allowing for enhanced signal resolution in contrast to the cytoplasmic GFP produced in current mouse models.

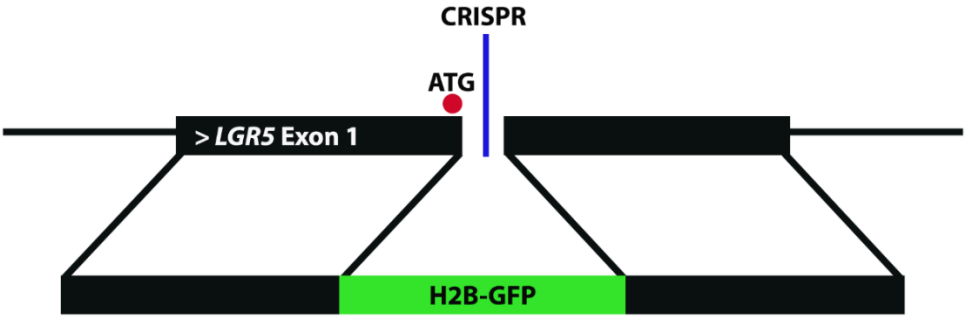

Figure 1. Transgenic approach for generating the LGR5-H2B-GFP pig. Schematic representation of the H2B-GFP insert into the targeted LGR5 locus via CRISPR/Cas9.

LGR5-H2B-GFP pigs exhibit normal intestinal architecture

To demonstrate normal intestinal architecture of LGR5-H2B-GFP transgenic pigs, histologic sections of duodenum, jejunum, ileum, and ascending colon were compared to wild type

control pigs (Figure 2A). LGR5-H2B-GFP pigs showed no differences in villus height or crypt depth compared to wild type animals (Figure 2B), suggesting there were likely no major intestinal mucosal architecture differences within the transgenic pigs. Next, we wanted to further define the specific location, phenotype, and function of LGR5-H2B-GFP^{hi} cells within the intestinal mucosal epithelium in order to show that they are consistent with known ISC identifying features in other species.

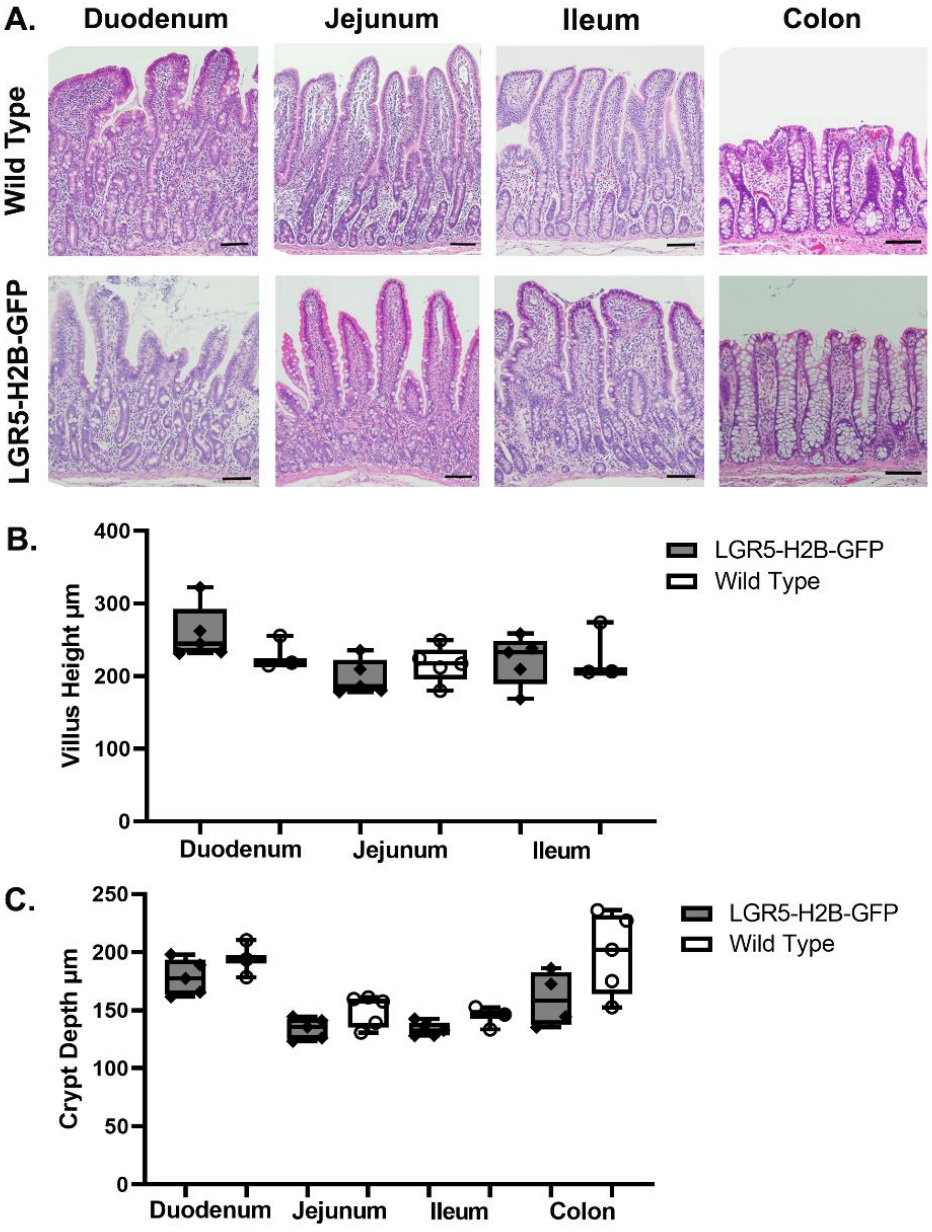

Figure 2. LGR5-H2B-GFP pig intestinal architecture does not differ from wild type pigs. ***A.*** Representative hematoxylin and eosin staining of duodenum, jejunum, ileum, and ascending colon from wild type and LGR5-H2B-GFP pigs. Scale bar 50 µm. ***B.*** Villus length and crypt depth measurements (µm) from wild type and LGR5-H2B-GFP pigs using ImageJ line tool (NIH). Statistical analysis by student's t-test for each intestinal segment revealed no significant differences in measurements between pigs ($p>0.05$); data points represent 3-5 pigs per section with 10 villi/crypt axis measured per pig. Images acquired on an IX83 inverted fluorescent microscope (Olympus) using DP26 color camera (Olympus), 10X objective (LIC Plan FLN; Olympus), and cellSens software (Olympus).

LGR5-H2B-GFP cells are crypt-base epithelial cells that co-express known ISC biomarkers

In the pig, small intestinal and colon crypt epithelial cell populations include ISCs, Paneth-like cells, and transit-amplifying cells. [41, 42] The ISCs and Paneth-like cells are positioned in an alternating fashion within the crypt-base. Transit-amplifying cells, progeny of the cycling ISCs, migrate up the crypt axis as they differentiate into mature intestinal epithelial cell populations. To define the location of LGR5-H2B-GFP$^+$ cells and determine if GFP$^+$ cell location was consistent with known ISC location based on previous literature, [14, 41] endogenous GFP expression in LGR5-H2B-GFP porcine intestine was analyzed using fluorescent microscopy (Figure 3A). Consistently, GFP positive cells localized to the crypt-base epithelium within all segments of intestine (Figure 3A). In jejunal and colon crypts, GFP fluorescent intensity normalized to DAPI was quantified for each nucleus starting at the crypt-base cell position 0 up to cell position 30 in the crypt neck. This quantification revealed a gradient of GFP expression. The brightest cells were noted at the crypt-base (cell position 0) and intensity decreased as cell position increased up the crypt axis (Figure 3B and C). These findings are expected given the construct of the model (Figure 1). [43] As crypt-base LGR5-H2B-GFP$^+$ ISCs divide to give rise to LGR5$^-$ transit-amplifying populations, intranuclear H2B-GFP is still present and its GFP signal intensity is diluted by half for each cell division of the daughter cells. Thus, loss of H2B-GFP signal can be used as a "clock" to examine cell lineage within the intestinal epithelium. While the majority of transit-amplifying daughter cells migrate upwards towards the villus tip during differentiation, a small subset is expected to move down towards cell position 0 as they develop into Paneth-like cells. [44] Therefore, quantification of fluorescence intensity from cell position 0 to 30 does not create a precise linear plot (Figures 3B and C). However, visualization of the highest intensity GFP

expression only within the crypt-base epithelium supported the conclusion that the LGR5-H2B-GFP positive cells are in the known location of ISCs.

Figure 3. GFP expressing cells are crypt base epithelial cells and GFP expression decreases in a gradient along the crypt axis. *A.* Representative images of endogenous GFP expression **(Figure 3 cont.)** (green) and bisbenzimide H 33342 (blue) within duodenum, jejunum, ileum, and spiral colon of LGR5-H2B-GFP pigs. Scale bar 100 µm, insets 50 µm. Images acquired on a Fluoview FV3000 upright confocal microscope (Olympus), 10X and 30X objectives, and cellSens software (Olympus). ***B and C.*** Means and standard deviations of GFP intensity normalized to bisbenzimide H 33342 intensity quantifications per cell nucleus within jejunum and colon crypts, with representative image of cell positions in jejunum and colon crypt; data points represent means and standard deviations from n=3-8 pigs with 3-5 crypts measured per pig. Images acquired as in *A.* Intensity measured using ImageJ measure tool (NIH). Scale bar 50 µm.

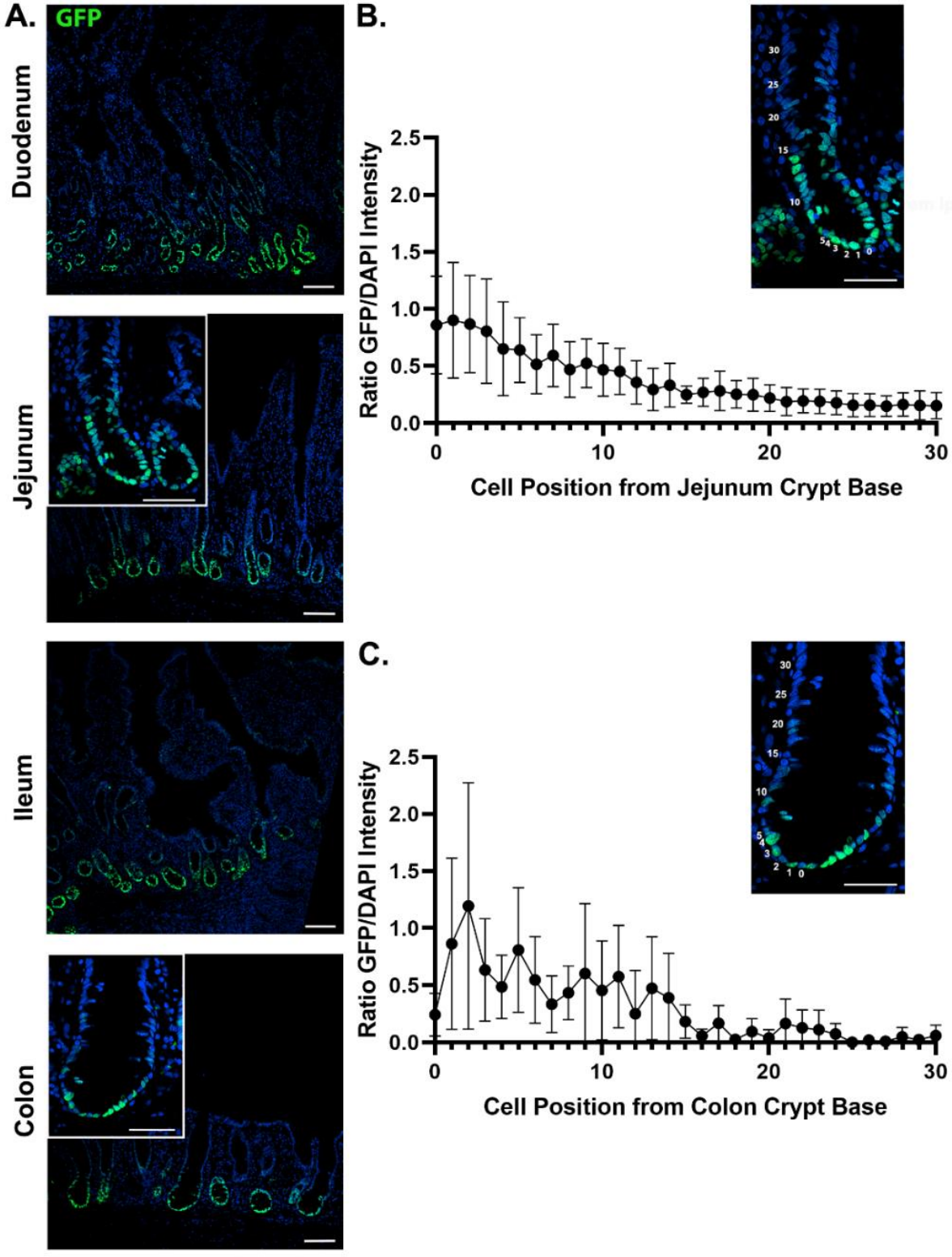
A.
GFP
Duodenum
Jejunum
Ileum
Colon
B.
Ratio GFP/DAPI Intensity
Cell Position from Jejunum Crypt Base
C.
Ratio GFP/DAPI Intensity
Cell Position from Colon Crypt Base

In the process of examining endogenous GFP expression by fluorescent microscopy, it became apparent that not every intestinal crypt-base expressed comparable levels of GFP (Figure 4A). As shown in the histologic image of endogenous GFP expression in the colon, clusters of adjacent crypts appeared negative for GFP (GFP^{dim}). The calculated percentage of GFP^{dim} crypts showed that the colon had the highest rate of mosaic crypts (29.78+/-6.58%) followed by duodenum, jejunum, and ileum (15+/-8.72%; 4.2+/14.03%; 0.8+/-1.79% respectively) (Figure 4B). To verify that GFP^{dim} crypts still expressed *LGR5*, fluorescent *in situ* hybridization using RNAscope technology was performed on sections of colon (Figure 4C). Overlay with α-GFP antibody demonstrated that all crypts expressed *LGR5*.

Despite the lack of GFP expression, GFP^{dim} colon crypts grew as expected in 3-D culture and developed into colonoids that remained GFP^{dim} (Figure 6D). These GFP^{dim} colonoids were individually isolated from culture and analyzed by flow cytometry to quantify GFP expression compared to GFP positive (GFP^{pos}) colonoids (Figure 4E). Rare GFP positive cells were still apparent in the GFP^{dim} colonoid population and mean fluorescence intensity was reduced compared to GFP^{pos} ($1.36x10^5$+/-$7.33x10^4$ and $1.71x10^6$+/-$6.29x10^5$, respectively). The same populations of colonoids were analyzed by qRT-PCR to further quantify *LGR5* and *GFP* expression (Figure 4F), which revealed that the GFP^{dim} colonoids, while no different in *LGR5* expression compared to GFP^{pos} colonoids, did have significantly reduced *GFP* expression (0.01633+/-0.0074; $p<0.0001$). Together, these findings suggest that monoallelic silencing or alternate splicing of the LGR5-H2B-GFP allele may be driving the differential GFP expression, and this variation is carried along with the process of crypt fission in the growing intestine to create the adjacent populations of GFP^{dim} crypts. [45, 46]

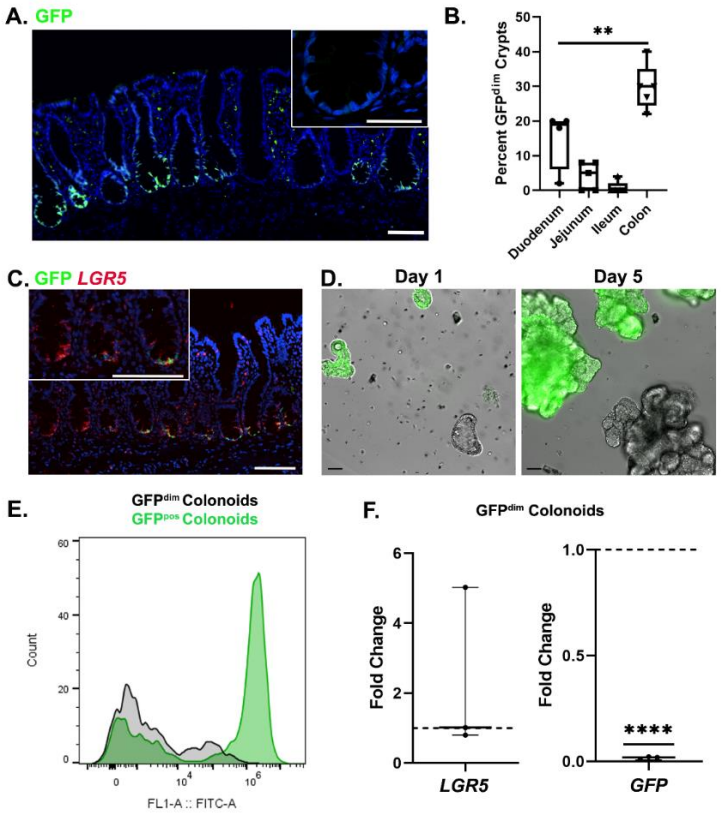

Figure 4. LGR5-H2B-GFP pigs exhibit mosaic expression of endogenous GFP between crypts. ***A.*** Representative colon histology showing both GFP^{pos} and GFP^{dim} crypts, adjacent to each other. Nuclei stained with bisbenzimide H 33342 (blue). Scale bar 100 µm, inset 50 µm. Images **(Figure 4 cont.)** acquired on both a Fluoview FV3000 upright confocal microscope (Olympus) using, 30x objective, and cellSens software (Olympus) and a IX83 inverted fluorescent microscope (Olympus) using monochrome digital camera (ORCA-flash 4.0, Hamamatsu), 10X objective (LIC Plan FLN; Olympus). ***B.*** Percentage of GFP^{dim} crypts counted in histologic slides from each segment of intestine; n=5 pigs; **p<0.01, two-way ANOVA with post-hoc Tukey's test. ***C.*** Colon histology of *LGR5* RNAscope probe (red) with GFP antibody (green) showing all crypts, GFP^{pos} and GFP^{dim}, express *LGR5* mRNA. Nuclei stained with bisbenzimide H 33342 (blue). Scale bars both 100 µm. Images acquired on a Fluoview FV3000 upright confocal microscope (Olympus), 10x objective, and cellSens software (Olympus). ***D.*** 3-D colon crypt culture of GFP^{dim} crypt on day one and day five in culture, demonstrating normal colonoid growth in culture. Images acquired on an IX83 inverted fluorescent microscope (Olympus) using monochrome digital camera (ORCA-flash 4.0, Hamamatsu), 20X objective (LIC Plan FLN; Olympus), and cellSens software (Olympus). Scale bar 50 µm. ***E.*** Representative flow cytometry histogram of GFP$^{pos/neg}$ populations from single live colonoid cells derived from GFP^{pos} (green) and GFP^{dim} (gray) colonoids after 7 days in culture, showing decreased GFP (FITC) expression in GFP^{dim} colonoids. ***F.*** qRT-PCR quantification of *LGR5* and *GFP* in isolated GFP^{dim} colonoids compared to GFP^{pos} colonoids after 7 days in culture. The $\Delta\Delta C_t$ method was used to measure relative fold change in gene expression compared with control (GFP^{pos} colonoids). Dotted horizontal line indicates control sample set = 1. *GAPDH* was used as the housekeeping gene. Samples were tested in triplicate; n=3 pigs; ****p<0.0001; statistical analysis by student's t-test.

To further characterize the LGR5-H2B-GFP positive cells and support their identity as ISCs, we examined the co-expression of GFP with previously validated porcine ISC protein biomarkers. Porcine research is somewhat limited by the availability of porcine-specific functional antibodies, thus, the antibody biomarkers Sex-determining region Y box 9 (SOX9) and proliferation marker Ki67 have been used in immunohistochemical analyses to identify ISCs. [4, 41] SOX9, a well-accepted biomarker of crypt-base cell populations, is not unique to the ISCs as Paneth cells and transit-amplifying cell populations also express the SOX9 protein. [47-49] Therefore, to identify the actively proliferating ISC phenotype with no porcine-specific antibodies available, co-localization of α-SOX9 with proliferation marker α-KI67 was necessary. [4] Immunofluorescent analysis of both jejunum and colon revealed that LGR5-H2B-GFP positive cells, identified by α-GFP antibody, co-localized with distinct cell populations of both $SOX9^+$ and $SOX9^+KI67^+$ cells within the crypt-base (Figure 5A). Cells that were $SOX9^+KI67^+$ were also GFP^+; these observations indicate that LGR5-H2B-GFP positive cells correlate with the previously identified porcine ISC pool.

The $SOX9^+Ki67^+GFP^+$ cells within the crypt-base were intercalated with $SOX9^+$ only cells – suspected to be the porcine Paneth-like cell population. [41, 42] To prove that these crypt-base GFP^-SOX9^+ cells were of the porcine Paneth-like cell phenotype distinct from the GFP^+ ISCs, additional co-localization with α-Ulex Europaeus Agglutinin I (UEA), a marker of Paneth cells, was performed. [50] Indeed, $\alpha\text{-}UEA^+$ cells were discrete GFP^- populations intercalated with the crypt-base GFP^+ cells (Figure 5B). This indicates that porcine Paneth-like cells are distinct from LGR5-H2B-GFP cells.

The co-localization of α-GFP and α-SOX9 within cells situated above the crypt-base stem cell zone (Figure 5A), along with the GFP intensity plot (Figure 3B and C), confirms that the

transit-amplifying cell population ($SOX9^{+}$) also carries some degree of GFP expression. Recognizing that the LGR5-H2B-GFP pig is a variation on lineage tracing given the expression of GFP in daughter progenitor cells, we hypothesized that the LGR5-H2B-GFP^{hi} cells are the ISCs. Therefore, we tested our hypothesis by evaluating these cells for their expression of ISC signature genes and ability to form enteroids from single cells.

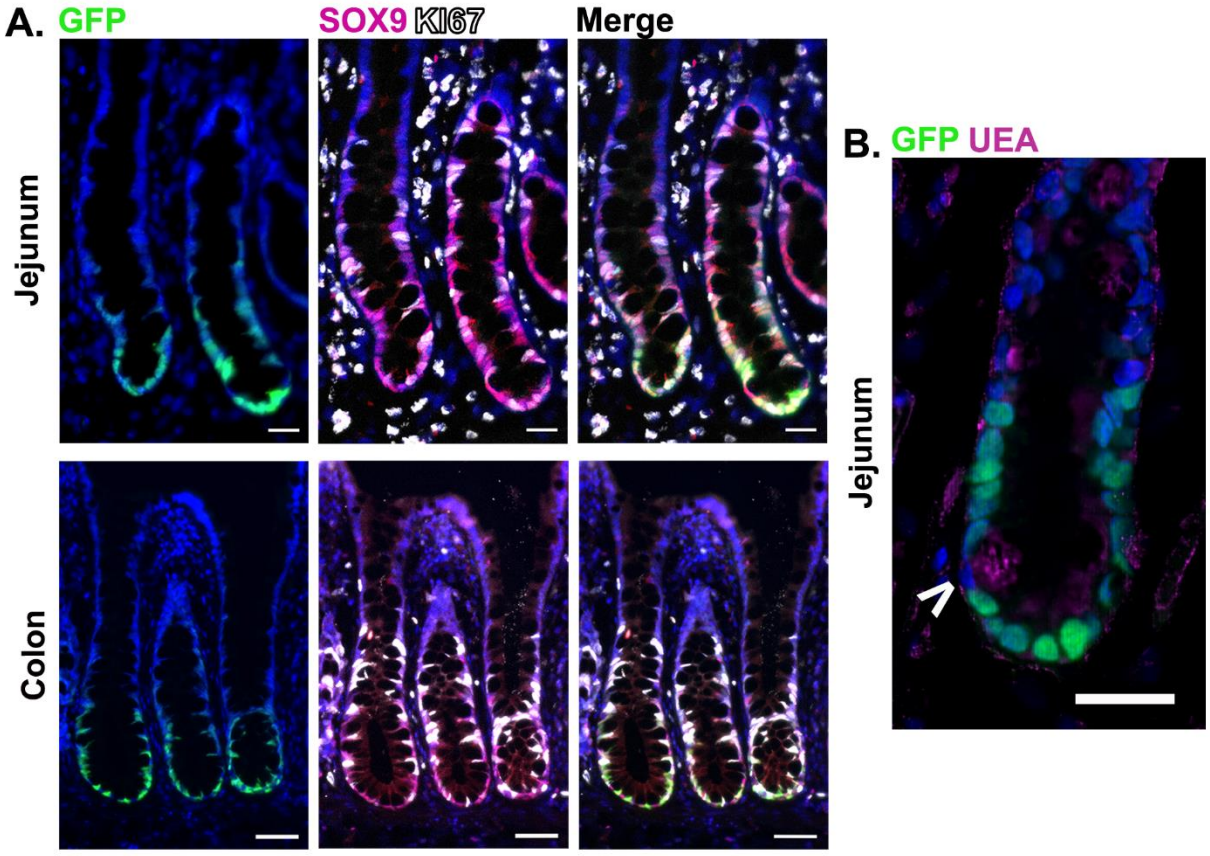

Figure 5. LGR5-H2B-GFP positive cells co-localize with ISC biomarkers and not Paneth-like cells. ***A.*** Immunofluorescent images of α-GFP^{+} cells (green), co-localized with two antibodies used to identify ISCs: α -Ki67 (white) and α -SOX9 (red) in jejunum and colon crypts. Nuclei were stained with bisbenzimide H 33342 (blue). Scale bar 20 µm. Images acquired on an IX83 inverted fluorescent microscope (Olympus) using monochrome digital camera (ORCA-flash 4.0, Hamamatsu), 40x objectives (LIC Plan FLN; Olympus), and cellSens software (Olympus). ***B.*** Immunofluorescent image of α -GFP^{+} cells (green), α -UEA^{+} (red) and bisbenzimide H 33342 (blue) in jejunum crypt. Arrow points to α-UEA^{+} α-GFP^{-} cell. Scale bar 20 µm. Image acquired on a Fluoview FV3000 upright confocal microscope (Olympus), 60X objective, and cellSens software (Olympus).

LGR5-H2B-GFP^{hi} cells are enriched in ISC gene biomarkers and exhibit increased growth potential of complex enteroids in culture

To show that LGR5-H2B-GFP^{hi} cells have both the enteroid-forming capacity characteristic of ISCs and enriched levels of ISC gene biomarker expression, jejunal epithelial cells were fluorescence activated cell (FACS) sorted into LGR5-H2B-GFP$^{hi/med/lo/neg}$ populations (Figure 6A). These populations were compared by quantitative real-time polymerase chain reaction (qRT-PCR) to measure known ISC biomarker gene expression. There are two described subgroups of ISCs, active and reserve, with the active population marked by *LGR5* and *OLFM4* expression. [2, 22, 51] The LGR5-H2B-GFP^{hi} cells had significantly increased expression of *LGR5* compared to LGR5-H2B-GFP$^{med/lo/neg}$ populations (9.74+/-5.25; 0.88+/-0.81; 0.34+/-0.21; 0.25+/-0.18; $p<0.01$) as well as *OLFM4* (15.06+/-11.2; 1.52+/-1.07; 0.48+/-0.34; 0.16+/-0.06; $p<0.05$) (Figure 6B).

Additionally, each FACS sorted LGR5-H2B-GFP population was cultured to assess enteroid growth potential. Jejunal LGR5-H2B-GFP^{hi} single cells sorted for 3-D culture grew into complex enteroids typical of porcine jejunum crypt culture. These enteroids exhibited classic budding of crypt-like structures with a central lumen by day 7 in culture (Figure 6C). Additionally, LGR5-H2B-GFP^{hi} cell cultures exhibited significantly higher percentage of enteroid growth efficiency compared to LGR5-H2B-GFP$^{med/lo/neg}$ populations (2.47+/-0.52; 0.2+/-0.1; 0.12+/-0.13; 0.16+/-0.28; $p<0.0001$) (Figure 6D). Furthermore, passaged enteroids from LGR5-H2B-GFP^{hi} sorted cells continued to proliferate in culture (3 passages performed) (Figure 6E). To demonstrate that enteroids derived from GFP^{hi} cells had the capacity to produce the post-mitotic intestinal epithelial cell types, we evaluated complex enteroids grown from LGR5-H2B-GFP^{hi} FACS sorted cells and confirmed gene biomarker expression by PCR (*LYZ*, *MUC2*, *CCK*, *ITF*, *CGA*, *SGLT-1*, and *FABP*; Figure 6F). [41, 52-54]

Figure 6. LGR5-H2B-GFP^{hi} cells are enriched for aISC genes and develop enteroids in culture. ***A.*** Representative flow sorting gating strategy to collect LGR5-H2B-GFP cells for gene expression and culture based on forward scatter (FSC), side scatter (SSC), live/dead marker **(Figure 6 cont.)** (Propidium Iodide/AutoF), and GFP expression. ***B.*** qRT-PCR analysis of active ISC gene biomarker expression in sorted LGR5-H2B-GFP $^{hi/med/lo/neg}$ cell populations. The $\Delta\Delta C_t$ method was used to measure relative fold change in gene expression compared with control (whole crypt epithelium). Dotted horizontal line indicates control sample set = 1. *GAPDH* was used as the housekeeping gene. Samples were tested in triplicate; data points represent 3 different pigs *p<0.05 **p<0.01, two-way ANOVA with post-hoc Tukey's test. ***C.*** Representative time course of growth of LGR-H2B-GFP^{hi} jejunum single cell in 3-D culture. Scale bar 20 µm. ***D.*** Percentage of LGR5-H2B-GFP$^{hi/med/lo/neg}$ single cells that developed into enteroids by day 10 in 3D culture; data points represent 3 different pigs, ***p<0.0001, two-way ANOVA with post-hoc Tukey's test. ***E.*** Representative image of LGR5-H2B-GFP^{hi} cells by third passaging, day 5 in 3-D culture; n=2 pigs. Scale bar 200 µm. All figure images acquired on an IX83 inverted fluorescent microscope (Olympus) using monochrome digital camera (ORCA-flash 4.0, Hamamatsu), 10X, 20X and 40X objectives (LIC Plan FLN; Olympus), and cellSens software (Olympus). ***F.*** Image of gel electrophoresis confirming presence of differentiated intestinal epithelial cell biomarker genes expressed within enteroids grown from LGR5-H2B-GFP^{hi} cells after 10 days in culture; n=3 pigs, 30-60 enteroids per pig. Image acquired using ChemiDoc-It 2.

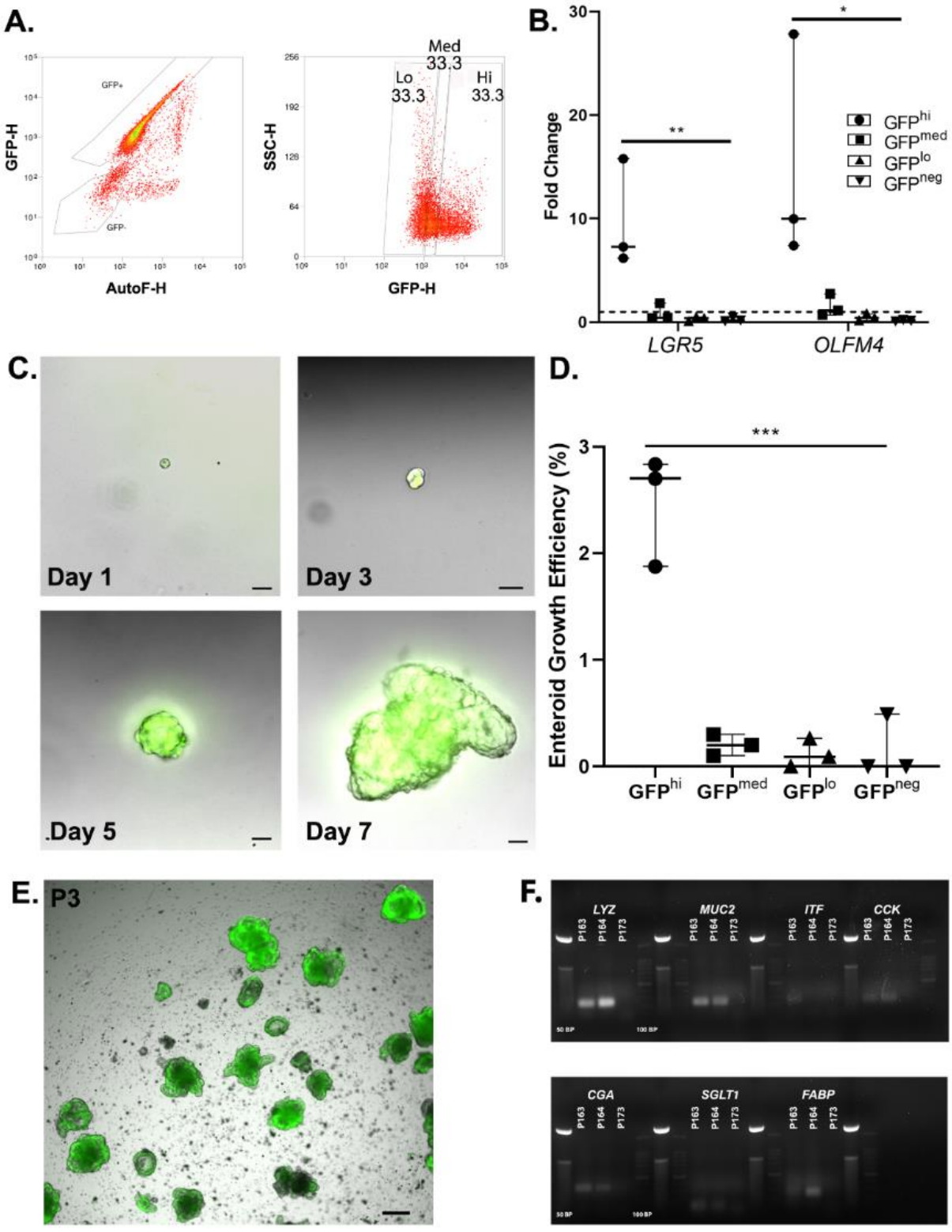
A.
GFP+
GFP-
GFP-H
AutoF-H
Med
33.3
Lo
33.3
Hi
33.3
SSC-H
GFP-H
B.
Fold Change
GFPhi
GFPmed
GFPlo
GFPneg
LGR5
OLFM4
C.
Day 1
Day 3
Day 5
Day 7
D.
Enteroid Growth Efficiency (%)
GFPhi
GFPmed
GFPlo
GFPneg
E.
P3
F.
LYZ
MUC2
ITF
CCK
CGA
SGLT1
FABP
P163
P164
P173

***In situ* comparison of crypt-base gene biomarkers shows similarities between pigs and humans that are not present in mice**

The LGR5-H2B-GFP pig has a large potential impact as an improved translational large animal model of human intestinal health and disease. To help further underscore the utility of this porcine model over traditional murine models, we used RNAscope fluorescent *in situ* hybridization (FISH) to compare key, crypt-base biomarker gene expression between LGR5-H2B-GFP pig, mouse, and human ileal and colonic biopsies. In ileum and colon for all species, *LGR5* expression was identified as expected within crypt-base cells (Figure 7).

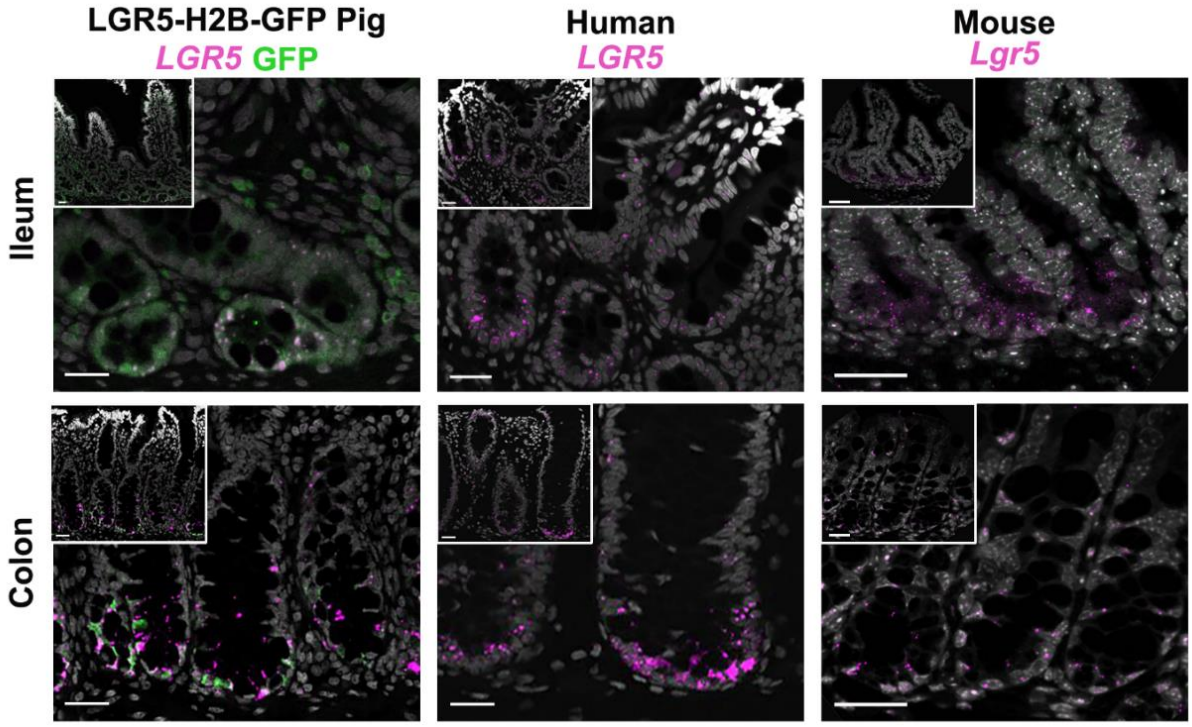

Figure 7. Crypt-base *LGR5* expression is similar between human and pigs. Representative histologic images from ileum and colon of healthy human donors, LGR5-H2B-GFP pigs, and mice with *LGR5* mRNA probe (magenta) and with α-GFP antibody (green). Nuclei stained with bisbenzimide H 33342 (gray). Scale bar 25 µm. Two to three animals/patients per species were analyzed. Images acquired on a Fluoview FV3000 upright confocal microscope (Olympus), 10X and 40X objective, and cellSens software (Olympus).

As previously noted, active ISCs have numerous biomarkers in addition to *LGR5*, including *OLFM4*. [51] In human samples of both small intestine and colon, *OLFM4* was previously shown by van der Flier et al. to overlap with *LGR5*, which was also demonstrated here (Figure 8A). Similar to humans, *OLFM4* was expressed both in small intestinal ISCs and in colonic ISCs of pigs (Figure 8A). This is in direct contrast to the mouse, in which *Olfm4* expression is restricted to small intestinal ISCs only (Figure 8A). [51] Separate from the actively cycling ISCs ($LGR5^+$ and $OLFM4^+$) are the quiescent, slower-cycling ISCs, also known as the "+4" position stem cell population. [55] While this population has a biomarker set once thought to be unique identifiers of "+4" ISCs, several studies have demonstrated that these markers, including *Hopx*, are also expressed in murine $Lgr5^+$ cells. [56, 57] Here, we again demonstrated the overlap of *Hopx* and *Lgr5* in mouse small intestinal and colonic ISCs (Figure 8B). Furthermore, both pig and human exhibited similar overlap in ISC expression of *LGR5* and *HOPX* within both small intestine and colon (Figure 8B).

The intestinal crypt-base contains other cell types in addition to ISCs, namely progenitor cells sitting just above ISCs and Paneth cells interspersed between ISCs. Common gene biomarkers for these cells include *SOX9* (Paneth, ISCs, and progenitor cells) and *LYZ* (Paneth cells). [47, 48, 58-60] Humans, mice, and pigs produce LYZ in the small intestine. [42, 58] However, while humans are known to express *LYZ* in the colon, rodents do not. [58] In the pig, colonic *in situ LYZ* expression has yet to be defined. Here, we demonstrated *LYZ* expression in human, pig, and mouse ileum and colon. In direct contrast to the mouse, both human and pig colon crypt-bases contained LYZ^+ cells (Figure 9). When we identified $SOX9^+$ cells between species, as expected, *SOX9* overlapped with $LGR5^+$ and LYZ^+ crypt-base cells, indicating both ISC and Paneth cell populations, respectively (Figure 9). [47, 48, 59, 60] In the human and pig transit-

amplifying/progenitor cell region, *SOX9*+ cells were also positive for *LGR5* and *LYZ*. This phenomenon was not appreciated in the murine tissues, where *LYZ* was restricted to the crypt-base small intestinal cells only (Figure 9).

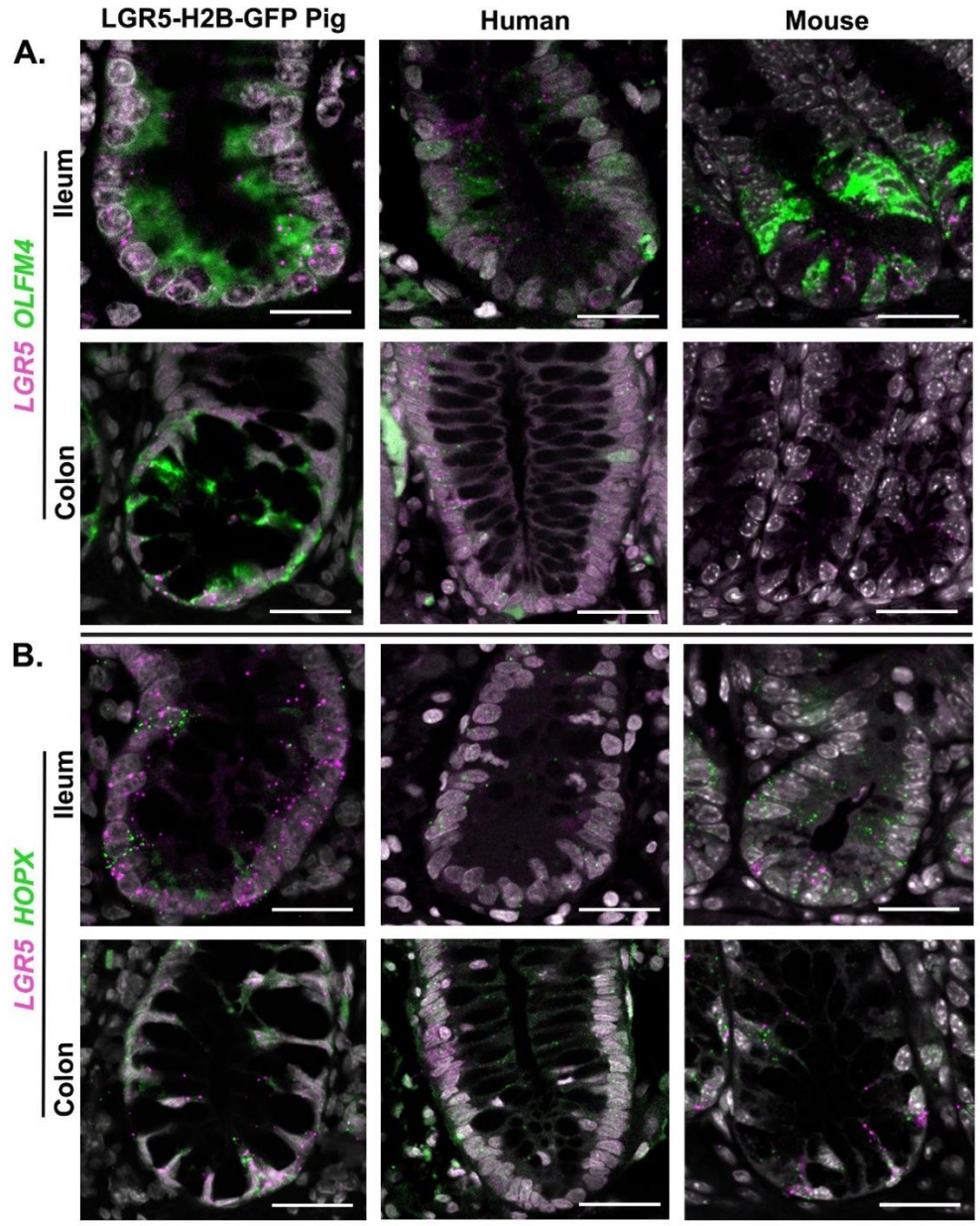

Figure 8. *OLFM4* and *HOPX* are similarly expressed between pig and human. Representative histologic images from ileum and colon of healthy human donors, LGR5-H2B-GFP pigs, and mice with *LGR5* (magenta) and either ***A.*** *OLFM4* or ***B.*** *HOPX* mRNA probes (green). Nuclei stained with DAPI (gray). Scale bar 25 µm. Two to three animals/patients per species were analyzed. Images acquired on a Zeiss LSM 880 microscope with 40X objective.

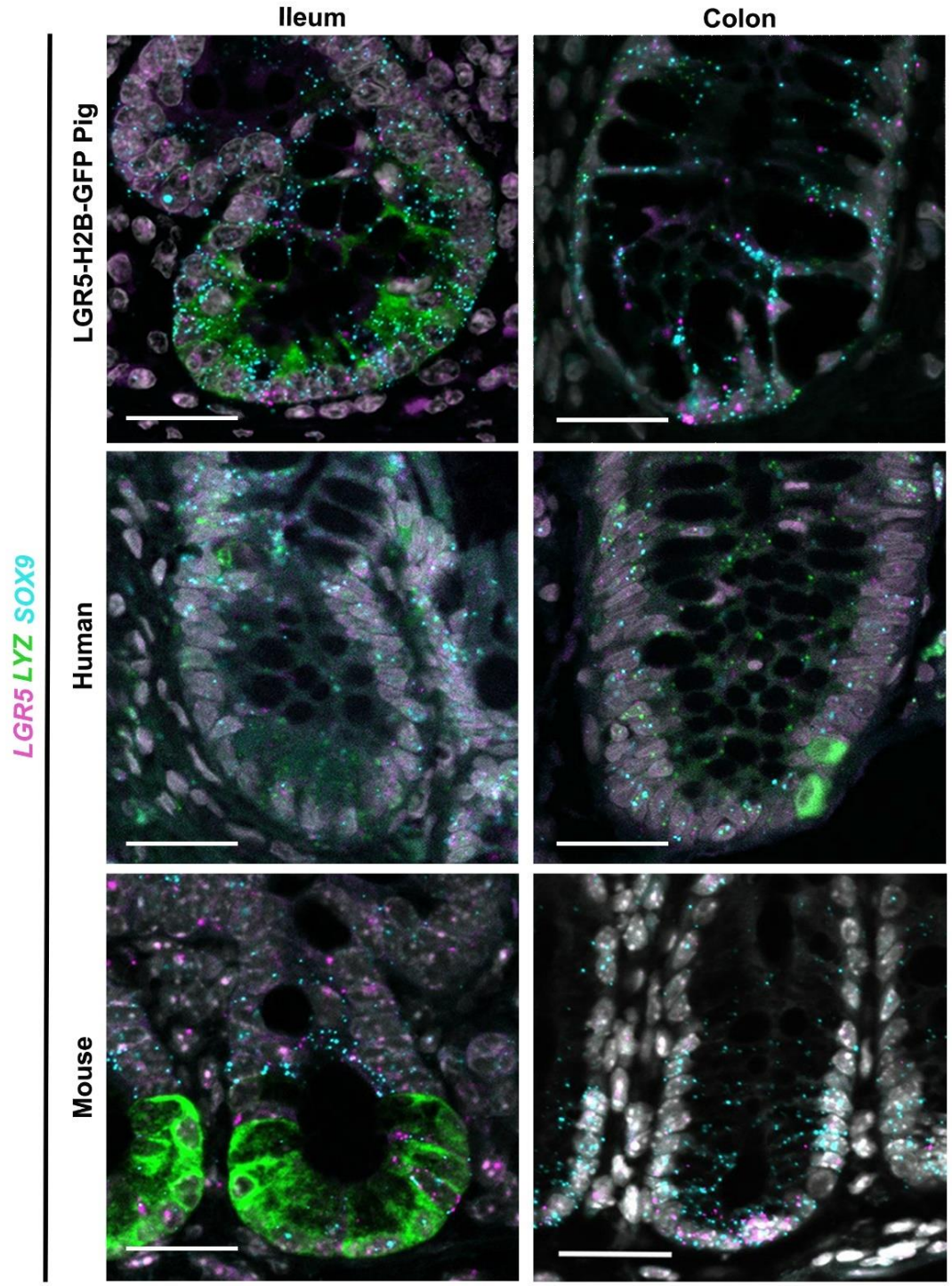

Figure 9. Colon crypt cells express *LYZ* and *SOX9* in humans and pigs. Representative histologic images from ileum and colon of healthy human donors, LGR5-H2B-GFP pigs, and mice with *LGR5* (magenta), *SOX9* (cyan), and *LYZ* (green) mRNA probes. Nuclei stained with DAPI (gray). Scale bar 25 μm. Two to three animals/patients per species were analyzed. Images acquired on a Zeiss LSM 880 microscope with 40X objective.

Disruption of *APC* in LGR5-H2B-GFP colonoids leads to cystic growth in culture and constitutive WNT/β-catenin signaling

To demonstrate the utility of the transgenic porcine model for the study of human intestinal disease, specifically colorectal cancer, we disrupted *APC* in LGR5-H2B-GFP colonoids. To achieve this goal of an *APC* edited LGR5-H2B-GFP model, we used CRISPR/Cas9 editing to target part of the *APC* sequence in exon 9 via nucleofection in LGR5-H2B-GFP colonoids. Colonoid editing efficiency was confirmed by tracking of indels by decomposition (TIDE) after the edited colonoids were grown in complete media for 7 days (58.73+/-19.76%). Colonoids were then passaged into selective media, depleted of Wnt, R-spondin, and CHIR, which enriched editing efficiency to 82.20+/-17.87% (Figure 10A). These LGR5-H2B-GFP/*APC*^{null} colonoids in selective media demonstrated cystic growth that paralleled similar previous murine and human *APC* edited colonoid models, while unedited colonoids failed to survive (Figure 10B). [13, 61]

As APC serves to suppress WNT/β-catenin signaling in unedited epithelial cells, [62, 63] we confirmed that *APC* mutation in the LGR5-H2B-GFP colonoids led to constitutive activation of WNT/β-catenin. This constitutive activation can be identified by increased *AXIN2* expression, a well-described WNT/β-catenin pathway target gene. [15, 61, 64] Compared to non-edited, complete media-grown colonoids (control), selective media-grown *APC* edited colonoids had significantly upregulated *AXIN2* (fold change 7.97+/-3.98; $p<0.05$; Figure 10C). The same *APC*^{null} colonoids also had significantly increased expression of other WNT/β-catenin signaling targets including *CCND1, LGR5, OLFM4,* and *WNT3a* (fold changes 6.41+/-4.93, 4.20+/-2.95, 24.42+/-11.06, 53.08+/-49.21, respectively; $p<0.05$). To assess potential tumorgenicity, colonoscopy-guided submucosal injection of the LGR5-H2B-GFP/*APC*^{null} organoids was performed in NOD.Cg-Prkdc^{scid} Il2rg^{tm1Wjl}/SzJ (NSG) mice as previously described. [65, 66] Engraftment of LGR5-H2B-GFP/*APC*^{null} colonoids was confirmed by visual evidence of tumor formation upon

recheck colonoscopy 10 days post-injection (Figure 10D). Furthermore, these tumors were positive for GFP expression, indicating the presence of LGR5-H2B-GFP cells.

Figure 10. Development, *in vitro* culture, and *in vivo* engraftment of LGR5-H2B-GFP/*APC*^{null} colonoids. *A.* Representative readout of editing efficiency as determined by tracking of indels by **(Figure 10 cont.)** decomposition (TIDE) in LGR5-H2B-GFP/*APC*^{null} colonoids. Bar graph below represents TIDE percent editing efficiency data from LGR5-H2B-GFP/*APC*^{null} colonoids in complete media for 7 days (magenta) compared to after passaging in selective media for 7 days (blue). Data points represent independent transfection replicates from 2 pigs, >100 colonoids used per data point. ***B.*** Representative images of LGR5-H2B-GFP/*APC*^{null} colonoids grown in complete media compared to selective media, and unedited LGR5-H2B-GFP colonoids grown in selective media. Images captured at 7 days in culture. Scale bar 100 μm. Images acquired on an IX83 inverted fluorescent microscope (Olympus) using monochrome digital camera (ORCA-flash 4.0, Hamamatsu), 10X objective (LIC Plan FLN; Olympus), and cellSens software (Olympus). ***C.*** qRT-PCR analysis of *AXIN2* expression in LGR5-H2B-GFP/*APC*^{null} colonoids grown in selective media for 3-7 days. The $\Delta\Delta C_t$ method was used to measure relative fold change in gene expression compared with control (unedited colonoids grown in complete media). Dotted horizontal line indicates control sample set=1. *GAPDH* was used as the housekeeping gene. Samples were tested in triplicate; data points represent independent transfection replicates from 2 different pigs, >100 colonoids used per data point. Statistical analysis by student's t-test, * $p<0.05$ ***D.*** Representative colonoscopy images from LGR5-H2B-GFP/*APC*^{null} submucosal injection into NSG mice colons at injection and at 10 days post injection recheck to confirm tumor formation. Tumor GFP expression outlined by dotted line.

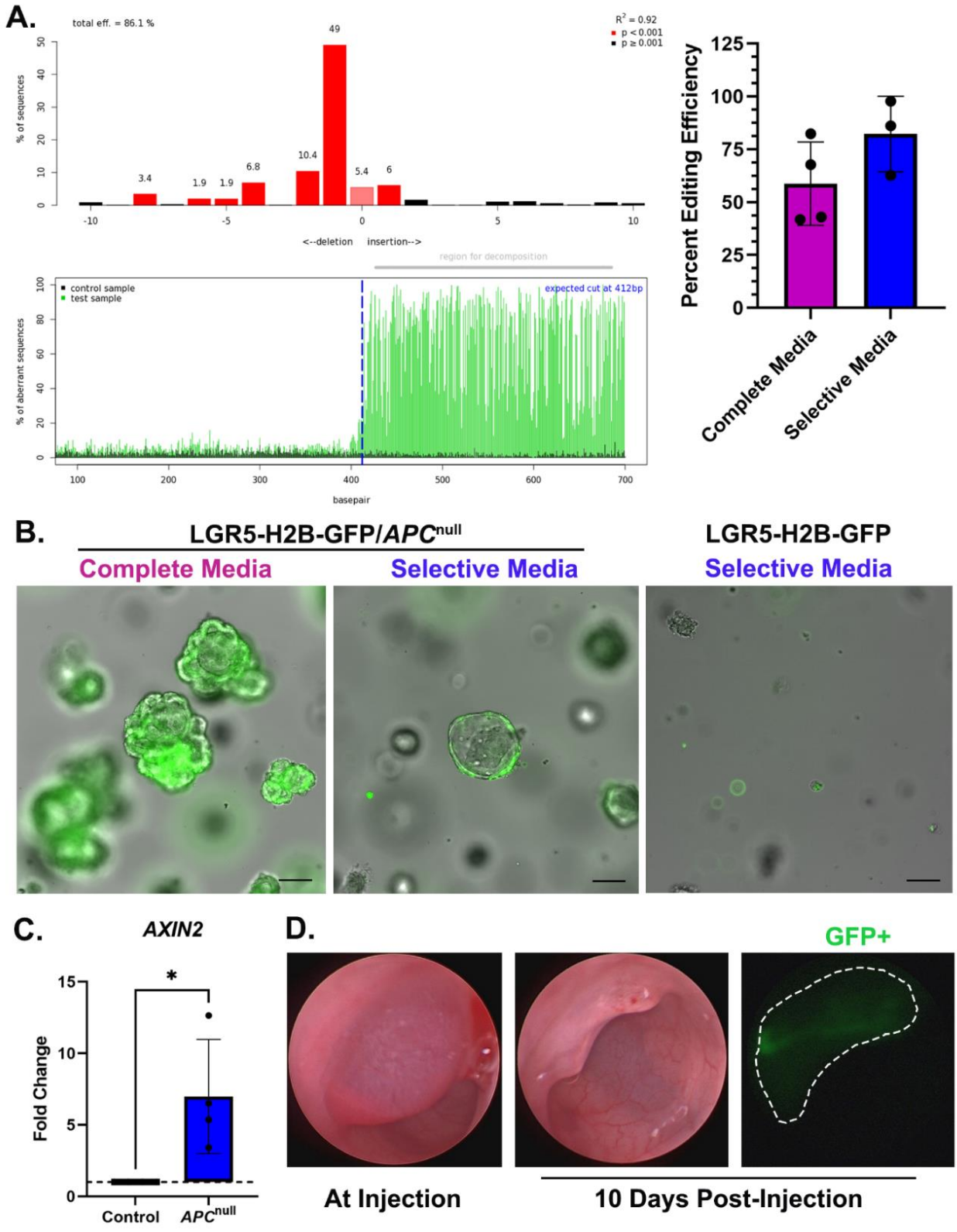
A.
total eff. = 86.1 %
R² = 0.92
p < 0.001
p ≥ 0.001
% of sequences
3.4
1.9
1.9
6.8
10.4
49
5.4
6
<--deletion insertion-->
region for decomposition
control sample
test sample
expected cut at 412bp
% of aberrant sequences
basepair
Percent Editing Efficiency
Complete Media
Selective Media
B.
LGR5-H2B-GFP/APCnull
Complete Media
Selective Media
LGR5-H2B-GFP
Selective Media
C.
AXIN2
Fold Change
Control
APCnull
D.
GFP+
At Injection
10 Days Post-Injection

DISCUSSION

To date, intestinal epithelial stem cell research has relied nearly completely on murine ISC transgenic models as the gold standard for advanced analysis of ISC biology, repair, and tumorigenesis. [2, 8, 16, 25] However, porcine models are increasing in popularity for translational gastrointestinal research because human and porcine intestinal anatomy and physiology are closely paralleled in size, diet, microbiome, and immune cell biology. [30, 31, 39] Further advancement of these porcine intestinal models for more mechanistic studies of human disease has been limited by a paucity of transgenic models.

In this study, we characterized a transgenic LGR5 reporter pig, the first of its kind, to validate its use as a large animal model to identify and isolate intestinal epithelial stem cells. Collectively, our findings reveal that the LGR5-H2B-GFP^{hi} cells, expressing nuclear GFP, are the LGR5^{+} ISCs. These findings were verified by histologic location of GFP^{+} cells in the crypt-base, ISC signature protein biomarker co-localization with GFP^{+} cells, significantly increased *LGR5* gene expression within the LGR5-H2B-GFP^{hi} population, and enteroid formation in culture from LGR5-H2B-GFP^{hi} single cells. Each of these findings underscore the utility of the LGR5-H2B-GFP pig as a translational model to identify and interrogate ISCs.

In addition, ileal and colonic biopsies of human, mouse, and pig were compared by *in situ* hybridization to underscore the utility of the pig as a model for crypt-base cell studies. While all three species demonstrated similar expression of *LGR5*, further *in situ* examination of other crypt-base cell markers *OLFM4*, *HOPX*, *LYZ*, and *SOX9* highlighted important similarities between pig and human that were not present in the mouse. Notably, previous literature detected *OLFM4* expression in porcine colonic epithelium by qRT-PCR; [67] however, to the authors knowledge, this is the first *in situ* identification of porcine *OLFM4* in both small intestine and colon, which

also mirrors human *OLFM4* expression. This is in direct contrast to the mouse, which does not express *OLFM4* in the colon. Similar *OLFM4* expression in both human and porcine colon could be important for future improved modeling of intestinal diseases such as colorectal cancer where *OLFM4* is a known marker for a subset of cancer cells and potential metastasis. [51, 68, 69]

Moreover, both porcine and human tissue also exhibit similar *in situ* co-expression of *LGR5* and *HOPX*, which further validates several recent studies showing overlap of *LGR5* and the proposed unique quiescent/ "+4" stem cell markers. [56, 57, 70] Comparison of *in situ LYZ* expression between species revealed that pig colon crypt-base cells are positive for *LYZ*, similar to humans, while mice are not. This finding may be important for potential future studies of intestinal diseases such as Inflammatory Bowel Disease (IBD). In human patients suffering from IBD, LYZ producing Paneth cells are over-expressed in the colon. [71] Previous studies have attempted to further investigate this disease pathophysiology by creating transgenic mice that overexpress Lyz in the colon; [58] however, given the naturally occurring similarity in *LYZ* expression between humans and pigs, the pig has the potential to be an improved translational large animal model for IBD research. Furthermore, similar co-expression of *LYZ*, *LGR5*, and *SOX9* located in the progenitor cell zone within both human and pig cells, but not in mouse, highlights the need for additional comparative transcriptomic and proteomic analysis between pig and human crypt-base cells. Such analysis in the LGR5-H2B-GFP model could potentially use the crypt-base cell GFP intensity gradient to identify different progeny of $LGR5^{+}$ ISCs, thereby expanding the possible model utility.

To specifically demonstrate the use of the LGR5-H2B-GFP porcine model for intestinal disease research, we utilized CRISPR/Cas9 editing to create *APC* disrupted colonoids (Figure 10). These LGR5-H2B-GFP/APC^{null} colonoids showed *APC* editing efficiency of over 80%, developed

cystic organoid structures in growth factor depleted selective media, and had increased expression of WNT target gene *AXIN2*. Similar characteristics have been previously described in human and murine *APC* knock-out colonoid experiments. [13, 61] Furthermore, orthotopic, submucosal injection of these colonoids into immunodeficient mice led to tumor growth that expressed GFP. This novel combination of ISC reporter and CRC gene mutation in a translational porcine model is important to progress the field of CRC research. Previously, Flisikowska et al. created an *APC* mutated pig line which develops dysplastic adenomas in the large intestine, similar to the precancerous lesions in human patients. [72] These pigs have contributed greatly to understanding CRC cellular mechanisms and improving diagnostics/therapeutics for human CRC patients in ways that previous mouse models could not. [73-76] Historically, colon cancer has been difficult to model completely in genetically modified mice due to the tendency of tumors to form in the small intestine instead of the colon. [77] Furthermore, the small size of mice makes it difficult for clinicians and researchers to improve endoscopic and surgical technique to detect and remove CRC. Additional porcine CRC models would significantly advance the field of translational CRC research in these areas. In particular, given the previously described role of $LGR5^{+}$ cancer stem cell in CRC tumor development, [7-9, 14] the LGR5-H2B-GFP pig will allow critical *in vivo* ISC tracking and isolation from tumors. Additionally, inducing the other common sequential CRC gene mutations in the LGR5-H2B-GFP colonoids beyond *APC* (*KRAS*, *SMAD4*, and *TP53*) will likely allow modeling of the adenoma-carcinoma sequence with potential to form invasive carcinoma upon orthotopic auto-transplantation. [61, 65, 66, 77]

The GFP^{dim} crypts observed in this study has also been demonstrated in ISC transgenic mice. Mosaicism has been long known to occur in the crypts of LGR5-eGFP-IRES-CreERT2 mice. [2, 78] It is unknown, in that model, what specific mechanisms drive the process, although it has

been hypothesized to be due to the inserted DNA sequence itself or the location of the insertion. [79] Research on other transgenes supports that during development, alterations to the DNA sequence can result in variegation that leads to stochastic levels of expression of transgenes from cell to cell, and this is especially true in essential genes, termed "spatial effect variegation" (different than position effect variegation due to random insertion) .[80, 81] Our data confirm that this pattern is also observed within a different species (porcine), with a different transgene organization, and insertion in the 5' end, and further that the silencing alters H2B-GFP expression but not LGR5 expression, as confirmed by RNAscope *in situ* hybridization and qRT-PCR (Figure 3C-F). Because GFP^{dim} crypts were observed in adjacent clusters (Figure 3A), our data support the idea that the mechanism driving differential GFP expression is likely occurring early in intestinal development. Subsequent crypt fission of a GFP^{dim} crypt as the intestine grows leads to adjacent populations of GFP^{dim} crypts. Further research needs to be done to determine if this observation is reflective of a previously unreported LGR5 gene transcriptional regulatory system (i.e., splicing variants, alternate promoters or other epigenetic modifications) in the colon.

The variable percentage of mosaic crypts noted between sections of intestine (Figure 3B) can likely be attributed to differential rates of crypt fission. In both porcine and murine studies, compared to small intestine and cecum, the rate of crypt fission in the colon is markedly increased. [45, 82, 83] Despite the mosaic pattern in the crypts, it is still clear that within the crypts that express GFP, we can reliably define the LGR5-H2B-GFP^{hi} cells as LGR5+ ISCs. Furthermore, this mosaic expression has not been observed in other tissues in this pig line. This suggests that this mosaicism is unique to certain tissues, in this case the intestinal tract. [40]

The LGR5-H2B-GFP transgenic pig serves as a milestone large animal model to reliably identify and isolate intestinal epithelial stem cells using the *LGR5* gene. Such advancement in large

animal transgenic models allows for critical improvement in translational basic science studies involving intestinal pathophysiology. In combination with previous ISC knowledge gained from murine studies and this new development in ISC identification in a translational large animal model, we can better model pathophysiology and discover treatments for numerous clinical intestinal disease processes including colorectal cancer, ischemia-reperfusion injury, inflammatory bowel diseases, neonatal necrotizing enterocolitis, allograft failure, and short bowel syndrome.

ACKNOWLEDGEMENTS

The authors would like to thank Yanet Murphy and Joshua Ginzel for their assistance in production of RNAscope images, Dr. Diana Cardona at Duke University for providing human samples, Javid Mohammed and the NCSU-CVM Flow Cytometry and Cell Sorting Laboratory for FACS sorting, the NCSU-CVM Histology Laboratory for processing H&E slides, and the NCSU-CVM Central Procedures Laboratory and Lab Animal Resource Veterinarians and technicians for their pig care and assistance in tissue collection.

METHODS

Porcine Models

Healthy, crossbred LGR5-H2B-GFP littermate male and female pigs (10-40 weeks) were used for this study. All LGR5-H2B-GFP animals were bred and raised in the animal facility of NCSU CVM. A mix of healthy male and female (10-40 weeks) Yorkshire cross pigs were used as normal control animals (wild type). The Institutional Animal Care and Use Committee of North Carolina State University approved all animal use (17-028-B and 19-019-B).

Human Samples

Endoscopic biopsies from adult human small bowel and colon deemed normal collected at Duke University. These samples were blinded for identity of the individuals. Sample use approved by IRB # 2020-10-733.

Murine Models

For orthotopic injection of LGR5-H2B-GFP/*APC*^{null} colonoids, NOD.Cg-Prkdc^{scid} Il2rg^{tm1Wjl}/SzJ (NSG) male mice, approximately 8-12 weeks old were used (Jackson Laboratory; Strain # 005557; RRID:IMSR_JAX:005557). The Institutional Animal Care and Use Committee of Duke University approved all animal use (A234-21-12).

Tissue Collection

Pigs were sedated with Telazol/Ketamine/Xylazine (TKX, 0.04 mL/kg IM) prior to euthanasia (60 mg/kg IV pentobarbital sodium). Loops (10-12 cm) of duodenum, jejunum, ileum, and spiral colon were collected and rinsed with 1x phosphate-buffered saline (PBS).

Histology

Full-thickness sections of duodenum, jejunum, ileum, and spiral colon were fixed in 10% formalin and washed in 70% ethanol. Paraffin embedded samples were sectioned (5-8 µm thickness) and stained with hematoxylin and eosin by the North Carolina State University Histology Core to visualize crypt/villus morphology.

Tissue Immunofluorescence

To identify specific cell types within whole tissue, sections of intestine were fixed in 4% paraformaldehyde (PFA) (14-18 h; 4^{O} C). Tissue was then transferred to 30% sucrose solution (24 h; 4^{o} C), embedded in optimal cutting temperate (OCT) media, and frozen. Frozen blocks were sectioned at 5-8 µm thickness. To look for endogenous GFP fluorescence, slides were washed with

PBS, stained with bisbenzimide H 33258 nuclear stain (1:1000, Sigma Aldrich), and sealed with a coverslip (Prolong Gold Antifade Mount; Thermo Fisher). For each slide evaluated for mosaic expression, only well-oriented crypts were used to obtain counts (crypt-base closely opposed to the muscularis mucosa layer and that extended and opened fully into the gut lumen). At least 100 total well-oriented crypts for each section of intestine per pig were counted and the percentage GFP negative crypts were calculated.

To co-localize ISC protein biomarkers SOX9 and KI67 with GFP expression in multiplex immunofluorescence assay, fixed-frozen sections of jejunum and spiral colon underwent heat-induced epitope retrieval (HIER) by placing slides in reveal decloaker solution (Biocare Medical, Concord) in a Pascal pressure chamber (DakoCytomation). Tissue permeabilization was performed with PBS-0.3% Triton X-100. The α-GFP (rabbit, 1:2,000; Abcam catalogue #: ab183734) antibody was diluted in antibody diluent (SignalStain Antibody Diluent; Cell Signaling Technology) and applied. Washes between reagents were in 1× Tris-Buffered Saline, 0.1% Tween. Following antibody binding, HRP boost reagent [SignalStain Boost Detection Reagent (HRP, rabbit); Cell Signaling Technology] was applied, followed by a specific fluorophore-conjugated tyramide signal amplification (TSA) reagent [green fluorescent protein (GFP)]. Slides were boiled in citrate stripping solution (SignalStain Citrate Unmasking Solution; Cell Signaling Technology) and then incubated in blocking reagent (Dako). Additional primary antibodies were applied overnight at 4^{o} C [α-SOX9 (rabbit, 1:500; Millipore catalogue #:AB5535), α-KI67 (mouse, 1:250; Dako catalogue #:M7240)] diluted in antibody diluent (Dako)]. The host-specific secondary antibodies (conjugated to Cyan3 and Cy5; Sigma Aldrich) were applied at 1:500 in antibody diluent. Slides were then counterstained with bisbenzimide H 33258 nuclear staining and cover slipped (Hydromount; National Diagnostics).

To co-localize α-GFP and α-UEA, the same procedure as above was followed, incubating first with α-GFP. The α-UEA antibody (rabbit, 1:500; Millipore Sigma-Aldrich catalogue #:U4754) diluted in antibody diluent (Dako) was applied overnight at 4° C. The secondary antibody (conjugated to Cyan3; Sigma Aldrich) was diluted 1:500 in antibody diluent and slides were counterstained with bisbenzimide H 33258 nuclear stain before coverslip application.

Crypt Isolation

Intestinal crypt isolation was performed as previously described.[4] Briefly, sections of intestine, with the mucosa exposed, were washed with cold PBS. The segments were then incubated in ethylenediaminetetraacetic acid [EDTA (30 mM)], Y-27632 (10 mM), dithiothreitol [DTT (1 mM)], and 1x antibiotic-antimycotic (anti-anti, Life Technologies; Primocin, InvivoGen) for 30 min at 4° C. Tissue was transferred and incubated in EDTA (30mM), Y-27632 (10 mM), and anti-anti for 10 min at 37° C. During incubation, tissue was intermittently shaken vigorously to mobilize the crypt epithelium. After incubation, tissues were transferred to ice-cold PBS washes with anti-anti. Tissue was shaken and transferred to additional washes until crypts were observed with minimal background debris. Crypts were then pelleted and snap-frozen in liquid nitrogen for total RNA extraction and additional crypts immediately dissociated into single cell for fluorescence activated cell sorting (FACS).

Single Cell Isolation

Crypts from each intestinal segment were independently incubated with Dispase (36 U; Corning, Corning), Y-27632 (10 mM), and DNase I (300 μg; Alfa Aeser) in 1x Hank's Balanced Salt Solution (HBSS) for 10 min at 37° C. Single cells were washed with 1x HBSS, resuspended in flow cytometry buffer (2% Bovine Serum Albumin in 1x PBS), and passed sequentially through

100 µm, 70 µm, and 40 µm filters. Cells were then stained with Propidium Iodide (BioLegend) for FACS sorting.

Fluorescence Activated Cell Sorting and Flow Cytometry

Fluorescence activated cell sorting was conducted by the NCSU-CVM Flow Cytometry and Cell Sorting Core using a Beckman Coulter MoFlo XDP. Dead cells were identified by Propidium Iodide. Based on GFP expression, single live cells were gated into Lgr5-H2B-GFP^{neg} and Lgr5-H2B-GFP$^{hi/med/lo}$. Single cells for culture were collected in cell culture media while cells for gene expression were collected in 1x PBS with 4% Fetal Bovine Serum, pelleted, and snap frozen in liquid nitrogen until RNA isolation. Flow cytometry analysis of GFP$^{pos/neg}$ colonoid single, live, GFP expressing cells was performed using Beckman Coulter CytoFLEX. Data were further analyzed using FlowJo (BD Biosciences).

Real-time PCR

Total RNA from whole crypt and LGR5-H2B-GFP single cells was extracted using Ambion PureLink RNA mini kit (Thermo Fisher Scientific). Yield and quality control of the extracts were determined by an Agilent 2100 BioAnalyzer performed by the North Carolina State University Genomic Sciences Laboratory Core using Agilent Eukaryote Total Pico Series II chips (Agilent Technologies). Samples were used with an RNA Integrity Score >6 and RNA concentration of >100 pg/µl. RNA (1 µg) was converted to cDNA using the iScript cDNA synthesis kit. Expression of intestinal stem cell genes was determined by quantitative real-time PCR (QuantStudio 6 Flex, Applied Biosystem) using cDNA samples and the iTaq Universal SYBR green Supermix. Primers included *GAPDH* (F- ATCCTGGGCTACACTGAGGAC; R- AAGTGGTCGTTGAGGGCAATG), *LGR5* (F- CCTTGGCCCTGAACAAAATA; R- ATTTCTTTCCCAGGGAGTGG), *OLFM4* (F- GTCAGCAAACCGGCTATTGT; R-

TGCCTTGGCCATAGGAAATA) [4, 41], and *eGFP* (F- AAGGGCATCGACTTCAAGG; R-TGCTTGTCGGCCATGATATAG). The $\Delta\Delta C_t$ method was used to measure relative changes in gene expression, and samples were tested in triplicate.

Single Cell Culture

Sorted LGR5-H2B-GFP cells were resuspended directly in growth factor-reduced Matrigel (BD Bioscience) supplemented with 50 ng/ml recombinant human Epidermal Growth Factor (Life Technologies), 10 µM Y-27632, 10 µM SB-202190 (Sigma-Aldrich), 500 nM LY-2157299 (Selleck Chemicals), 10 nM Gastrin (Sigma-Aldrich, St. Louis), 1mM Nicotinamide (Sigma-Aldrich), 500 nM A-83-01 (Tocris Bioscience), and 2.5 µM Glycogen Synthase Kinase 3 inhibitor (GSK3i, CHIR99021, Tocaris Bioscience). Approximately 4,000 cells were plated in 50 µl of Matrigel. Each well was then overlaid with a total of 500 ml of conditioned media: 250 ml of recombinant human noggin, recombinant human R-spondin, recombinant wingless/integrated 3a (Wnt-3a) (L-WRN) media with an additional 250 ml of culture media [advanced DMEM-F-12 (Thermo Fisher Scientific) supplemented with 1x N-2 supplement (Life Technologies), 1x B-27 supplement minus vitamin A (Life Technologies), 1x Glutamax (Life Technologies), 1x anti-anti, and 1 mM HEPES buffer (Life Technologies)]. The entire volume of growth factors and conditioned media were changed 48 h after plating and subsequent 48 h intervals.

Whole Crypt Culture

The pelleted whole crypts from epithelial crypt dissociation were resuspended directly in growth factor-reduced Matrigel at a concentration of approximately 50 crypts per 50 µl of Matrigel. The crypts were cultured in the same conditioned media and growth factors as the single cells.

Organoid Isolation, RNA Extraction, and cDNA Conversion

Organoids were isolated from Matrigel using Corning Cell Recovery Solution as per the manufacturer's instructions. Organoids were pelleted, snap-frozen in liquid nitrogen, and stored at −80°C. RNA was extracted using the Ambion PureLink RNA mini kit (Thermo Fisher Scientific). RNA quality control and quantification were performed with the Agilent 2100 Bioanalyzer as described above. Reverse transcription and was performed as previously described for cDNA derived from crypts. A PCR reaction for each sample was performed using the following primers: *LYZ* (F- GGTCTATGATCGGTGCGAGT; R- AACTGCTTTGGGTGTCTTGC), *MUC2* (F- GGCTGCTCATTGAGAGGAGT; R- ATGTTCCCGAACTCCAAGG), *ITF* (F- TCGGTTCCCCAGAACCTGCCC; R- CGGGGATGCTGGAGTCGAAGC), *CCK* (F- CAAAAGGTAGACGGCGAGTC; R- GCGGGGTCTTCTAGGAGGTA), *CGA* (F- GACCTCGCTCTCCAAGGAGCCA; R- TGTGCGCCTGGGCGTTTCTT), *SGLT1* (F- GCAGCTGTCTTCCTCTTGC; R- GCAAACTCGGTAATCATACGG), and *FABP* (F- CCGGCAAATACCAAGTACAGAGCC; R- CCTTCTCCCCAGTCAGGGTCTCC)[41] and iTaq Universal SYBR Green Supermix (BioRad) in an iCycler thermal cycler. To visualize the products of PCR reaction, a 1.5% agarose gel was prepared from heating agarose (Sigma Aldrich) and 1X TAE buffer (Thermo Fisher Scientific). SYBER safe DNA gel stain (10µl, Invitrogen) was added to the melted agarose. Once the gel was set, PCR samples and ladder were mixed with DNA loading dye, loaded into lanes, and allowed to run until the DNA migrated ¾ of the length of the gel. The gel was imaged using ChemiDoc-It 2 (Ultra-Violet Products, Upland).

***APC* Editing in Colonoids**

The *APC* guide plasmid for CRISPR was designed using Benchling (San Francisco, CA) and created following the Joung Lab Cloning Protocol, and MLM3636 (Addgene plasmid # 43860;

http://n2t.net/85ddgene:43860; RRID:Addgene 43860) was a gift from Keith Joung. Once the guide plasmid was constructed, it was transfected into porcine fetal fibroblasts with the Cas9 plasmid VP12 (Addgene plasmid # 72247; http://n2t.net/85ddgene:72247; RRID:Addgene 72247)[84] using the Nucleofector 2b device (Lonza) setting U-023. Post-transfection, a PCR product of transfected cells was used to determine the editing efficiency by tracking of indels by decomposition (TIDE)[85]. This optimized *APC* guide (sequence 5'-gtgttgttgggaaattcccg-3') for exon 9 was ordered as a sgRNA from Synthego.

To develop the LGR5-H2B-GFP/APC^{null} colonoids, LGR5-H2B-GFP colon crypts were isolated and plated in Matrigel with conditioned media as described above. The resulting colonoids were passaged using the cell recovery protocol described previously and dissociated to single cells by incubation in TrypLE (Thermo Fisher Scientific) and Y-27632 (1:1000). Single colonoid cells were then aliquoted to 250,000 cells per nucleofection. For this process, CRISPR-Cas9 was assembled as ribonucleoprotein (RNP) complex by combining 5 ug of sgRNA and 5 ug of Cas9 protein in 100 ul of nucleofector solution and incubated at room temperature for 20 min. Human Stem Cell Solution 1 within the Human Stem Cell Nucleofector™ Starter Kit (Lonza) was used for nucelofection. The aliquoted single LGR5-H2B-GFP colon cells were pelleted and resuspended with the RNP complex and nucleofector solution by gently pipetting, transferred into a cuvette, and then placed into the nucleofector device for nucleofection. Once the nucleofection was complete, cells were washed with culture media and plated at a density of 5,000 cells per 50 µl Matrigel with conditioned media for 7 days to permit for Cas9-mediated editing of *APC*. To select for *APC* edited cell population, LGR5-H2B-GFP/*APC*^{null} colonoids were passaged as single cells and grown in growth factor reduced media without Wnt-3a, R-spondin, or CHIR. Knockout efficiency of *APC* immediately following nucleofection and after growth in selective media was

determined through TIDE analysis. For gene expression, LGR5-H2B-GFP/*APC*^{null} colonoids were passaged at least twice in selective media and then processed for RNA isolation and qRT-PCR as described above. Primers for *AXIN2* were F- ATTGTTGTTTCCCCGCACTC and R- CTGCTCATGGTGAGGGAGTT; *CCND1* F- GCATCTACACCGACAACTCC and R- TGATCTGTTTGTTCTCCTCG; *WNT3a* GCGACTTCCTCAAGGACAAG and *R*- GGTCACGTGTACCGAAGGAT.

Murine Colonoscopy and Injection

Optical colonoscopy was performed as previously described. [65, 66] For mucosal injections, LGR5-H2B-GFP/*APC*^{null} colonoids, after 2 passages in selective media and grown for 72 hours prior to injection, were suspended in 1:1 culture media/Matrigel at a concentration of 50 organoids/µl. Colonoids were delivered beneath the colon mucosa of 8-12 week old male recipient NOD.Cg-Prkdc^{scid}Il2rg^{tm1Wjl}/SzJ (NSG) mice (JAX #005557) mice by optical colonoscopy as previously described using a custom injection needle (Hamilton Inc., 33 gauge, small Hub RN NDL, 16 inches long, point 4, 45-degree bevel, part number 7803-05), a syringe (Hamilton Inc., part number 7656-01), a transfer needle (Hamilton Inc., part number 7770-02), and a colonoscope with integrated working channel (Karl Storz, 61029 C). [65, 66] For each mouse, 2-3 injections of 50-70 µl were performed as previously described. [65] Mice underwent colonoscopy 1-2 weeks following injection to assess tumor formation and were followed weekly by colonoscopy. Mice were euthanized between 3-5 weeks post injection. Just prior to euthanasia, mice received 2 mg intraperitoneal Bromodeoxyuridine (BrdU) 2 hrs prior to tissue collection injection. After euthanasia, the distal 3 cm colon was collected and fixed in 10% formalin.

Multiplex RNA FISH

Fluorescent *in situ* hybridization to detect mRNA targets (RNAscope, Advanced Cell Diagnostics) was performed in accordance with the manufacturer's instructions. Briefly, formalin-fixed paraffin embedded intestinal tissue from human, mouse, or pig was sectioned at 7 μm. Slides were deparaffinized with xylene, then heat induced epitope retrieval treated followed by protease digestion. The tissue was hybridized with the species-specific probes targeting *LGR5, HOPX, SOX9, LYZ, and OLFM4* mRNA or a positive control probe peptidylprolyl isomerase B (*PPIB*) (Advanced Cell Diagnostics), followed by chromogenic or Tyramide Signal Amplification technology development per user manual. Porcine tissue slides were then incubated in primary antibody α-GFP (abcam catalogue # ab183734), diluted (1:50) followed by secondary antibody (Alexa Fluor 488). Slides were washed, then mounted with Prolong Gold Antifade Mount with DAPI (Thermo Fisher) and imaged by confocal microscopy.

Image Acquisition

Images were captured on an inverted fluorescence microscope (Olympus IX83, Tokyo) fitted with a monochrome digital camera (ORCA-flash 4.0, Hamamatsu) and color camera (DP26; Olympus). Additional images were also captured on a Fluoview FV3000 upright confocal microscope (Olympus) and on a Zeiss LSM 880 microscope.

Crypt/Villus and Fluorescent Intensity Measurements

Crypt depth and villus length was measured using line tool in ImageJ (NIH). Intensity of GFP and bisbenzimide H 33342 fluorescence was also measured by the measure tool in ImageJ.

Statistics

All statistical analyses were performed using Prism software (GraphPad Software, La Jolla). Outliers were identified by ROUT method and a Shapiro-Wilk normality test was

performed on raw data, followed by either student's t-test or two-way ANOVA with Tukey's multiple comparisons. Data are reported as means with standard deviations. The α-level for statistical significance was defined as $p<0.05$.

REFERENCES

[1] Cheng H, Leblond CP. Origin, differentiation and renewal of the four main epithelial cell types in the mouse small intestine V. Unitarian theory of the origin of the four epithelial cell types. American Journal of Anatomy 1974;141(4):537-61.

[2] Barker N, van Es JH, Kuipers J, Kujala P, van den Born M, Cozijnsen M, Haegebarth A, Korving J, Begthel H, Peters PJ, Clevers H. Identification of stem cells in small intestine and colon by marker gene Lgr5. Nature 2007;449(7165):1003-7.

[3] Barker N, van der Wetering M, Clevers H. The intestinal stem cell. Genes and Development 2008;22(14):1856-64.

[4] Gonzalez LM, Amy SS, Freund J, Cecilia RK, Dekaney CM, Magness ST, Blikslager AT. Preservation of reserve intestinal epithelial stem cells following severe ischemic injury. American Journal of Physiology-Gastrointestinal and Liver Physiology 2019;316(4):G482-G94.

[5] Yan KS, Chia LA, Li X, Ootani A, Su J, Lee JY, Su N, Luo Y, Heilshorn SC, Amieva MR, Sangiorgi E, Capecchi MR, Kuo CJ. The intestinal stem cell markers Bmi1 and Lgr5 identify two functionally distinct populations. Proceedings of the National Academy of Sciences of the United States of America 2012;109(2):466-71.

[6] Siegel RL, Miller KD, Goding Sauer A, Fedewa SA, Butterly LF, Anderson JC, Cercek A, Smith RA, Jemal A. Colorectal cancer statistics, 2020. CA: A Cancer Journal for Clinicians 2020;70(3):145-64.

[7] Schepers Arnout G, Snippert Hugo J, Stange Daniel E, van den Born M, van Es Johan H, van de Wetering M, Clevers H. Lineage Tracing Reveals Lgr5+ Stem Cell Activity in Mouse Intestinal Adenomas. Science 2012;337(6095):730-5.

[8] Barker N, Ridgway RA, van Es JH, van de Wetering M, Begthel H, van den Born M, Danenberg E, Clarke AR, Sansom OJ, Clevers H. Crypt stem cells as the cells-of-origin of intestinal cancer. Nature 2009;457(7229):608-11.

[9] Zhou Y, Xia L, Wang H, Oyang L, Su M, Liu Q, Lin J, Tan S, Tian Y, Liao Q, Cao D. Cancer stem cells in progression of colorectal cancer. Oncotarget 2017;9(70):33403-15.

[10] Miyoshi Y, Nagase H, Ando H, Horii A, Ichii S, Nakatsuru S, Aoki T, Miki Y, Mori T, Nakamura Y. Somatic mutations of the APC gene in colorectal tumors: mutation cluster region in the APC gene. Hum Mol Genet 1992;1(4):229-33.

[11] Laken SJ, Papadopoulos N, Petersen GM, Gruber SB, Hamilton SR, Giardiello FM, Brensinger JD, Vogelstein B, Kinzler KW. Analysis of masked mutations in familial adenomatous polyposis. Proc Natl Acad Sci U S A 1999;96(5):2322-6.

[12] Huang D, Sun W, Zhou Y, Li P, Chen F, Chen H, Xia D, Xu E, Lai M, Wu Y, Zhang H. Mutations of key driver genes in colorectal cancer progression and metastasis. Cancer and Metastasis Reviews 2018;37(1):173-87.

[13] Yamazaki D, Hashizume O, Taniguchi S, Funato Y, Miki H. Role of adenomatous polyposis coli in proliferation and differentiation of colon epithelial cells in organoid culture. Scientific Reports 2021;11(1):3980.

[14] Barker N, Clevers H. Leucine-rich repeat-containing G-protein-coupled receptors as markers of adult stem cells. Gastroenterology 2010;138(5):1681-96.

[15] Sato T, Stange DE, Ferrante M, Vries RGJ, van Es JH, van den Brink S, van Houdt WJ, Pronk A, van Gorp J, Siersema PD, Clevers H. Long-term Expansion of Epithelial Organoids From Human Colon, Adenoma, Adenocarcinoma, and Barrett's Epithelium. Gastroenterology 2011;141(5):1762-72.

[16] Sato T, Vries RG, Snippert HJ, van de Wetering M, Barker N, Stange DE, van Es JH, Abo A, Kujala P, Peters PJ, Clevers H. Single Lgr5 stem cells build crypt-villus structures in vitro without a mesenchymal niche. Nature 2009;459(7244):262-5.

[17] van der Flier LG, van Gijn ME, Hatzis P, Kujala P, Haegebarth A, Stange DE, Begthel H, van den Born M, Guryev V, Oving I, van Es JH, Barker N, Peters PJ, van de Wetering M, Clevers H. Transcription factor achaete scute-like 2 controls intestinal stem cell fate. Cell 2009;136(5):903-12.

[18] Montgomery RK, Carlone DL, Richmond CA, Farilla L, Kranendonk MEG, Henderson DE, Baffour-Awuah NY, Ambruzs DM, Fogli LK, Algra S, Breault DT. Mouse telomerase reverse transcriptase (mTert) expression marks slowly cycling intestinal stem cells. Proceedings of the National Academy of Sciences of the United States of America 2011;108(1):179-84.

[19] Powell Anne E, Wang Y, Li Y, Poulin Emily J, Means Anna L, Washington Mary K, Higginbotham James N, Juchheim A, Prasad N, Levy Shawn E, Guo Y, Shyr Y, Aronow Bruce J, Haigis Kevin M, Franklin Jeffrey L, Coffey Robert J. The Pan-ErbB Negative Regulator Lrig1 Is an Intestinal Stem Cell Marker that Functions as a Tumor Suppressor. Cell 2012;149(1):146-58.

[20] Sangiorgi E, Cappechi MR. Bmi1 is expressed in vivo in intestinal stem cells. Nature Genetics 2008;40(7):915-20.

[21] Takeda N, Jain R, LeBoeuf MR, Wang Q, Lu MM, Epstein JA. Interconversion Between Intestinal Stem Cell Populations in Distinct Niches. Science 2011;334(6061):1420.

[22] Tian H, Warming S, Leong KG, Rangell L, Klein OD, de Sauvage FJ. A reserve stem cell population in small intestine renders Lgr5-positive cells dispensable. Nature 2011;478:255-9.

[23] Barker N, van Oudenaarden A, Clevers H. Identifying the Stem Cell of the Intestinal Crypt: Strategies and Pitfalls. Cell Stem Cell 2012;11(4):452-60.

[24] Tan SH, Swathi Y, Tan S, Goh J, Seishima R, Murakami K, Oshima M, Tsuji T, Phuah P, Tan LT, Wong E, Fatehullah A, Sheng T, Ho SWT, Grabsch HI, Srivastava S, I M, Denil SLIJ, Mustafah S, Tan P, Shabbir A, So J, Yeoh KG, Barker N. AQP5 enriches for stem cells and cancer origins in the distal stomach. Nature 2020;578(7795):437-43.

[25] Metcalfe C, Kljavin NM, Ybarra R, de Sauvage FJ. Lgr5+ stem cells are indispensable for radiation-induced intestinal regeneration. Cell Stem Cell 2014;14(2):149-59.

[26] Kararli TT. Comparison of the gastrointestinal anatomy, physiology, and biochemistry of humans and commonly used laboratory animals. Biopharmaceutics & Drug Disposition 1995;16(5):351-80.

[27] Mak IW, Evaniew N, Ghert M. Lost in translation: animal models and clinical trials in cancer treatment. American journal of translational research 2014;6(2):114-8.

[28] Mestas J, Hughes CCW. Of Mice and Not Men: Differences between Mouse and Human Immunology. The Journal of Immunology 2004;172(5):2731.

[29] Seok J, Warren HS, Cuenca AG, Mindrinos MN, Baker HV, Xu W, Richards DR, McDonald-Smith GP, Gao H, Hennessy L, Finnerty CC, López CM, Honari S, Moore EE, Minei JP, Cuschieri J, Bankey PE, Johnson JL, Sperry J, Nathens AB, Billiar TR, West MA, Jeschke MG, Klein MB, Gamelli RL, Gibran NS, Brownstein BH, Miller-Graziano C, Calvano SE, Mason PH, Cobb JP, Rahme LG, Lowry SF, Maier RV, Moldawer LL, Herndon DN, Davis RW, Xiao W, Tompkins RG. Genomic responses in mouse models poorly mimic human inflammatory diseases. Proc Natl Acad Sci U S A 2013;110(9):3507-12.

[30] Gonzalez LM, Moeser AJ, Blikslager AT. Porcine models of digestive disease: the future of large animal translational research. Translational Research 2015;166(1):12-27.

[31] Yandza T, Tauc M, Saint-Paul MC, Ouaissi M, Gugenheim J, Hebuterne X. The pig as a preclinical model for intestinal ischemia-reperfusion and transplantation studies. Journal of Surgical Research 2012;178(2):807-19.

[32] P. Nejdfors MEBJBRW. Mucosal in Vitro Permeability in the Intestinal Tract of the Pig, the Rat, and Man: Species- and Region-Related Differences. Scandinavian Journal of Gastroenterology 2000;35(5):501-7.

[33] Mair KH, Sedlak C, Käser T, Pasternak A, Levast B, Gerner W, Saalmüller A, Summerfield A, Gerdts V, Wilson HL, Meurens F. The porcine innate immune system: An update. 45. 2014:321-43.

[34] Patterson JK, Lei XG, Miller DD. The pig as an experimental model for elucidating the mechanisms governing dietary influence on mineral absorption. Exp Biol Med (Maywood) 2008;233(6):651-64.

[35] Käser T. Swine as biomedical animal model for T-cell research—Success and potential for transmittable and non-transmittable human diseases. Molecular Immunology 2021;135:95-115.

[36] Lunney Joan K, Van Goor A, Walker Kristen E, Hailstock T, Franklin J, Dai C. Importance of the pig as a human biomedical model. Science Translational Medicine;13(621):eabd5758.

[37] Stewart AS, Schaaf CR, Luff JA, Freund JM, Becker TC, Tufts SR, Robertson JB, Gonzalez LM. HOPX+ injury-resistant intestinal stem cells drive epithelial recovery after severe intestinal ischemia. American Journal of Physiology-Gastrointestinal and Liver Physiology 2021;321(5):G588-G602.

[38] Llanos JC, Bakonyi Neto A, Lerco MM, Clark RMO, Polachini do Valle A, Sousa MMF. Induction of Short Gut Syndrome and Transplantation in a Porcine Model. Transplantation Proceedings 2006;38(6):1855-6.

[39] Jiminez JA, Uwiera TC, Douglas Inglis G, Uwiera RRE. Animal models to study acute and chronic intestinal inflammation in mammals. Gut pathogens 2015;7:29-.

[40] Polkoff KM, Chung J, Simpson SG, Gleason K, Piedrahita JA. In Vitro Validation of Transgene Expression in Gene-Edited Pigs Using CRISPR Transcriptional Activators. The CRISPR Journal 2020;3(5):409-18.

[41] Gonzalez LM, Williamson I, Piedrahita JA, Blikslager AT, Magness ST. Cell Lineage Identification and Stem Cell Culture in a Porcine Model for the Study of Intestinal Epithelial Regeneration. Public Library of Science One 2013;8(6).

[42] van der Hee B, Loonen LMP, Taverne N, Taverne-Thiele JJ, Smidt H, Wells JM. Optimized procedures for generating an enhanced, near physiological 2D culture system from porcine intestinal organoids. Stem Cell Research 2018;28:165-71.

[43] Tumbar T, Guasch G, Greco V, Blanpain C, Lowry WE, Rendl M, Fuchs E. Defining the Epithelial Stem Cell Niche in Skin. Science 2004;303(5656):359.

[44] Gassler N. Paneth cells in intestinal physiology and pathophysiology. World journal of gastrointestinal pathophysiology 2017;8(4):150-60.

[45] St. Clair WH, Osborne JW. Crypt fission and crypt number in the small and large bowel of postnatal rats*. Cell Proliferation 1985;18(3):255-62.

[46] Totafurno J, Bjerknes M, Cheng H. The crypt cycle. Crypt and villus production in the adult intestinal epithelium. Biophysical journal 1987;52(2):279-94.

[47] Formeister EJ, Sionas AL, Lorance DK, Barkley CL, Lee GH, Magness ST. Distinct SOX9 levels differentially mark stem/progenitor populations and enteroendocrine cells of the small intestine epithelium. American Journal of Physiology-Gastrointestinal and Liver Physiology 2009;296(5):G1108-G18.

[48] Ramalingam S, Daughtridge GW, Johnston MJ, Gracz AD, Magness ST. Distinct levels of Sox9 expression mark colon epithelial stem cells that form colonoids in culture. American Journal of Physiology-Gastrointestinal and Liver Physiology 2011;302(1):G10-G20.

[49] Bastide P, Darido C, Pannequin J, Kist R, Robine S, Marty-Double C, Bibeau F, Scherer G, Joubert D, Hollande F, Blache P, Jay P. Sox9 regulates cell proliferation and is required for Paneth cell differentiation in the intestinal epithelium. J Cell Biol 2007;178(4):635-48.

[50] Jang WH, Park A, Wang T, Kim CJ, Chang H, Yang B-G, Kim MJ, Myung S-J, Im S-H, Jang MH, Kim Y-M, Kim KH. Two-photon microscopy of Paneth cells in the small intestine of live mice. Scientific Reports 2018;8(1):14174.

[51] van der Flier LG, Haegebarth A, Stange DE, van de Wetering M, Clevers H. OLFM4 Is a Robust Marker for Stem Cells in Human Intestine and Marks a Subset of Colorectal Cancer Cells. Gastroenterology 2009;137(1):15-7.

[52] Portela-Gomes GM, Stridsberg M, Johansson H, Grimelius L. Complex Co-localization of Chromogranins and Neurohormones in the Human Gastrointestinal Tract. Journal of Histochemistry & Cytochemistry 1997;45(6):815-22.

[53] Johansson MEV, Sjövall H, Hansson GC. The gastrointestinal mucus system in health and disease. Nature Reviews Gastroenterology & Hepatology 2013;10(6):352-61.

[54] Farin HF, Van Es JH, Clevers H. Redundant Sources of Wnt Regulate Intestinal Stem Cells and Promote Formation of Paneth Cells. Gastroenterology 2012;143(6):1518-29.e7.

[55] Potten CS, Kovacs L, Hamilton E. CONTINUOUS LABELLING STUDIES ON MOUSE SKIN AND INTESTINE. Cell Proliferation 1974;7(3):271-83.

[56] Muñoz J, Stange DE, Schepers AG, van de Wetering M, Koo B-K, Itzkovitz S, Volckmann R, Kung KS, Koster J, Radulescu S, Myant K, Versteeg R, Sansom OJ, van Es JH, Barker N, van Oudenaarden A, Mohammed S, Heck AJR, Clevers H. The Lgr5 intestinal stem cell signature: robust expression of proposed quiescent '+4' cell markers. The EMBO journal 2012;31(14):3079-91.

[57] Itzkovitz S, Lyubimova A, Blat IC, Maynard M, van Es J, Lees J, Jacks T, Clevers H, van Oudenaarden A. Single-molecule transcript counting of stem-cell markers in the mouse intestine. Nature Cell Biology 2012;14(1):106-14.

[58] Yu S, Balasubramanian I, Laubitz D, Tong K, Bandyopadhyay S, Lin X, Flores J, Singh R, Liu Y, Macazana C, Zhao Y, Béguet-Crespel F, Patil K, Midura-Kiela MT, Wang D, Yap GS, Ferraris RP, Wei Z, Bonder EM, Häggblom MM, Zhang L, Douard V, Verzi MP, Cadwell K, Kiela PR, Gao N. Paneth Cell-Derived Lysozyme Defines the Composition of Mucolytic Microbiota and the Inflammatory Tone of the Intestine. Immunity 2020;53(2):398-416.e8.

[59] Blache P, van de Wetering M, Duluc I, Domon C, Berta P, Freund J-Nl, Clevers H, Jay P. SOX9 is an intestine crypt transcription factor, is regulated by the Wnt pathway, and represses the CDX2 and MUC2 genes. Journal of Cell Biology 2004;166(1):37-47.

[60] Bastide P, Darido C, Pannequin J, Kist R, Robine S, Marty-Double C, Bibeau Fdr, Scherer G, Joubert D, Hollande Fdr, Blache P, Jay P. Sox9 regulates cell proliferation and is required for Paneth cell differentiation in the intestinal epithelium. Journal of Cell Biology 2007;178(4):635-48.

[61] Drost J, van Jaarsveld RH, Ponsioen B, Zimberlin C, van Boxtel R, Buijs A, Sachs N, Overmeer RM, Offerhaus GJ, Begthel H, Korving J, van de Wetering M, Schwank G, Logtenberg M, Cuppen E, Snippert HJ, Medema JP, Kops GJPL, Clevers H. Sequential cancer mutations in cultured human intestinal stem cells. Nature 2015;521(7550):43-7.

[62] Sansom OJ, Reed KR, Hayes AJ, Ireland H, Brinkmann H, Newton IP, Batlle E, Simon-Assmann P, Clevers H, Nathke IS, Clarke AR, Winton DJ. Loss of Apc in vivo immediately perturbs Wnt signaling, differentiation, and migration. Genes & development 2004;18(12):1385-90.

[63] Kim J-H, Park S-Y, Jun Y, Kim J-Y, Nam J-S. Roles of Wnt Target Genes in the Journey of Cancer Stem Cells. International Journal of Molecular Sciences 2017;18(8).

[64] Lustig B, Jerchow B, Sachs M, Weiler S, Pietsch T, Karsten U, van de Wetering M, Clevers H, Schlag Peter M, Birchmeier W, Behrens J. Negative Feedback Loop of Wnt Signaling through Upregulation of Conductin/Axin2 in Colorectal and Liver Tumors. Molecular and Cellular Biology 2002;22(4):1184-93.

[65] Roper J, Tammela T, Cetinbas NM, Akkad A, Roghanian A, Rickelt S, Almeqdadi M, Wu K, Oberli MA, Sánchez-Rivera FJ, Park YK, Liang X, Eng G, Taylor MS, Azimi R, Kedrin D, Neupane R, Beyaz S, Sicinska ET, Suarez Y, Yoo J, Chen L, Zukerberg L, Katajisto P, Deshpande V, Bass AJ, Tsichlis PN, Lees J, Langer R, Hynes RO, Chen J, Bhutkar A, Jacks T, Yilmaz ÖH. In vivo genome editing and organoid transplantation models of colorectal cancer and metastasis. Nature Biotechnology 2017;35(6):569-76.

[66] Roper J, Tammela T, Akkad A, Almeqdadi M, Santos SB, Jacks T, Yilmaz ÖH. Colonoscopy-based colorectal cancer modeling in mice with CRISPR-Cas9 genome editing and organoid transplantation. Nature protocols 2018;13(2):217-34.

[67] Barnett AM, Mullaney JA, Hendriks C, Le Borgne L, McNabb WC, Roy NC. Porcine colonoids and enteroids keep the memory of their origin during regeneration. American Journal of Physiology-Cell Physiology 2021;320(5):C794-C805.

[68] Okamoto T, duVerle D, Yaginuma K, Natsume Y, Yamanaka H, Kusama D, Fukuda M, Yamamoto M, Perraudeau F, Srivastava U, Kashima Y, Suzuki A, Kuze Y, Takahashi Y, Ueno M, Sakai Y, Noda T, Tsuda K, Suzuki Y, Nagayama S, Yao R. Comparative Analysis of Patient-Matched PDOs Revealed a Reduction in OLFM4-Associated Clusters in Metastatic Lesions in Colorectal Cancer. Stem Cell Reports 2021;16(4):954-67.

[69] Besson D, Pavageau A-H, Valo I, Bourreau A, Bélanger A, Eymerit-Morin C, Moulière A, Chassevent A, Boisdron-Celle M, Morel A, Solassol J, Campone M, Gamelin E, Barré B, Coqueret O, Guette C. A Quantitative Proteomic Approach of the Different Stages of Colorectal Cancer Establishes OLFM4 as a New Nonmetastatic Tumor Marker *. Molecular & Cellular Proteomics 2011;10(12).

[70] Beumer J, Clevers H. Regulation and plasticity of intestinal stem cells during homeostasis and regeneration. Development 2016;143(20):3639-49.

[71] Tanaka M, Saito H, Kusumi T, Fukuda S, Shimoyama T, Sasaki Y, Suto K, Munakata A, Kudo H. Spatial distribution and histogenesis of colorectal Paneth cell metaplasia in idiopathic inflammatory bowel disease. Journal of Gastroenterology and Hepatology 2001;16(12):1353-9.

[72] Flisikowska T, Merkl C, Landmann M, Eser S, Rezaei N, Cui X, Kurome M, Zakhartchenko V, Kessler B, Wieland H, Rottmann O, Schmid RM, Schneider G, Kind A, Wolf E, Saur D, Schnieke A. A Porcine Model of Familial Adenomatous Polyposis. Gastroenterology 2012;143(5):1173-5.e7.

[73] Sikorska A, Stachowiak M, Flisikowska T, Stachecka J, Flisikowski K, Switonski M. Polymorphisms of CSF1R and WISP1 genes are associated with severity of familial adenomatous polyposis in APC(1311) pigs. Gene 2020;759:144988.

[74] Sikorska A, Flisikowska T, Stachowiak M, Kind A, Schnieke A, Flisikowski K, Switonski M. Elevated expression of p53 in early colon polyps in a pig model of human familial adenomatous polyposis. J Appl Genet 2018;59(4):485-91.

[75] Rogalla S, Flisikowski K, Gorpas D, Mayer AT, Flisikowska T, Mandella MJ, Ma X, Casey KM, Felt SA, Saur D, Ntziachristos V, Schnieke A, Contag CH, Gambhir SS, Harmsen S. Biodegradable Fluorescent Nanoparticles for Endoscopic Detection of Colorectal Carcinogenesis. Advanced Functional Materials 2019;29(51):1904992.

[76] Yim JJ, Harmsen S, Flisikowski K, Flisikowska T, Namkoong H, Garland M, van den Berg NS, Vilches-Moure JG, Schnieke A, Saur D, Glasl S, Gorpas D, Habtezion A, Ntziachristos V, Contag CH, Gambhir SS, Bogyo M, Rogalla S. A protease-activated, near-infrared fluorescent probe for early endoscopic detection of premalignant gastrointestinal lesions. Proceedings of the National Academy of Sciences 2021;118(1):e2008072118.

[77] Clevers H, Tuveson DA. Organoid Models for Cancer Research. Annual Review of Cancer Biology 2019;3(1):223-34.

[78] Dehmer JJ, Garrison AP, Speck KE, Dekaney CM, Van Landeghem L, Sun X, Henning SJ, Helmrath MA. Expansion of Intestinal Epithelial Stem Cells during Murine Development. PLOS ONE 2011;6(11):e27070.

[79] Koo B-K, Clevers H. Stem Cells Marked by the R-Spondin Receptor LGR5. Gastroenterology 2014;147(2):289-302.

[80] Noordermeer D, de Wit E, Klous P, van de Werken H, Simonis M, Lopez-Jones M, Eussen B, de Klein A, Singer RH, de Laat W. Variegated gene expression caused by cell-specific long-range DNA interactions. Nature Cell Biology 2011;13(8):944-51.

[81] Ashe A, Morgan DK, Whitelaw NC, Bruxner TJ, Vickaryous NK, Cox LL, Butterfield NC, Wicking C, Blewitt ME, Wilkins SJ, Anderson GJ, Cox TC, Whitelaw E. A genome-wide screen for modifiers of transgene variegation identifies genes with critical roles in development. Genome Biology 2008;9(12):R182.

[82] Mandir N, FitzGerald AJ, Goodlad RA. Differences in the effects of age on intestinal proliferation, crypt fission and apoptosis on the small intestine and the colon of the rat. International Journal of Experimental Pathology 2005;86(2):125-30.

[83] Brunsgaard G. Morphological Characteristics, Epithelial Cell Proliferation, and Crypt Fission in Cecum and Colon of Growing Pigs. Digestive Diseases and Sciences 1997;42(11):2384-93.

[84] Kleinstiver BP, Pattanayak V, Prew MS, Tsai SQ, Nguyen NT, Zheng Z, Joung JK. High-fidelity CRISPR-Cas9 nucleases with no detectable genome-wide off-target effects. Nature 2016;529(7587):490-5.

[85] Brinkman EK, Chen T, Amendola M, van Steensel B. Easy quantitative assessment of genome editing by sequence trace decomposition. Nucleic Acids Research 2014;42(22):e168-e.

CHAPTER 4

DISSERTATION SUMMARY AND FUTURE DIRECTIONS

The research in this dissertation highlights an intracellular mechanism (HOPX) that drives intestinal stem cell (ISC) mediated epithelial repair following severe ischemic injury, as well as the timeline for this epithelial repair (Chapter 2). Additionally, to improve upon translational porcine intestinal disease models, a novel, transgenic ISC porcine model was validated (Chapter 3). Through this work, the intestinal LGR5-H2B-GFP^{hi} cells were defined as the LGR5+ ISC population and comparative *in situ* gene expression between human, mouse, and pig crypt-base cells underscored the translational potential of the porcine model. To demonstrate the utility of this model for study of ISC mechanisms during disease, a gene mutation was introduced into LGR5-H2B-GFP colonoids to produce a novel model of colorectal cancer. Future work, as outlined in the Appendix, will utilize the LGR5-H2B-GFP pig to investigate an additional signaling pathway during post-ischemic repair. Specifically, this proposal will investigate the impact of neighboring intestinal T-cells and their cytokines on ISC-mediated repair with the goal to identify therapeutic targets to improve barrier repair for both human and veterinary patients.

APPENDIX

SPECIFIC AIMS

Severe intestinal damage caused by ischemia-reperfusion (IR) injury accounts for 1/1000 US hospital admissions. Mortality rates are devastating, approaching -- 80%. While intestinal IR injury can be initiated by numerous pathologic events (e.g. trauma, emboli, intestinal strangulation), the result is the same: progressive epithelial barrier loss that leaves patients susceptible to bacterial translocation, inflammation, and sepsis. Current treatment options for the IR-injured intestine are only supportive care and/or surgical removal, with limited success. There are no therapeutic options to hasten critical intestinal epithelial barrier repair.

Endogenous epithelial barrier repair is directly achieved by proliferation of crypt-base intestinal epithelial stem cells (ISCs). This process can be substantially influenced by mucosal immune cells; during both homeostasis and infection, T-cell subsets (T-regulatory, T-helper, TCRγδ) produce cytokines (IL-10, IL-13, IL-22, KGF, IL-17a, IFNγ) that promote ISC proliferation and differentiation. However, after IR injury, the nature of localized T-cell subset populations and their responses, and how these influence critical ISC-mediated epithelial regeneration, has not been elucidated. A full knowledge of these T-cell subsets and their products, and how these provoke ISC proliferation in IR repair, can dramatically improve our understanding of intestinal injury and repair and provide new therapeutic targets.

A recurring problem in assessing intestinal IR-induced injury/repair is lack of valid animal models to investigate associated T-cell and ISC parameters. To this end, our group recently developed and validated a translational, large animal model of jejunal IR injury and recovery, the porcine surgical model. In preliminary studies using this model, and forming the basis of this application, we have shown:

a) acute injury causes significant $CD3^+$ mucosal T-cell loss and ISC apoptosis (Fig 2);

b) surviving ISCs reach peak proliferative activity 2 days post injury (2 DPI) (Fig 1);

c) coinciding with 2 DPI, $CD3^+$ T-cells repopulate around the crypt-base near proliferating ISCs (Fig 2); and

d) also at 2 DPI, $CD3^+CD4^+$ T-cells increase in number and $CD3^+FoxP3^+$ T-regulatory cells are specifically identified around the crypt-base (Fig 3 and 4).

Thus, our data suggest that $CD3^+CD4^+$ T-cells, including $FoxP3^+$ T-regulatory cells, are a crucial component promoting early epithelial regeneration. It is known that T-regulatory cells can produce anti-inflammatory cytokines. Importantly, in both intestinal homeostasis and infection models in the mouse, T-regulatory cell production of IL-10 supports ISC renewal; this may occur through signaling of JAK/STAT pathways within ISCs. Here, we propose that *T-regulatory cells, IL-10, and JAK/STAT signaling* are critical components in the mechanism of ISC proliferation during repair from IR injury.

***The specific hypothesis is that during peak ISC activation following severe small intestinal IR injury, T-regulatory cells repopulate around the crypt-base and produce IL-10 to stimulate ISC proliferation via JAK/STAT pathways*.** To address this hypothesis, we will take advantage of a major advancement to the above-described pig model, a novel transgenic ISC reporter pig, LGR5-H2B-GFP (validated in our lab [manuscript in preparation; Fig 5]), which allows, for the first time, specific *in vivo/ex vivo* ISC interrogation in a clinically relevant large animal model. The specific aims are:

1. To determine whether IL-10 producing T-regulatory cells (Foxp3+) are the predominant subset around crypt-base ISCs, and if proliferating ISCs express the IL-10 receptor in jejunum recovering from IR injury. 1a. Quantify T-cell phenotypes in early mucosal repair by flow cytometry analysis ($CD4^+$, $CD8^+$, $TCR\gamma\delta^+$, $Foxp3^+$). 1b. Map proximity of

T-cell subsets to ISCs by immunofluorescent microscopy of recovering jejunum. 1c. Profile transcriptome of T-cell cytokines and corresponding receptors on ISCs using RNAseq of both laser micro-dissected crypt-base area mucosa and sorted LGR5-H2B-GFP ISCs from recovering tissue.

2. To determine, following severe jejunal ischemic injury, whether IL-10 produced by T-regulatory cells activates JAK/STAT pathways within ISCs to promote proliferation. 2a. In *ex vivo* 3-D culture, measure proliferation of ischemic injured LGR5-H2B-GFP ISCs in the presence of IL-10 and other T-cell cytokines that promote normal ISC function (IL-13, IL-22, KGF, IL-17a, IFNγ) and determine downstream ISC pathway transcriptome by RNAseq. 2b. Measure proliferation and downstream ISC pathway transcriptome of injured LGR5-H2B-GFP ISCs co-cultured with individual T-cell subsets present in recovery, including T-regulatory cells.

Successful completion of the aims will provide critical understanding of how intestinal T-cell dynamics and signaling impact ISC proliferation following severe IR injury. Our results will identify novel therapeutic pathways that can promote epithelial regeneration and increase survival. Training goals: Develop expertise in immune cell profiling, bioinformatics analysis, advanced ISC co-culture, and immune aspects of ISC activation. This work will provide preliminary data for a future K01 application. Collaboration with other labs through this work will develop my research and technical skills to advance my portfolio as I pursue a career as a clinician-scientist.

RESEARCH STRATEGY

(A) Significance:

Significant patient mortality rates – 80% -- are associated with severe small intestinal ischemia reperfusion (IR) injury. [1, 2] While intestinal IR injury is induced by numerous pathologic events (e.g. emboli, shock, intestinal strangulation), the result is the same: progressive epithelial barrier loss leaving patients susceptible to bacterial translocation, inflammation, and sepsis. [1-3] Because the majority of IR injury is not preventable, aggressive medical and/or surgical interventions are necessary to mitigate the sequelae of epithelial loss, but this has limited success. Therefore, there is a critical need to develop therapies that promote epithelial barrier regeneration.

The small intestinal epithelial barrier is comprised of a single layer of cells, continually renewed by intestinal epithelial stem cells (ISC). Severe IR damage (≥3hr ischemia) leads to over 75% acute loss of surface epithelium, extending down to the crypt-base ISCs. [3] Preliminary studies, using our translational porcine model of IR injury and recovery, demonstrated that the surviving ISCs begin barrier renewal starting at 2 days post injury (DPI) (**Fig 1**). Limited research has been conducted to evaluate signaling mechanisms that control this ISC mediated epithelial repair; even less has focused on clinically relevant disease states such as IR injury. This represents a critical limitation in our ability to improve patient survival from IR injury.

A potential source of ISC epithelial repair signals resides in the mucosa adjacent to ISCs – intestinal immune cells. Expanding literature shows that in both homeostasis and non-IR disease models, intestinal immune cell populations promote ISC proliferation and differentiation. [4-7] One such population is intestinal T-cells. While in some immune-mediated injury states (e.g. graft-vs-host disease), T-cells have been shown to have detrimental effects on ISC viability and

proliferation, [5, 8, 9] recent studies now show that T-cell subsets (T-helper, T-regulatory, TCRγδ) and their cytokine products promote ISC functions. Specifically, CD4+ T-helper cells, including T-regulatory cells, and their cytokines (interleukin [IL]-10, IL-22, IL-13, IL-17a, and interferon-γ [IFNγ]) are critical for ISC renewal and differentiation, both in homeostasis and following enteric infection. [4, 5, 9] These ISC renewal and differentiation functions are, in part, due to cytokine signaling of JAK/STAT pathways within ISCs. [5, 10, 11] A recent paper showed that after acute intestinal inflammation, JAK/STAT signaling is required for activation of ISCs to repair the epithelial barrier. [12] However, in repair stages after severe IR injury, the interactions of T-cells and their products with ISCs and subsequent signaling of ISC JAK/STAT pathways have not been investigated.

In murine acute intestinal IR injury studies, overall T-cell numbers decrease. [13-16] Preliminary data from our translational porcine model of severe IR injury confirms acute T-cell loss. Once acute injury ceases and epithelial repair begins, CD3+ T-cells repopulate around crypt-based ISCs,including increase in CD3+CD4+ T-cells (T-helper, T-regulatory) (**Fig 2, 3**); however, the role of these T-cells in ISC-mediated epithelial repair is unknown. Non-intestinal IR models showed a similar increase of CD4+CD25+ T-regulatory cells in recovering kidney, liver, and muscle, starting 3 days after injury. These T-regulatory cells supported healing through production of IL-10, which inhibited inflammation and promoted tissue regeneration and vessel formation. [17-19] The critical role of T-regulatory cells in homeostatic ISC renewal, [4] as well as the ability of T-regulatory cells to repopulate and promote healing in non-intestinal IR damage, [17-19] justifies our **hypothesis that T-regulatory cells repopulate the ISC niche after severe IR injury and produce IL-10 to signal ISC proliferation via JAK/STAT pathways**.

After IR damage, T-cells likely serve as a critical source of cytokine signals to initiate ISC proliferation for epithelial repair. Without quick epithelial barrier repair, bacteria translocate from the lumen, induce systemic inflammation, and lead to sepsis; these sequelae result in the devastatingly high IR injury mortality rates. *To prevent these high mortality rates in IR patients, it is critical to define the relationship between T-cells and ISC proliferation and, thereby, identify novel therapies to promote ISC-mediated epithelial regeneration.*

To investigate dynamics of T-cells and their products in IR injury/recovery (**Aim 1**) and their role in ISC-mediated epithelial repair (**Aim 2**), this proposal utilizes an innovative combination of a novel transgenic ISC reporter pig, LGR5-H2B-GFP, developed by my co-sponsor (Dr. Piedrahita) and validated in our lab (**Fig 5**, manuscript in preparation) to be used in our well-published porcine model of reversible, prolonged ischemic injury. [3, 20, 21] Pigs are an incredibly advantageous translatable human health model; their size, intestinal physiology, and immune system is closely matched to that of humans, making pigs the ideal clinical disease model. [20-24] With availability of the first transgenic ISC reporter pig and my background as a veterinary scientist, this proposal is uniquely poised to answer targeted questions on both ISC and T-cell dynamics with IR injury. This proposal will help me develop a better understanding of immune cell roles in ISC biology while I work towards an independent career focused on therapeutics to improve outcome for patients suffering from gastrointestinal disease.

(B) Approach: ***The specific hypothesis is that during peak ISC activation following severe small intestinal IR injury, T-regulatory cells repopulate around the crypt-base and produce IL-10 to stimulate ISC proliferation via JAK/STAT pathways*****.**

Background/Supporting Data

Timeline of ISC mediated epithelial repair: In a porcine model of reversible intestinal mesenteric vascular occlusion, ischemia of varying duration can be induced within a single animal. The intestinal epithelium can be collected immediately post ischemic injury for analysis and *ex vivo* culture, or the animal can be recovered to study *in vivo* intestinal repair 1-3 days post injury (DPI). [3] Using this approach, performed prior to LGR5-H2B-GFP pig model availability, we identified significant loss of ISCs by apoptosis in severe acute ischemia (≥3hr). [3] In new preliminary histomorphometric and immunofluorescent (IF) analysis of acute IR injury and 1-3 DPI jejunum (n=3 per time point), our lab mapped out the timeline of ISC-mediated epithelial repair. Histologic analysis revealed both an increase in crypt epithelium mitotic figures and a shift to a cuboidal phenotype at 2 DPI, indicative of increased cellular proliferation. To demonstrate that these proliferating cells are ISCs, cell counts using ISC biomarker (SOX9) co-localized with proliferative marker KI67 showed a significant increase in percent of activated ISCs (SOX9+KI67+) per total ISCs (SOX9+) per crypt at 2 DPI compared to non-injured control (p=0.007) (**Fig 1**). Given this marked increase in proliferative features and

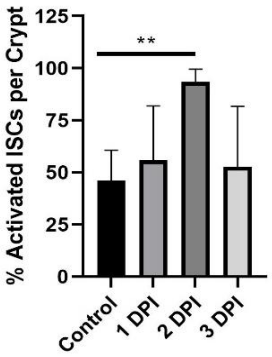

Fig 1: Percent activated ISCs/crypt increases at 2 DPI. IF analysis to quantify SOX9+KI67+ ISCs per total ISCs (SOX9+) per crypt.

T-cell Loss at 1 DPI and Rebound at 2 DPI Using IF and FCM Analysis

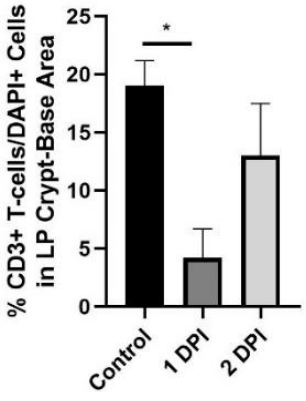

Fig 2: IF analysis of crypt-base LP demonstrates loss in percent of CD3+ T-cells/DAPI+ cells at 1 DPI.

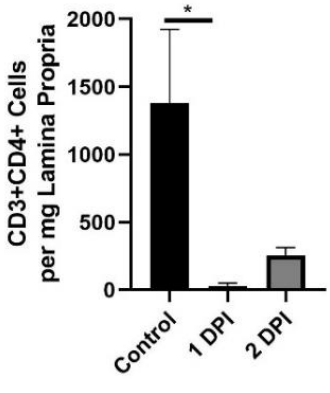

Fig 3: FCM analysis of total LP confirm loss of CD3+CD4+ T-cells per mg of tissue at 1 DPI.

significant ISC activation, 2 DPI was labeled the early regenerative stage with peak ISC activation. By 3 DPI, histologic analysis showed complete restitution of the luminal epithelium, indicative of advanced healing. [25] Despite strong evidence, these studies in non-transgenic animals are limited to histologic analysis. The LGR5-H2B-GFP animal, proposed for use in this study, will enable the identification and isolation of live ISCs for thorough analysis.

Mucosal T-cell dynamics in a porcine model of severe IR injury: In the intestine, peripheral lymphocytes located outside of gut associated lymphoid tissue (GALT; Peyer's patches and mesentery lymph nodes) are classified by their effector locations -- intraepithelial lymphocytes (IELs) or lamina propria (LP) lymphocytes (LPLs). Both populations contain major T-cell subsets: TCRγδ, T-helper, T-regulatory, and cytotoxic T-cells. These cells function locally to respond to luminal microbes, support epithelial barrier maintenance, and balance inflammatory responses. Consistent with recent literature that describes loss of both IEL and LPL populations during acute IR injury in the intestine, [13, 26] our preliminary investigations, using IF and flow cytometry (FCM) analysis, confirm a time line of T-cell loss and re-population when evaluating porcine tissue immediately following acute injury and 1-2 DPI (n=2 per time point). Quantification by IF analysis showed significant loss in percent of CD3+ T-cells per total DAPI+ cells around the crypt base at 1 DPI compared to control ($p=0.02$), followed by an increase at 2 DPI, the early regenerative stage (**Fig 2**). Additional T-cell subset quantification by FCM analysis of total LPLs in control and 1-2 DPI jejunum revealed significant loss of CD3+CD4+ T-cells at 1 DPI ($p=0.045$) followed by an increase at 2 DPI (**Fig 3**). These CD3+CD4+ T-cells include T-helper and T-regulatory cells. Specific analysis by IF of 2 DPI tissue confirmed the presence of CD3+FoxP3+ T-regulatory cells in crypt-base LP (**Fig 4**) Using multiple modalities we have, therefore, preliminarily identified an increase in CD3+CD4+ T-cell number near the crypt-base that coincides with peak ISC activation,

suggesting a role of T-cell subsets in critical epithelial repair processes following severe IR injury.

Aim 1. To determine whether IL-10 producing T-regulatory cells (Foxp3+) are the predominant subset around crypt-base ISCs and if proliferating ISCs express the IL-10 receptor in jejunum recovering from IR injury.

Subaim.1A *Quantify T-cell phenotypes in early regenerative intestinal mucosa by flow cytometry analysis.* Using the porcine surgical ischemia model developed in the Gonzalez lab, [27] ischemic injury will be induced by reversible occlusion of jejunal mesenteric vessels in 6-8 week old LGR5-H2B-GFP male and female pigs. In this pig, ISCs are specifically identified by gating for GFP^{hi} cells (publication in preparation). Within a single animal, 10 cm segments of jejunum will be isolated and ischemia will be induced for 3hrs to create severe injury. An additional segment will be identified at the start of surgery as an internal control. Animals will either be euthanized immediately following ischemic injury or recovered for 1, 2, or 3 DPI prior to euthanasia and tissue collection.

Table 1: T-Cell immunophenotyping strategy for flow cytometry.

T-Cell Type	**Markers**
All T-cells	CD3+
TCRγδ	CD3+TCRγδ+
TCRαβ	CD3+TCRγδ-
Subsets:	
CD8	CD3+TCRγδ-CD8α+
CD4 (Th1, Th2, Th17)	CD3+TCRγδ-CD4+; IFNγ+; GATA3+; IL-17a+
T-reg	CD3+TCRγδ-CD4+FoxP3+

From control and injured jejunum at each time point, GALT will be excluded by dissection, and LPLs and IELs will be separately collected using an established intestinal immune cell isolation protocol in our lab. Briefly, the entire intestinal epithelium, including IELs, will be collected through dissociation with EDTA and DTT. The remaining denuded LP will be digested both enzymatically (Liberase TM, Sigma Aldrich) and mechanically (gentleMACS dissociator, Miltenyi Biotec) to create a single cell suspension that includes the LPLs. Both IELs and LPLs

will be independently analyzed by FCM using a porcine specific multi-color antibody panel developed and validated with the help of our collaborator, Dr. Kaeser (**Table 1**). [24, 28, 29]

Data Analysis and Sample Size: T-cell phenotypes from control, acute injured, and 1-3 DPI jejunum will be evaluated by FCM analysis of LP lymphocytes and IELs independently. Analysis will be performed using a Beckman Coulter CytoFLEX available through the NCSU Flow Cytometry and Cell Sorting Core (see support letter). Flow cytometry data will be analyzed using FlowJo 10 (BD Biosciences). Statistical analyses will be performed using GraphPad Prism 8.0. Statistical differences between T-cell phenotype percentages and total cell number per gram of tissue from all injury/recovery timepoints will be both performed using a one-way ANOVA with a post-hoc Tukey's test for multiple comparisons. Interactions with $p<0.05$ will be considered significant. Based on preliminary cell count data, and with a power of 0.80 and a p-value of 0.05, and to account for potential sex differences, a minimum sample size of 6 animals for each time point is needed (acute and 1, 2, 3 DPI; 24 animals total for Aim 1; JMP Pro 15). Equal numbers of males (3) and females (3) will be used per time point.

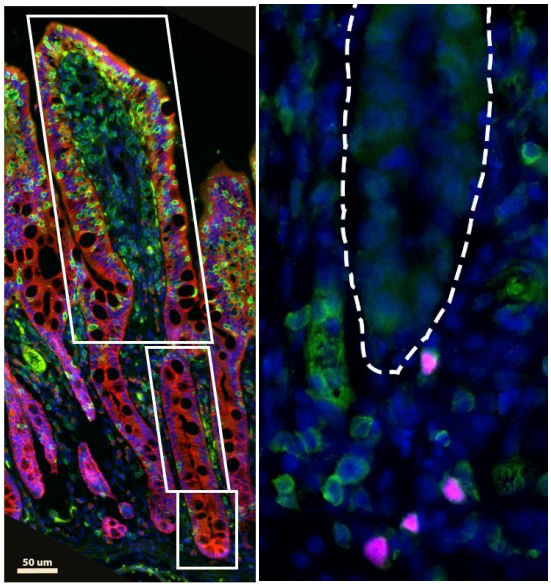

Fig 4: Spatial quantification of CD3 and FoxP3 T-cells by IF analysis. (Left) Representative IF image of CD3+ T-cells (green), E-cadherin+ epithelium (red), and DAPI+ cells (blue) in control jejunum. Boxes demarcate crypt-base, crypt-neck, and villus. **(Right)** T-regulatory cells are identified in crypt-base LP of 2 DPI tissue by FoxP3 (magenta) and CD3 (green) co-localization. Crypt epithelium outlined by white dotted line.

Subaim.1B *Map proximity of T-cell subsets to ISCs by immunofluorescent microscopy of recovering jejunum.* To quantify an increase in repopulating T-cell subsets specifically surrounding the recovering crypt-base ISCs, fixed and embedded

samples of jejunum from pigs in 1A will be analyzed by immunofluorescent analysis. Porcine specific antibodies will be used to identify numbers of CD3+, CD4+, FoxP3+, CD8+, and TCRγδ+ T-cells (Bio-rad, SouthernBiotech, Invitrogen, Kingfisher Biotech) and E-Cadherin+ (Abcam) epithelium containing ISCs (GFP+, Abcam).

Data Analysis: For quantitative analysis, 10-20 images (20x magnification) per T-cell subset (CD3+, CD4+, FoxP3+, CD8+, or TCRγδ+) per time point from all pigs in 1A (control, acute, and 1-3 DPI) will be collected, with each image containing a complete villus-crypt axis that extends from muscularis mucosa to lumen. Using ImageJ (NIH), identically measured areas will be drawn on each image to demarcate crypt-base region (containing ISCs and adjacent LP), crypt neck region (containing partially differentiated transit-amplifying, progenitor epithelial cells and adjacent LP), and villus region (**Fig 4**). T-cell subset and total cell (DAPI+ for LP and DAPI+E-cadherin+ for epithelium) number will be counted for both LP and epithelial populations in each area (Cell Counter, ImageJ). At least 10 total areas per region (crypt-base, crypt neck, villus) per time point will be counted. Evaluators will be blinded to time point. Statistical differences in T-cell subset counts between each image area and between time points will be assessed using two-way ANOVA with post-hoc analysis for multiple comparisons, with $p<0.05$ considered significant.

Subaim.1C *Spatially profile T-cell cytokine transcriptomics and corresponding cytokine receptors on ISCs within early regenerative mucosa.* To elucidate T-cell transcriptomics and highlight potential T-cell cytokine interactions with recovering ISCs, jejunum from pigs in 1A (acute injured and 1-3 DPI) will be collected for laser capture microdissection (LMD; Leica). Briefly, fresh tissue sections will be snap frozen, embedded in Optimal Cutting Temperature media (OCT, TissueTek) and stored at -80^{o} C until cryostat sectioning. Cut, frozen sections will then be briefly fixed in 70% ethanol, stained for H&E, and then the lamina propria surrounding crypt-base

(LPLs) and crypt-base epithelium (IELs) will be separately collected via LMD.[30] Bulk RNA-sequencing (RNAseq) of dissected lamina propria and epithelium will be separately assessed (to keep LPLs and IELs distinct) for differences in T-cell stimulatory markers, proliferation, cytokines, and chemokine expression. To identify the corresponding cytokine receptors on ISCs, fresh intestinal epithelium from all pigs in 1A will be isolated immediately at euthanasia, as described previously by our lab[27] and then dissociated to single cell suspension by Dispase (Corning). From this, LGR5-H2B-GFP^{hi} cells (ISCs, **Fig 5**) will be isolated using Fluorescence Activated Cell Sorting (FACS) and sequenced. Directional RNA library prep and mRNA sequencing will be performed with assistance from NCSU Genomic Sciences Lab (see letter of support), utilizing the NovaSeq 6000 platform (Illumina). Based on bulk sequence analysis, *in situ* validation of cytokine gene expression, particularly IL-10, in the same sections of porcine tissue will be performed using RNAscope fluorescent *in situ* hybridization (ACDBio). This technology is already in use in our lab to identify ISC gene expression and will utilize previously developed and validated porcine mRNA probes for cytokines, their receptors, and T-cell marker targets highlighted by RNAseq. Porcine-specific IL-10 antibody (R&Dsystems) is also available to validate *in situ* protein production by IF.

Data Analysis: Results will be analyzed with support of the Bioinformatics Core and Biostatisticians at NCSU (see letter of support). After sequencing, samples will be mapped to the *Sus scrofa* transcriptome plus the additional genomic insertions included in the transgenic LGR5-H2B-GFP pig. Transcriptome mappings will be quantified via the software package Salmon; those will be loaded into the R package DESeq2 (r-project.org). After filtering and quality control steps, DESeq2 will be used to perform likelihood ratio tests of a model that contains information for sex and time versus a model that contains only sex. This will allow adjustment for any differences in

gene expression due to sex while testing for differences across time. Genes that have been differentially expressed will be used as input for Gene Ontology and KEGG pathway classification.

Expected Outcomes – Aim 1: As indicated by preliminary data and previous literature, I expect, by IF analysis, a significant increase in crypt-base CD4+ T-helper cells (which include T-regulatory cells) at 2 DPI compared to the loss seen in 1 DPI tissue. More specifically, by FCM analysis, I expect a significant increase in CD4+FOXP3+ T-regulatory cells at 2 DPI, consistent with previous non-intestinal IR-injury models. [17-19] This population increase may be due to proliferation of resident, inducible T-regulatory cells that remain following severe IR injury. [31] Detailed RNAseq analysis and confirmation by RNAScope *in situ* hybridization of crypt-base lamina propria and epithelium at 2 DPI will also show an increased expression of cytokines previously associated with ISC proliferation, including IL-10, IL-22, Keratinocyte Growth Factor (KGF), as well as increased expression of markers of T-cell activation (CD69, Helios, CD40L, etc). Reciprocal cytokine receptors will be expressed by recovering ISCs. Overall, these experiments will highlight specific T-cell subsets and their cytokines present at the time of peak ISC activation following severe IR injury.

Training Goals – Aim 1: To develop proficiency in advanced FCM techniques for immune cell phenotyping with the collaboration of Dr. Kaeser (1A), as well as implementing and understanding complex bioinformatics analyses (1C). By learning RNAseq methods and analysis with the collaboration of Dr. Piedrahita, the Genomic Sciences Lab, and the Bioinformatics Core, I will gain an invaluable skill set of next generation sequencing and open doors for detailed examination of cell signaling pathways. I will also learn, through advanced FCM analysis and RNAseq, increasingly detailed methods of T-cell phenotyping, thereby improving my knowledge

of T-cell biology. Drs. Piedrahita and Gonzalez will provide additional guidance in the use and interpretation of this novel large animal translational model. Dr. Gonzalez will provide guidance for IF imaging interpretation (1B).

Potential Problems/Alternative Approach/Future Directions – Aim 1: Limitations include the inability to differentiate by IF between all porcine CD4+ T-helper cell subsets (e.g. T-reg, Th1, Th2, Th17), due to a lack of validated antibodies for IF. While using a mouse model would allow for more specific histologic T-cell differentiation, the use of RNAseq and RNAscope in 1C will provide detailed information on porcine T-cell phenotypes. Additionally, 2-D imaging techniques (1B) may not capture the full extent of T-cell dynamics in recovering tissue. Three-dimensional analysis of cell count per tissue volume (e.g. immunolabeling-enabled imaging of solvent-cleared organs) is an alternative approach.[8, 32] (Chen 2021) Future directions include performing single cell RNAseq on mucosal immune cell populations to identify individual detailed T-cell phenotypes, as well as delineating if T-cell re-population around the crypt base is primarily due to proliferation of resident T-cells remaining after injury or homing of newly activated T-cells. Performing single cell RNAseq will also help to determine other potential sources of IL-10 in the recovering intestine, which, in homeostasis and other disease models, includes macrophages, B-cells, innate lymphoid cells, and even some intestinal epithelial cells. Additional prolonged recovery studies (i.e. 7-14 DPI) are also warranted to investigate any long-term changes to T-cell subsets and tissue remodeling.

Aim 2. To determine, following severe jejunal ischemic injury, whether IL-10 produced by T-regulatory cells activates JAK/STAT pathways within ISCs to promote proliferation.

Subaim.2A *Using ex vivo 3-D culture, measure proliferation of ischemic injured LGR5-H2B-GFP ISCs in the presence of IL-10 and other T-cell cytokines that promote normal ISC function.* Juvenile LGR5-H2B-GFP transgenic pigs will undergo acute ischemic injury without recovery as described in 1A, and 3hr ischemic tissue will be collected at the time of euthanasia (n=6; 3 male and 3 female). In these pigs, ISCs express GFP tagged to Histone 2B (H2B-GFP), and this H2B-GFP expression is driven by the *Lgr5* promoter, a gene specific to adult stem cells. Experiments from our lab (gene expression, histology, stem cell culture) confirms that FACS sorted intestinal LGR5-H2B-GFP^{hi} cells are bona fide ISCs (**Fig 5**, manuscript in preparation). For this proposal, single LGR5-H2B-GFP^{hi} ISCs will be isolated after injury and sorted as described in 1C, and subsequently plated in 3-D Matrigel (Corning) for enteroid culture. [27, 33] Recombinant, bioactive T-cell cytokines IL-10, IFN-γ (porcine) and IL-22, IL-13, IL-17a, KGF (human) (R&D Systems), as well as vehicle controls, will be added in previously published concentrations, both individually and together as a "cytokine soup" to culture media at time of plating. [4, 5, 34-36] These cytokines are both produced by intestinal T-cells (T-helper, T-regulatory, TCRγδ) and promote ISC proliferation/differentiation in homeostasis and non-IR intestinal disease models. [4, 34-36] Cytokines will be supplemented to the media every 48hr with media changes. Resultant enteroids will be imaged and processed out to 192hr post-plating (Day 8) to define injured ISC response to cytokine signaling. This will allow for development of mature, budding enteroids that contain post-mitotic enterocytes (**Fig 5B**).

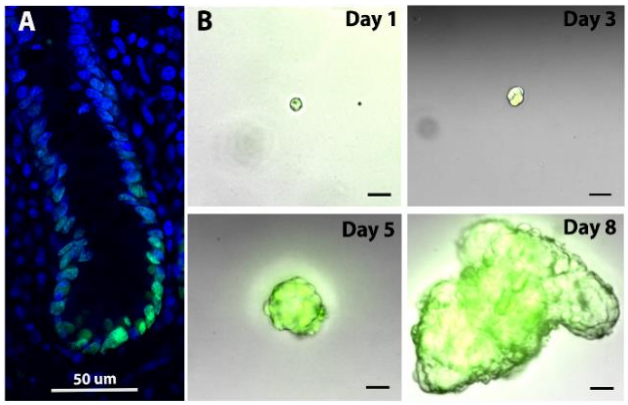

Fig 5: Intestinal LGR5-H2B-GFP^{hi} cells are ISCs. (A) Endogenous GFP (green) expression in crypt-base ISCs, (B) growth of enteroid from single LGR5-H2B-GFP^{hi} cell. Scale 20 μm.

Enteroid growth will be assessed through daily efficiency counts, area measurements, and proliferative bud unit counts. Enteroids will be collected for histologic assessment of proliferation (EdU; Click-it Kit, Invitrogen) and RNAseq to examine expression of ISC/post-mitotic gene signatures and proliferation pathways.

Data Analysis: Based on previous published cell culture work (power of 0.80; p-value of 0.05), and to account for potential sex differences, a minimum n of 6 animals is needed (3 males, 3 females). All samples in culture will be plated with 3 technical replicates; evaluators will be blinded to treatment group. Growth efficiency will be determined by dividing the number of enteroids grown over 192hrs by the number of single cells plated at time 0. Resultant enteroids will be counted and imaged for area/bud measurements every 24hrs. Enteroid area, bud count, and proliferative biomarkers will determine ISC activation and proliferation. For histologic proliferative biomarkers, enteroids grown to 72hr and 192hr will be EdU pulsed one hour prior to collection to identify cells within the S phase of the cell cycle. Enteroids will then be fixed and processed for IF assays to visualize and quantify proliferating ISCs by EdU co-localization with ISC biomarkers (GFP, Abcam; SOX9, Millipore; HOPX, Abcam), allowing comparison between groups.[37] Statistical differences of efficiency, area, bud unit count, and EdU/biomarker counts between ischemic-injured crypts grown in the presence or absence of cytokines will be performed using a two-way ANOVA with a post-hoc Tukey's test for pairwise comparisons with $p<0.05$ considered significant. RNAseq of 72hr enteroids, an ISC enriched timepoint, will be performed as described in 1C to quantify differences in gene expression of ISC biomarkers and proliferation signatures (e.g. *SOX9, HOPX, LRIG, LGR5, OLFM4, Ki67, PCNA*) and mature, differentiated cell signatures (e.g. *LYZ, MUC2, CGA, SGLT1, CCK, ATOH1, FABP*), as well as up-regulated proliferation pathways including JAK/STAT.

Subaim.2B *Measure proliferation of ischemic injured LGR5-H2B-GFP ISCs co-cultured with individual T-cell subsets present in recovery, including T-regulatory cells, and determine downstream ISC pathway transcriptome.* To create a co-culture system of ISCs and stimulated, cytokine-producing T-cells from the same animal, T-cells will be isolated and activated to produce cytokines 3 days prior to surgical induction of ischemic injury in the pigs from 2A (n=6; 3 male and 3 female). Citrated whole blood will be collected from the pig by jugular venipuncture. Peripheral blood mononuclear cells (PBMCs) will be isolated by Ficoll density-gradient separation. The following T-cell isolation and stimulation protocols have been validated and published by Dr. Kaeser. [28, 38-40] Briefly, CD4+ lymphocytes will be sorted by magnetic activated cell sorting using anti-CD4 and corresponding microbeads (Miltenyi Biotec). CD4+CD25- (T-helper) and CD4+CD25+ (T-regulatory) cells will then be FACS sorted and cultivated/stimulated by plate-bound anti-CD3 (PPT7, 1.5 µg/ml), ConA (GE Helathcare, 2.5 µg/ml), and rpIL-2 (R&D Systems, 20 ng/ml). To isolate and stimulate TCRγδ T-cells, TCRγδ+ cells will be FACS sorted from PBMCs and stimulated and cultivated with ConA and rpIL-2.[39]

On the day of surgery, LGR5-H2B-GFP^{hi} ISC single cells will be FACS sorted from 3hr ischemic injured jejunum. Individual, stimulated, CellTrace Violet (ThermoFisher) stained T-cell subsets (T-helper, T-regulatory, or TCRγδ) and injured ISCs from the same pig will be co-cultured in Matrigel in a ratio of approximately 20:1. [4, 5, 41, 42] To account for potential cell-to-cell contact signaling versus cell cytokine signaling, T-cells will be both mixed into the Matrigel with ISCs (to allow for cell contact) in one set of wells or suspended in the media in a separate set of wells (reduce cell contact). [42] The CellTrace Violet staining will allow visual confirmation of T-cells in the culture system. T-cell cytokine production in co-culture supernatant will be quantified every 48hrs by porcine ELISAs (Biosource). As a control, ischemic injured LGR5-

H2B-GFP^{hi} ISCs will be cultured without T-cells. To define activated T-cell subset impact on ISC proliferation, enteroid growth will be assessed by daily efficiency counts, area measurements, proliferative bud unit counts out to 96hr, and be collected for histology (EdU proliferation assay, 72 and 96hr). Enteroids at 72hrs in culture will be collected for RNAseq to identify both ISC/post-mitotic gene signatures and ISC cellular proliferation pathways, including JAK/STAT.

Data Analysis: All samples in culture will be plated with 3 technical replicates, with sample size of 6 animals (2A). Evaluators will be blinded to T-cell subset co-culture group. Analysis of enteroid growth by area measurement, efficiency, proliferative biomarkers and bud unit count will be performed as described (2A). RNAseq analysis of co-cultured and control enteroids at 72hrs post-plating will be performed as described (2A).

Expected Outcomes – Aim 2: Addition of recombinant IL-10 to ischemic injured ISC culture will increase overall enteroid growth efficiency, area, and cell proliferation (EdU+) compared to injured ISCs grown alone (2A). LGR5-H2B-GFP^{hi} ISCs and T-cell subset co-cultures (2B) will show that compared to ischemic injured ISCs grown alone, injured ISCs grown with T-regulatory cells that produce IL-10 will significantly increase ISC proliferation (overall enteroid growth efficiency, area, and cell proliferation). Additionally, through RNAseq analysis, more proliferative enteroids will have upregulated JAK/STAT signaling, in-line with recent literature.[11, 12]

Training Goals – Aim 2: To develop proficiency in paracrine cell signaling models in a translational porcine model. This will be accomplished using co-cultured enteroids/T-cells to assess functional outcome. Drs. Kaeser and Gonzalez, well published in porcine T-cell and ISC cultures, respectively, will guide me in the co-culture systems. [3, 28, 37-39] Dr. Piedrahita will again provide valuable guidance in the interpretation of findings in a transgenic model. Completion

of this aim and its findings will build my foundations in study design of advanced co-culture methods, RNAseq for signaling pathway analysis, large animal transgenic models, and collaboration with multiple labs to develop a future K01 application.

Potential Problems/Alternative Strategies/Future Directions – Aim 2: Some human recombinant proteins will be used since the bioactive porcine recombinant proteins are not currently available (2A). The human analogue protein sequences are closely aligned to porcine (BLAST alignment, NCBI NIH); the Kaeser lab has successfully utilized recombinant human cytokines to induce porcine cell responses. [28, 38] Also, *in vivo* ischemia is used because we believe that it best represents the clinical conditions, however an alternative method to study T-cell subset and cytokine impact on enteroid development is the use of a hypoxia chamber (Dako, available in the Gonzalez lab) to induce injury *ex vivo*. Additionally, RNAseq analysis of enteroids will not reveal individual cell transcriptomes; single cell RNAseq may be performed here, time allowing. Also, it is likely that other cytokines in 2A and TCRγδ co-cultures will also increase injured ISC proliferation *ex vivo* as those cytokines and cells have shown to promote ISC function in homeostasis. [4, 34-36] However, considering few TCRγδ T-cells are present at 2 DPI (preliminary data), the *in vivo* relevance of these findings will be limited. Future, longer-term *in vivo* recovery studies could identify when other T-cell subsets contribute to epithelial repair.

Timeline and Feasibility: The timeline to complete the above experiments and training goals is 2 years. Surgical modeling and ISC culture techniques are routinely used in the Gonzalez laboratory, and I have extensive experience with the porcine surgical ischemia model, crypt isolation/cell culture, and subsequent analysis techniques. Porcine IR injury with recovery surgeries are on-going in the Gonzalez lab, making samples readily available. Dr. Kaeser (NCSU) has extensive experience with both FCM analysis and T-cell culture; he will continue to guide me

in those portions of the study. Both Drs. Piedrahita and Gonzalez will provide key mentorship regarding the study design in a transgenic large animal model, data analysis, and dissemination of results through presentations and publications. Core facilities at NCSU will provide additional support for experiments and data analyses. I will complete the experiments efficiently with specific benchmarks to assess progress, concluding with a K01 application and PhD training completion.

Future Directions: The aims in this F32 proposal will elucidate signaling pathways between T-cell subsets and ISCs to mediate intestinal barrier repair after severe IR injury. Future directions include to block cytokine function *in vivo/ex vivo* and develop porcine T-cell subset knock-out models. Such models would both examine the effect of T-cell absence on epithelial regeneration and allow new T-cell biology studies in a clinically relevant large animal model. RNAseq (2A, B) will highlight specific ISC proliferation signaling pathways, including JAK/STAT, for future manipulation using methods such as pharmacologic blocking or silencing by interfering-RNA within recovering ISCs. By studying these pathways, I will develop the tools to build an independently funded research lab that effectively uses interdisciplinary and translational techniques including large animal modeling, bioinformatics, and signaling pathway manipulation. In the training plan outlined in this proposal, I will gain fundamental research, mentorship, and collaboration skills by directing this project from inception to dissemination of results. This will favorably position me to submit a K01 proposal using findings from this grant and support my career trajectory to be an independent and successful veterinarian clinician-scientist in gastrointestinal pathophysiology.

REFERENCES

[1] Grootjans J, Lenaerts K, Derikx JPM, Matthijsen RA, de Bruine AP, van Bijnen AA, van Dam RM, Dejong CHC, Buurman WA. Human intestinal ischemia-reperfusion-induced inflammation characterized: experiences from a new translational model. Am J of Path 2010;176(5):2283-91.

[2] Blikslager AT, Moeser AJ, Gookin JL, Jones SL, Odle J. Restoration of barrier function in injured intestinal mucosa. Physiological Reviews 2007;87(2):545-64.

[3] Gonzalez LM, Amy SS, Freund J, Cecilia RK, Dekaney CM, Magness ST, Blikslager AT. Preservation of reserve intestinal epithelial stem cells following severe ischemic injury. American Journal of Physiology-Gastrointestinal and Liver Physiology 2019;316(4):G482-G94.

[4] Biton M, Haber AL, Rogel N, Burgin G, Beyaz S, Schnell A, Ashenberg O, Su C-W, Smillie C, Shekhar K, Chen Z, Wu C, Ordovas-Montanes J, Alvarez D, Herbst RH, Zhang M, Tirosh I, Dionne D, Nguyen LT, Xifaras ME, Shalek AK, von Andrian UH, Graham DB, Rozenblatt-Rosen O, Shi HN, Kuchroo V, Yilmaz OH, Regev A, Xavier RJ. T Helper Cell Cytokines Modulate Intestinal Stem Cell Renewal and Differentiation. Cell 2018;175(5):1307-20.e22.

[5] Lindemans CA, Calafiore M, Mertelsmann AM, O'Connor MH, Dudakov JA, Jenq RR, Velardi E, Young LF, Smith OM, Lawernce G, Ivanov JA, Fu Y, Takashima S, Hua G, Martin ML, O'Rourke KP, Lo YMM, Romera-Hernandez M, Cupedo T, Dow LE, Nieuwenhuis EE, Shroyer NF, Liu C, Kolesnick R, van der Brink MRM, Hanash AM. Interleukin-22 promotes intestinal-stem-cell-mediated epithelial regeneration. Nature 2015;528(24/31):560-4.

[6] Parks OB, Pociask DA, Hodzic Z, Kolls JK, Good M. Interleukin022 Signaling in the Regulation of Intestinal Health and Disease. Frontiers in Cell and Developmental Biology 2016;3:1-13.

[7] Sonnenberg GF, Artis D. Innate lymphoid cells in the initiation, regulation, and resolution of inflammation. Nature Medicine 2015;21:698-708.

[8] Fu YY, Egorova A, Sobieski C, Kuttiyara J, Calafiore M, Takashima S, Clevers H, Hanash AM. T Cell Recruitment to the Intestinal Stem Cell Compartment Drives Immune-Mediated Intestinal Damage after Allogeneic Transplantation. Immunity 2019;51(1):90-103.e3.

[9] Takashima S, Matin M, Jansen S, Fu Y, Bos J, Chandra D, O'Connor M, Mertelsmann A, Vinci P, Kuttiyara J, SM D, Middendorp S, Calafiore M, Egorova A, Kleppe M, Lo Y, Shroyer N, Cheng E, Levine R, Liu C, Kolesnick R, Lindemans C, Hanash A. T cell-derived interferon gamma programs stem cell death in immune-mediated intestinal damage. 4. Science Immunology; 2019:eaay8556.

[10] Kominsky DJ, Campbell EL, Ehrentraut SF, Wilson KE, Kelly CJ, Glover LE, Collins CB, Bayless AJ, Saeedi B, Dobrinskikh E, Bowers BE, MacManus CF, Müller W, Colgan SP, Bruder D. IFN-γ–Mediated Induction of an Apical IL-10 Receptor on Polarized Intestinal Epithelia. The Journal of Immunology 2014;192(3):1267.

[11] Beebe K, Lee W-C, Micchelli CA. JAK/STAT signaling coordinates stem cell proliferation and multilineage differentiation in the Drosophila intestinal stem cell lineage. Developmental Biology 2010;338(1):28-37.

[12] Richmond CA, Rickner H, Shah MS, Ediger T, Deary L, Zhou F, Tovaglieri A, Carlone DL, Breault DT. JAK/STAT-1 Signaling Is Required for Reserve Intestinal Stem Cell Activation during Intestinal Regeneration Following Acute Inflammation. Stem cell reports 2018;10(1):17-26.

[13] Qiu Y, Yu M, Yang Y, Sheng H, Wang W, Sun L, Chen G, Liu Y, Xiao W, Yang H. Disturbance of intraepithelial lymphocytes in a murine model of acute intestinal ischemia/reperfusion. Journal of Molecular Histology 2014;45(2):217-27.

[14] Huang Y, Rabb H, Womer KL. Ischemia–reperfusion and immediate T cell responses. Cellular Immunology 2007;248(1):4-11.

[15] Linfert D, Chowdhry T, Rabb H. Lymphocytes and ischemia-reperfusion injury. Transplantation Reviews 2009;23(1):1-10.

[16] Rao J, Lu L, Zhai Y. T cells in organ ischemia reperfusion injury. Current opinion in organ transplantation 2014;19(2):115-20.

[17] Gandolfo MT, Jang HR, Bagnasco SM, Ko G-J, Agreda P, Satpute SR, Crow MT, King LS, Rabb H. Foxp3⁺ regulatory T cells participate in repair of ischemic acute kidney injury. Kidney International 2009;76(7):717-29.

[18] Feng M, Wang Q, Zhang F, Lu L. Ex vivo induced regulatory T cells regulate inflammatory response of Kupffer cells by TGF-beta and attenuate liver ischemia reperfusion injury. International Immunopharmacology 2012;12(1):189-96.

[19] van Weel V, Toes REM, Seghers L, Deckers MML, de Vries MR, Eilers PH, Sipkens J, Schepers A, Eefting D, van Hinsbergh VWM, van Bockel JH, Quax PHA. Natural Killer Cells and CD4+ T-Cells Modulate Collateral Artery Development. Arteriosclerosis, Thrombosis, and Vascular Biology 2007;27(11):2310-8.

[20] Gonzalez LM, Moeser AJ, Blikslager AT. Porcine models of digestive disease: the future of large animal translational research. Translational Research 2015;166(1):12-27.

[21] Yandza T, Tauc M, Saint-Paul MC, Ouaissi M, Gugenheim J, Hebuterne X. The pig as a preclinical model for intestinal ischemia-reperfusion and transplantation studies. Journal of Surgical Research 2012;178(2):807-19.

[22] Jiminez JA, Uwiera TC, Douglas Inglis G, Uwiera RRE. Animal models to study acute and chronic intestinal inflammation in mammals. Gut pathogens 2015;7:29-.

[23] Mair KH, Sedlak C, Käser T, Pasternak A, Levast B, Gerner W, Saalmüller A, Summerfield A, Gerdts V, Wilson HL, Meurens F. The porcine innate immune system: An update. 45. 2014:321-43.

[24] Dawson HD, Lunney JK. Porcine cluster of differentiation (CD) markers 2018 update. Research in Veterinary Science 2018;118:199-246.

[25] Stewart AS, Schaaf CR, Luff JA, Freund JM, Becker TC, Tufts SR, Robertson JB, Gonzalez LM. HOPX+ injury-resistant intestinal stem cells drive epithelial recovery after severe intestinal ischemia. American Journal of Physiology-Gastrointestinal and Liver Physiology 2021;321(5):G588-G602.

[26] Fukatsu K, Sakamoto S, Hara E, Ueno C, Maeshima Y, Matsumoto I, Mochizuki H, Hiraide H. Gut ischemia-reperfusion affects gut mucosal immunity: A possible mechanism for infectious complications after severe surgical insults*. Critical Care Medicine 2006;34(1).

[27] Stewart AS, Freund JM, Blikslager AT, Gonzalez LM. Intestinal Stem Cell Isolation and Culture in a Porcine Model of Segmental Small Intestinal Ischemia. Journal of Visualized Experiments 2018;135:57647.

[28] Käser T, Gerner W, Hammer SE, Patzl M, Saalmüller A. Phenotypic and functional characterisation of porcine CD4+CD25high regulatory T cells. Veterinary Immunology and Immunopathology 2008;122(1):153-8.

[29] Käser T, Pasternak JA, Delgado-Ortega M, Hamonic G, Lai K, Erickson J, Walker S, Dillon JR, Gerdts V, Meurens F. Chlamydia suis and Chlamydia trachomatis induce multifunctional CD4 T cells in pigs. Vaccine 2017;35(1):91-100.

[30] Espina V, Wulfkuhle JD, Calvert VS, VanMeter A, Zhou W, Coukos G, Geho DH, Petricoin EF, 3rd, Liotta LA. Laser-capture microdissection. Nat Protoc 2006;1(2):586-603.

[31] Hadis U, Wahl B, Schulz O, Hardtke-Wolenski M, Schippers A, Wagner N, Müller W, Sparwasser T, Förster R, Pabst O. Intestinal Tolerance Requires Gut Homing and Expansion of FoxP3⁺ Regulatory T Cells in the Lamina Propria. Immunity 2011;34(2):237-46.

[32] Renier N, Wu Z, Simon David J, Yang J, Ariel P, Tessier-Lavigne M. iDISCO: A Simple, Rapid Method to Immunolabel Large Tissue Samples for Volume Imaging. Cell 2014;159(4):896-910.

[33] Sato T, Vries RG, Snippert HJ, van de Wetering M, Barker N, Stange DE, van Es JH, Abo A, Kujala P, Peters PJ, Clevers H. Single Lgr5 stem cells build crypt-villus structures in vitro without a mesenchymal niche. Nature 2009;459(7244):262-5.

[34] Finch PW, Cheng AL. Analysis of the cellular basis of keratinocyte growth factor overexpression in inflammatory bowel disease. Gut 1999;45(6):848-55.

[35] Farmer DG, Ke B, Shen X-D, Kaldas FM, Gao F, Watson MJ, Busuttil RW, Kupiec-Weglinski JW. Interleukin-13 protects mouse intestine from ischemia and reperfusion injury through regulation of innate and adaptive immunity. Transplantation 2011;91(7):737-43.

[36] Cai Y-J, Wang W-S, Liang H-Y, Sun L-H, Teitelbaum DH, Yang H. Keratinocyte growth factor up-regulates Interleukin-7 expression following intestinal ischemia/reperfusion in vitro and in vivo. International journal of clinical and experimental pathology 2012;5(6):569-80.

[37] Gonzalez LM, Williamson I, Piedrahita JA, Blikslager AT, Magness ST. Cell Lineage Identification and Stem Cell Culture in a Porcine Model for the Study of Intestinal Epithelial Regeneration. Public Library of Science One 2013;8(6).

[38] Käser T, Mair KH, Hammer SE, Gerner W, Saalmüller A. Natural and inducible Tregs in swine: Helios expression and functional properties. Developmental & Comparative Immunology 2015;49(2):323-31.

[39] Rodríguez-Gómez IM, Talker SC, Käser T, Stadler M, Reiter L, Ladinig A, Milburn JV, Hammer SE, Mair KH, Saalmüller A, Gerner W. Expression of T-Bet, Eomesodermin, and GATA-3 Correlates With Distinct Phenotypes and Functional Properties in Porcine γδ T Cells. Frontiers in immunology 2019;10:396-.

[40] Käser T, Gerner W, Saalmüller A. Porcine regulatory T cells: Mechanisms and T-cell targets of suppression. Developmental & Comparative Immunology 2011;35(11):1166-72.

[41] Bar-Ephraim YE, Kretzschmar K, Clevers H. Organoids in immunological research. Nat Rev Immunol 2020;20(5):279-93.

[42] Chen S, Zheng Y, Ran X, Du H, Feng H, Yang L, Wen Y, Lin C, Wang S, Huang M, Yan Z, Wu D, Wang H, Ge G, Zeng A, Zeng YA, Chen J. Integrin αEβ7+ T cells direct intestinal stem cell fate decisions via adhesion signaling. Cell Research 2021;31(12):1291-307.